University of Nottingham

Characterisation of a Novel Microtubule Inhibitor and its Therapeutic Potential

Nikita Dave

BSc (Hons), MSc

Thesis submitted to the University of Nottingham towards the degree of Doctor of Philosophy

-

2024

Abstract

The dynamic instability of microtubules allows them to perform a diverse range of functions, including spindle formation and chromosome segregation during mitosis. Uncontrolled cell division is a hallmark of cancer, and drugs that inhibit microtubule dynamics to supress cell division are routinely used in chemotherapy. EFA6 and MCAK are microtubule destabilisers with differing modes of function, with the same result of an inhibition of microtubule dynamics. EFA6, a negative regulator of axonal growth, inhibits microtubule polymerisation through an 18-residue motif known as the microtubule elimination domain, or MTED. Apart from its microtubule inhibition abilities, little is known about the binding properties of this peptide. Here, I show that MTED has a strong affinity for the α/β-tubulin subunit, <10nM, and inhibits its polymerisation by directly binding to this subunit and sequestering it. Further investigations using an MTED-GFP DNA construct show that this peptide inhibits cell proliferation as a direct result of its microtubule inhibition activities, warranting attempts to recreate this result by externally adding synthetic peptide, an area still under investigation. Finally, I use a synthetic version of the kinesin-13 motor domain, Anc13, and study its depolymerisation abilities when placed in the context of the full length MCAK protein. This construct depolymerises microtubules nine-fold faster than wtMCAK, and promotes internal breakage of microtubules, suggesting that the ancestor of this family was a “super-depolymerase”. It is likely that the Kinesin-13 family, over time, moved away from this hyperactive depolymerisation activity to a slower, but much more controlled motor domain. By studying two microtubule destabilising proteins with differing modes of function, I aim to increase our understanding of microtubule targeting agents and aid in the development of novel therapeutics to combat the challenges posed by acquired drug resistance and lack of drug specificity.

Declaration of Academic Integrity

I confirm that all work presented in this thesis, unless explicitly mentioned, is the result of my own investigations carried out during my registered period of study at the University of Nottingham.

Nikita Dave

Acknowledgements

There are no words to express how grateful I am for the help and support I have received from family, friends, and colleagues during my PhD studies, but I will do my best.

Firstly, to my supervisors Dr Claire Friel and Dr Alan Huett – thank you for your endless support and wisdom. To Claire, I will forever be grateful for your kindness and words of encouragement when things were not going to plan, and your resourcefulness and determination to ensure I did not miss out on any experiences that comes with being a researcher, including helping me attend conferences and kickstarting my (hopefully long) publishing career. Thank you to Hanan Alghamdi, my Friel labmate, for your patience and generosity with protocols that you had devised yourself and never hesitating to help me despite having restrictions on your own time.

Thank you to Ian Ward of the School of Life Sciences Imaging Facility for training me on various equipment, checking to ensure that all was well during my booked sessions and being so friendly and approachable.

Thank you to Professor Dmitry Veprintsev for training and assisting me with light polarisation experiments, an area completely out of my field that I now feel somewhat comfortable with thanks to your expertise.

To Mom, Dad and Amit, – thank you for always acting impressed by my research despite having no idea what I'm talking about, especially my dad who liked to (and still does) send me every single biology-related news article he came across to show that he is interested in what I do.

To my wonderful network of friends: I relied on each and every one of you during my four years of trials and tribulations, and I truly believe I could not have accomplished what I have had I not had you behind me. Sharon, Euan, Louise, Kabi, Sareena, Aurelija, Arry, Talla, thank you for putting up with tears and late-night phone calls and last-minute plans cancellations and everything else. Love you all.

Of course, special mention to Callum and Mahari, my D119 partners in crime.

Last but not least, thank you to past me for having the determination to carry on and persevere throughout a pandemic, lab closures, illness, culture contamination, negative results and too-short trips home. She is the reason I am where I am today.

Table of Contents

Table of Figures

Abbreviations

2D – Two dimensional

3D – Three dimensional

AcNMPV – *Autographa californica* multiple nuclear polyhedrosis virus

ADP – Adenosine-5'-diphosphate

A-MTs – Astral microtubules

ANOVA – Analysis of variance

ATP – Adenosine -5'-Triphosphate

AU – Arbitrary units

BIIC - Baculovirus Infected Insect Cells

BSA – Bovine Serum Albumin

CEB – Cation Exchange Buffer

CNS – Central Nervous System

CPPs – Cell Penetrating Peptides

Da – Daltons

DMEM – Dulbecco's Modified Eagle Medium

DMSO – Dimethyl Sulfoxide

DNA – Deoxyribose Nucleic Acid

DOL – Degree of labelling

DP (μW) – Power differential

DTT – Dithiothreitol

ECM - Extracellular Matrix

EDTA – Ethylene Diamine Tetraacetic Acid

EFA6 – Exchange Factor for Arf6

EGTA – Ethylene Glycol Tetraacetic Acid

E-site – Exchangeable site

FACS – Fluorescence-activated Cell-sorting

FBS – Foetal Bovine Serum

GDP – Guanosine-5'-diphosphate

GEF-H1 – Guanine Exchange Factor – H1

GFP – Green Fluorescent Protein

GMPCPP – Guanylyl-(alpha-beta)-methylene-diphosphonate

GTP – Guanosie-5'-triphosphate

H_2O - Water

HDAC6 – Histone deacetylase 6

HEPES - 4-(2-hydroxyethyl)-1-piperazineethanesulfonic acid

hSgo2 - Human Shugoshin 2

IDT – Integrated DNA Technologies

Interpolar MTs – Interpolar microtubules

Isopropyl β-d-1-thiogalactopyranoside (IPTG)

ITC – Isothermal Titration Calorimetry

KCl – Potassium chloride

kDa - Kilodaltons

K-fibres – Kinetochore fibres

KHC - Kinesin heavy chain

K-MTs – Kinetochore microtubules

LB - Luria Broth

LCEA – Last Common Eukaryotic Ancestor

LN_2 - Liquid Nitrogen

LUCA - Last Universal Common Ancestor

MAP4 – Microtubule Associated Protein 4

MAP6 – Microtubule Associated Protein 6

MCAK – Mitotic Centromere Associated Kinesin

MgATP – Magnesium ATP

$MgCl_2$ – Magnesium chloride

mRNA – messenger RNA

MST – Microscale Thermophoresis

MTAs – Microtubule Targeting Agents

MTED – Microtubule Elimination Domain

MTOC – Microtubule Organisation Centre

N_2 – Nitrogen gas

NaCl – Sodium chloride

NCBI – National Centre for Biotechnology Information

NEB – New England Biolabs

NFL – Neurofilament derived

NFL-TBS – Neurofilament derived tubulin binding site

Ni buffer – nickel affinity buffer

NMR - Nuclear magnetic resonance

N-site - Non-exchangeable site

P/S – Penicillin / Streptomycin

P53-REs – p53 Response Elements

PBS – Phosphate Buffered Saline

PBST – PBS + TritonX-100

PCM - Pericentriolar Matrix

PCR – Polymerase Chain Reaction

PFA – Paraformaldehyde

pH – power of Hydrogen

PLMs - Posterior Lateral Microtubules

PMNs - Polymorphonuclear Neutrophils

PMSF – Phenylmethanesulphonyl Fluoride

PSD – Pleckstrin Sec7 Domain

PTDs – Protein Transduction Domains

PTMs – Post Translational Modification

RFP – Red Fluorescent Protein

Rhodamine – Tetramethylrhodamine

RNAi – RNA interference

rpm – Rounds per Minute

SDS-PAGE – Sodium dodecyl sulphate polyacrylamide gel electrophoresis

Sf9 – *Spodoptera frugipera* cells

Sgo2 - Shugoshin 2

Silane – Dimethyldichlorosilane

siRNA – small interfering RNA

SOC – Super Optimal Culture

STOP - Stable Tubule Only Peptide

TAE – Tris Acetate EDTA

TBS – Tubulin Binding Site

TCE – Trichloroethylene

TPPP1 - Tubulin Polymerising Promoting Protein 1

TRITC – Tetramethylrhodamine Isothiocyanate

WHO – World Health Organisation

α-TAT1 – alpha Tubulin acetyl Transferase

γ-TURC – Gamma Tubulin Ring Complex

ΔH - Enthalpy

Chapter 1) Introduction

1.1. The cytoskeleton

The cytoskeleton is an intricate and dynamic system with three main components: actin, intermediate filaments, and microtubules (**Figure 1.1**). Together, these filaments work to give shape and structure to the cell, provide networks for intracellular trafficking and generate force to allow for cell migration and movement (Hohmann & Dehghani, 2019).

Previously, it was thought that only the Eukaryota possessed a cytoskeleton. However, the discovery of actin and tubulin homologues in bacteria, such as *Mre*B and *Fst*Z, respectively, which provide some form of membrane structure and support, have disproved this idea, suggesting that the last universal common ancestor (LUCA) possessed a rudimentary cytoskeleton (RayChaudhuri and Park 1992, Strahl, Burmann et al. 2014).

Actin, the smallest of the three filaments (~7nm in diameter), is composed of monomers of globular actin (G-actin) that, upon binding to ATP, polymerise into filaments (F-actin) (Cooper 2000). Actin is crucial for a range of cellular functions; it provides mechanical support for the cell membrane, aids in cell migration by forming cellular protrusions, and interacts with the motor protein myosin to facilitate muscle contraction (Pollard & Cooper, 2013; Cooper, 2000).

However, actin does Intermediate filaments (~10nm diameter) are formed of long proteins with a conserved, central α-helical domain via which these subunits polymerise (Fraser, MacRae et al. 1964, Parry, Strelkov et al. 2007). Intermediate filaments are the main contributors to tensile strength of cells, being able to stretch over three times their original length (Fudge and Gosline 2004). Cell-cell adhesion and tissue integrity is also facilitated by intermediate filaments such as keratin.

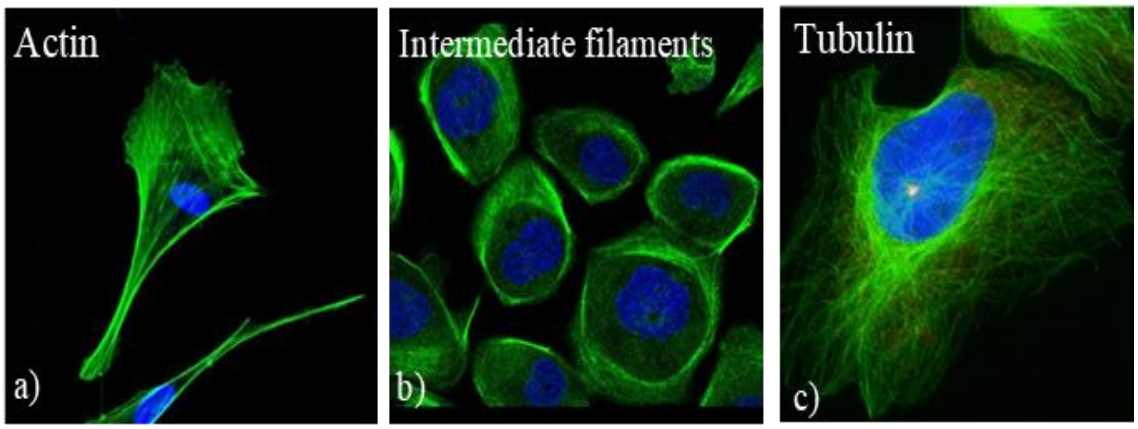

Figure 1.1) The three components of the cytoskeleton.

a) The actin cytoskeleton in human mesenchymal stromal cells; b) intermediate filaments in epidermoid carcinoma cells, c) the microtubule cytoskeleton in U2OS cells. DNA is stained blue in all images. Images adapted from (Zonderland, Wieringa et al. 2019) (actin); (Uhlen 2012) (intermediate filaments); (Sulimenko, Hajkova et al. 2017) (Tubulin).

1.2. Microtubules

Microtubules, the largest of the three filaments (~25nm in diameter), are polymers of tubulin, a globular heterodimeric protein with α- and β-tubulin subunits that polymerise into microtubules upon the binding of GTP. Microtubules are involved in several cellular functions such as the provision of networks for intracellular cargo transport, the formation of flagella and cilia, cell polarisation, structure and support, and the formation of the mitotic spindle during cell division (reviewed in (Logan and Menko 2019)).

1.2.1. Microtubule polymerisation

In cells, microtubule polymerisation typically initiates at the centrosome; a pair of centrioles surrounded by a pericentriolar matrix (PCM) with rings of γ-tubulin embedded on the surface, known as the γ-tubulin ring complex (γTuRC) **(Figure 1.2a,b).** These rings have 13-fold symmetry (Kollman, Polka et al. 2010) (although a recent study suggests that the ring is asymmetrically cone-shaped (Wieczorek, Urnavicius et al. 2020)) which aids in the polymerisation of 13 protofilaments into the hollow microtubule. γTuRC forms the nucleation site and negative end of the microtubule.

α- and β-tubulin are almost identical in structure, with both containing a nucleotide binding site; α- tubulin binds GTP at the non-exchangeable site (N-site) and β-tubulin at the exchangeable site (E-site) (Nogales, Wolf et al. 1998, Lowe, Li et al. 2001). These GTP-bound heterodimers assemble into straight protofilaments (Cote and Borisy 1981). α- and β-tubulin monomers in each protofilament form parallel, lateral associations with their counterparts in the adjacent filaments (i.e. α-α and β-β), with the 13 filaments coming together at a discontinuous seam, folding into a hollow, cylindrical lattice, the microtubule (**Figure 1.2c**).

Upon polymerisation, GTP is hydrolysed to GDP in the β-tubulin subunit and becomes non-exchangeable. The heterodimer now favours a curved conformation and reduces the dimer's affinity for its neighbouring subunits (Wang and Nogales 2005). However, lateral associations between GTP-bound subunits, and the GDP-bound dimer being "buried" in the microtubule and less exposed, exert a strong enough force to maintain the protofilament in a straight conformation (Nogales, Wolf et al. 1998, Wang and Nogales 2005, Horio and Murata 2014).

GTP at the α-tubulin site does not hydrolyse and remains stably bound. (Nogales, Wolf et al. 1998, Horio and Murata 2014).

As the microtubule continues to polymerise at the plus end, the incorporation of GTP-bound tubulin dimers can exceed the rate of GTP hydrolysis within the microtubule. When this occurs, a stable "GTP-cap" is formed with the tubulin heterodimers at the + end remaining in the high affinity GTP-bound state, further stabilising the microtubule in a straight conformation (Vale, Reese et al. 1985). A loss of this GTP cap results in "catastrophe"; the term used to define the moment the microtubule changes from a polymerising to depolymerising state, while the recovery of the GTP cap results in a "rescue", the moment when the microtubule changes from a depolymerising to polymerising state.

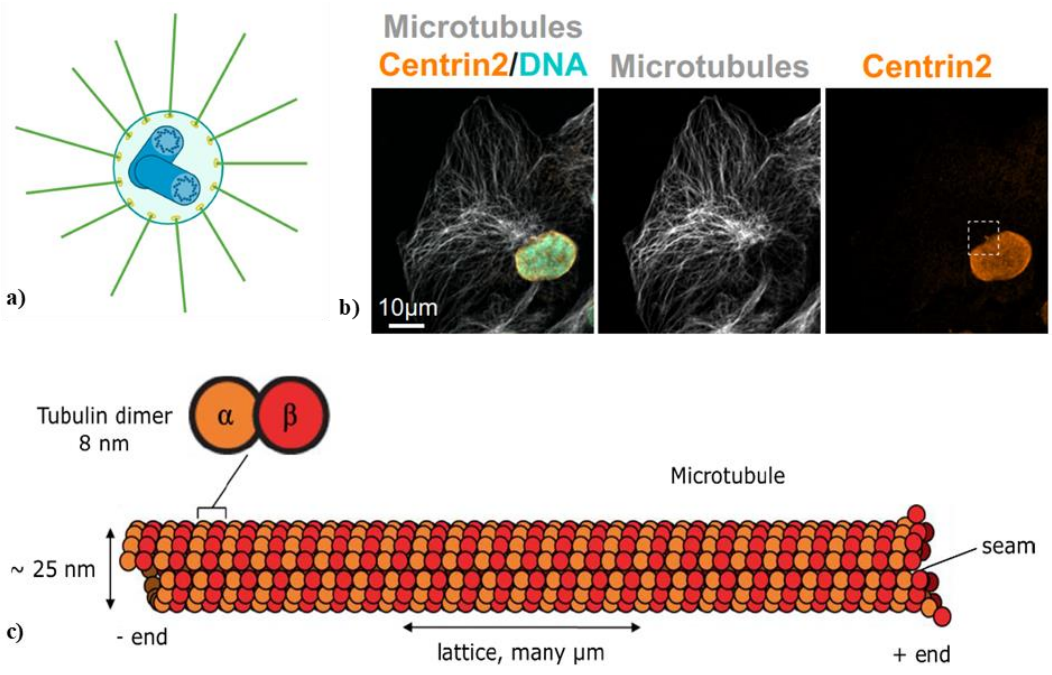

Figure 1.2) The centrosome is the origin of microtubule polymerisation.

a) Simplified schematic of a centrosome. Centrioles are blue, γ-TURC is yellow and microtubules are extending outwards in green. b) The position of the centrosome and the microtubules radiating from it (adapted from (Montieiro, Yeon et al. 2023)). c) simplified schematic of a microtubule. The 13 protofilaments come together at a single, discontinuous seam to form the hollow cylinder.

This ability of the microtubule to grow and shrink in repeated cycles is termed “dynamic instability” and is dependent on GTP hydrolysis. The idea of a GTP cap was sceptically received when first proposed, as kinetic measurements have shown that GTP hydrolysis is “closely coupled” with polymerisation (Hyman, Salser et al. 1992) (reviewed in (Caplow 1992)). The GTP cap has never been directly observed in microtubule dynamics and so its existence is yet to be proven (Gardner, Zanic et al. 2011). Microtubules polymerised with Guanosine-5’-(α,β)-methylene-triphosphate (GMPCPP), a non-hydrolysable analogue of GTP, do not exhibit any dynamic instability at the critical tubulin concentration of 20nM, where the critical concentration refers to the minimum concentration of tubulin necessary for microtubule polymerisation to occur, while those polymerised with GTP undergo such high rates of catastrophe that no polymerisation can be detected (Hyman, Salser et al. 1992). Additionally, molecular dynamics simulations and subsequent microtubule depolymerisation assays show that the proportion of GMPCPP nucleotides within the microtubule correlates with an increase in microtubule stability. A 40% GMPCPP content results in microtubules that remain stable for over 400s, increasing to over 600s at a GMPCPP content of >70%, compared to less than 100s in a 100% GTP control (Bollinger, Imam et al. 2020). Microtubule stability, therefore, is highly dependent on GTP hydrolysis, though this is not the sole factor, as catastrophe has been found to be influenced by a number of factors, many of which are still poorly understood.

1.2.2. Microtubule depolymerisation

Within the microtubule lattice, hydrolysis of GTP to GDP occurs at the β-tubulin E-site (Nogales, Wolf et al. 1998, Lowe, Li et al. 2001). GDP-bound tubulin favours a curved conformation, decreasing the strength of the lateral interactions of each heterodimer with its counterparts in neighbouring protofilaments, and destabilising the microtubule (Nogales, Wolf et al. 1998). However, destabilisation of the microtubule is not sufficient for depolymerisation. While microtubules do spontaneously depolymerise, they do so incredibly slowly; GMPCPP stabilised microtubules spontaneously depolymerise at a rate of 0.03µm/min^{-1} when fixed onto cover glass surfaces at 20°C (Gell, Bormuth et al. 2010). Therefore, depolymerisation is aided by the kinesin-13s, a subfamily within the Kinesin superfamily of microtubule motor proteins with depolymerisation as opposed to translocation activity. The mammalian members of this family are Kif2a, Kif2b and Kif2c (also known as

mitotic centromere-associated kinesin [MCAK]), the most well characterised member of this subfamily (Wordeman and Mitchison 1995). The kinesin-13s utilise ATPase activity to bind to the terminal tubulin dimer, stabilise it in the curved conformation induced upon GTP hydrolysis, and remove it from the microtubule (Hunter, Caplow et al. 2003). Depolymerisation and translocation along the microtubule are not mutually exclusive; the kinesin-8 subfamily are unique in that they have the dual function of plus-end translocation and microtubule depolymerisation (Su, Qiu et al. 2011, Weaver, Ems-McClung et al. 2011). However, the depolymerisation abilities of this protein are not as strong as that of MCAK. The rate of ATP turnover, used to measure the speed at which ATP-hydrolysing proteins function, shows that, in the presence of microtubules, MCAK has an ATPase rate of $4.97\pm0.53^{s-1}$, while Kif19a, the most well characterised member of the kinesin-8 subfamily, turns over ATP at a rate of $0.42\pm0.09^{s-1}$, much slower than MCAK (Friel and Howard 2011) (Wang, Ryo et al. 2016).

1.3. Microtubule functions

Microtubules are involved in a diverse set of functions within the cell. They provide networks for kinesin and dynein motor proteins to transport cargo, make up the structural components of flagella and cilia to allow for cell motility, aid in the determination of cell polarity and confer structure and support to the cell (reviewed in (Logan and Menko 2019)). These functions are all vital to cellular function and survival; however, there are two functions that are of particular interest and relevance to the work described in this thesis, mitosis and migration, and I will describe these in detail.

1.3.1. Mitosis

Uncontrolled cell division is often the first change in normal cellular function, in a series of genetic and cellular changes, that leads to cancer. Microtubules play an essential role in cell division, comprising the spindle fibres required for chromosome segregation during anaphase. Several different types of microtubules come together to orchestrate this complex process.

Mitotic microtubules can be broadly classified into those that interact with the kinetochore (K-MTs or K-fibres) and those that do not, polar microtubules (P-MTs), further divided into astral microtubules (A-MTs) and interpolar microtubules (interpolar MTs) (Meunier and Vernos 2012, Conduit, Wainman et al. 2015, Prosser and Pelletier 2017, Tolic 2018). Each of these types of microtubules have differing levels of stability, with K-fibres being the most stable, and play an essential role in cell division (**Figure 1.3**). At S phase, the singular centrosome duplicates, and the nucleating capabilities of each one increases more than three-fold, known as centrosome maturation (Robbins, Jentzsch et al. 1968, Kochanski and Borisy 1990, Khodjakov and Rieder 1999, Piehl, Tuli et al. 2004). Once duplicated, centrosomes localise to opposite ends of the cell, facilitated by A-MTs and specific kinesin motor proteins such as Eg5. Eg5 is essential for centrosome separation; depletion of this kinesin results in an up to 91% decrease in the distance of centrosomes during metaphase and can result in the formation of a monopolar spindle (She, Zhong et al. 2022). Post centrosome separation, A-MTs are essential for correct spindle orientation; depletion of A-MTs in yeast results in an increase in spindle misorientation and, while not inhibiting anaphase, increases the proportions of binucleated cells and aberrant mitoses (Palmer, Sullivan et al. 1992).

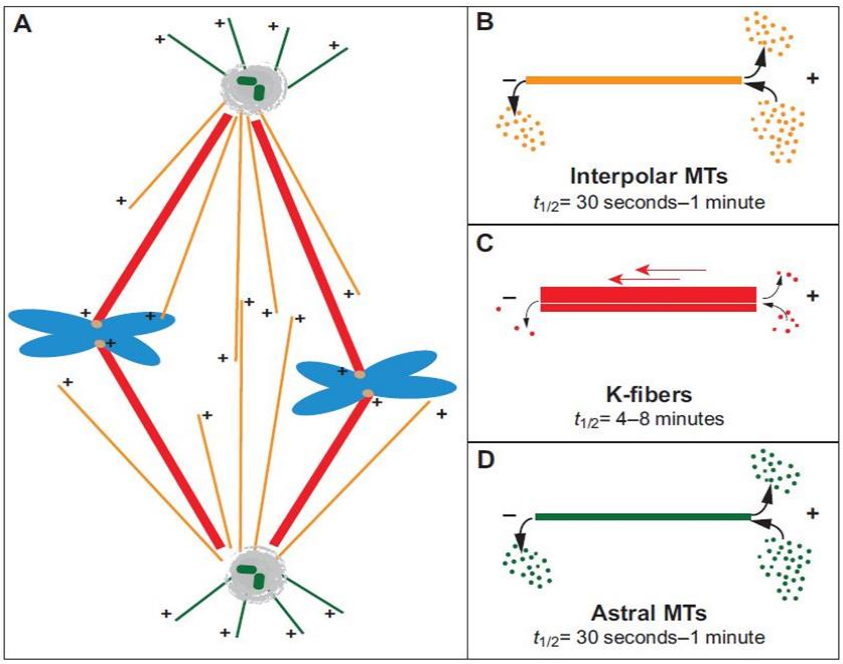

Figure 1.3) Types of microtubules involved in mitosis.

A) A simple schematic showing the various microtubule structures involved in mitotic spindle formation and chromosome segregation. Chromosomes are depicted in blue, kinetochores as orange circles, centrioles are green cylinders within the centrosome, the grey circle at either end. B-D) Images and descriptions of the different microtubule structures depicted in (A). + symbols refer to the plus end of the microtubule, and – symbols refer to the minus end in all panels. $t_{1/2}$ in B-D refers to the half-life of each type of microtubules. Adapted from (Meunier and Vernos 2012).

1.3.1.1. Interpolar MTs

During prometaphase and spindle fibre formation, interpolar MTs (**Figure 1.3**, yellow) strengthen and lengthen the K-fibres (**Figure 1.3**, red), leading them to the cell equator (Tanenbaum and Medema 2010). Interpolar MTs from opposite poles can interact and form antiparallel overlaps here, hence the name "interpolar" (Mastronarde, McDonald et al. 1993). Yeast and Drosophila studies demonstrated that force is generated by select kinesin motor proteins (e.g. Kinesin-5 proteins Eg5 and Cut7) walking along the interpolar MTs towards the + end and pulling them apart while others, such as NCD and HSET in the kinesin-14 family walk towards the - end, drawing the microtubules closer together (Hagan and Yanigida 1990, McDonald, Stewart et al. 1990, Sawin, LeGuellec et al. 1992, Cai, Weaver et al. 2009).

1.3.1.2. K-MTs

As cells progress from G2 to mitosis, K-MTs nucleate from the centrosomes, extending into their periphery in search of kinetochores, called "search and capture" (Kirschner and Mitchison 1986) (reviewed in (Prosser and Pelletier 2017)). The dynamic nature of microtubules allows K-MTs to grow and shrink as they examine the area around them, stabilising upon encountering a kinetochore, otherwise undergoing catastrophe (Kirschner and Mitchison 1986, Meunier and Vernos 2012). While the search-and-capture method has been extensively studied, it cannot be the only way in which K-MTs encounter kinetochores. In 2005, mathematical modelling and computer simulations determined the time needed for MTs growing at random to encounter all kinetochores present during metaphase completely unaided and on average, the process took 20-30 minutes for the final kinetochore to be captured (Wollman, Cytrynbaum et al. 2005). This is inconsistent with the length of metaphase, the stage at which K-MTs attach to kinetochores, and other factors have since been identified to aid this process (Paul, Wollman et al. 2009, Magidson, Paul et al. 2015). For example, a RanGTP gradient, produced by RCC1, a metaphasic chromosome-associated protein, around the kinetochores promotes centrosome-independent microtubule polymerisation, increasing the density of microtubules in the vicinity of kinetochores and increasing the likelihood of kinetochore capture by the microtubule plus end (reviewed in (Heald & Khodjakov, 2015).

1.3.1.3. K-fibres

Once bound to kinetochores, 20-40 K-MTs bundle together into K-fibres (Rieder 1981, Meunier and Vernos 2012). TACC3, clathrin and ch-TOG have been identified in cross-linking these fibres together by forming short inter-MT "bridges" (Royle, Bright et al. 2005, Booth, Hood et al. 2011). While the connecting strands look like bridges in two dimensions (2D), three dimensional (3D) analysis shows that the strands connecting the K-MTs contact multiple microtubules simultaneously in all directions (**Figure 1.4**) These interconnected structures are collectively known as a "mesh" and is a key regulator of K-MT stability (Nixon, Hood et al. 2015).

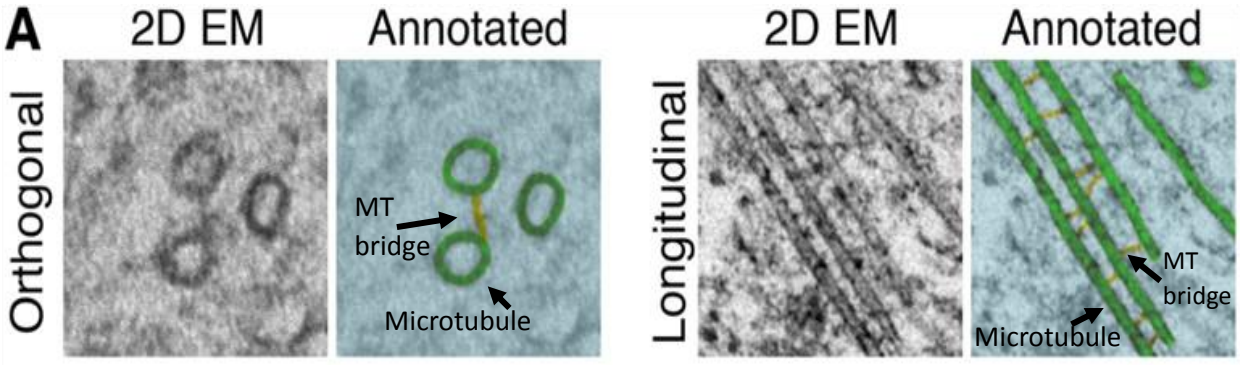

Figure 1.4) Microtubules (K-fibres) are supported by an interconnected mesh.

A) 2D-Electron Microscopy orthogonal and longitudinal slices showing the microtubule (dark grey ring) and an annotated image with microtubules in green and the mesh in yellow. Adapted from (Nixon, Hood et al. 2015).

1.3.2. Cell migration

The migration of cancer cells through the vasculature and invasion of distal tissue, a process known as metastasis, is of vital importance in cancer studies and is considered a target for therapy, as in most cases of cancer, it is not the primary tumour, but metastasis and invasion of cancer cells into distal tissue that proves fatal. Actin has long been known to the be primary driver of cell migration; it provides the structural basis for filopodial and lamellipodial protrusions, communicates with and transduces signals from the extracellular matrix (ECM) through focal adhesions and undergoes rapid polymerisation/depolymerisation to facilitate the "crawling" of the cell (reviewed in (Schaks, Giannone et al. 2019)). However, actin does not work alone, as microtubules too are involved in the process of cell migration, and the two networks are in constant communication with each other.

1.3.2.1. Determination of cell polarity

Directional movement of the cell requires polarity within the cell to define the leading edge. In most non-migrating, interphasic cells, the centrosome / microtubule organisation centre (MTOC) is centrally positioned, near the nucleus (Eddy, Pierini et al. 2002, Burakov, Nadezhdina et al. 2003, Tang and Marshall 2012).

When stimulated with a chemoattractant, polymorphonuclear neutrophils (PMNs) become highly polarised; the MTOC is positioned directly behind the actin-rich lamella, and ~87% of microtubules radiate towards the rear of the cell, into the uropod (**Figure 1.5**) (Eddy, Pierini et al. 2002). The MTOC in unstimulated PMNs is centrally positioned, with microtubules radiating uniformly in all directions (Eddy, Pierini et al. 2002). Treatment of many immune cells with both microtubule stabilisers and destabilisers have been shown to impair the determination of polarity and migration directionality without negatively impacting migration itself, suggesting that this class of cells rely on the asymmetric organisation of the microtubules for polarity, but not migration (Keller, Naef et al. 1984, Niggli 2003, Yadav, Stojkov et al. 2019).

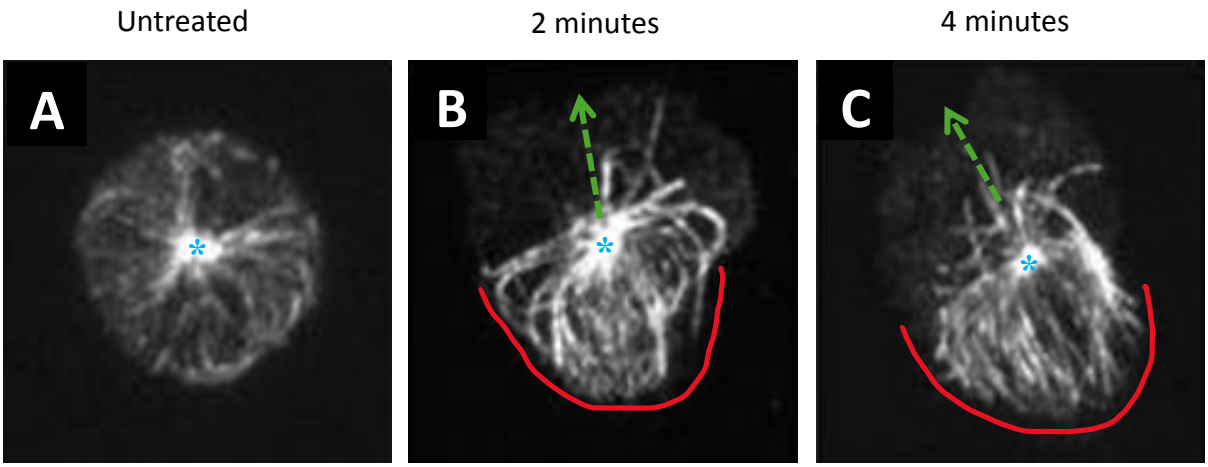

Figure 1.5) Microtubules reorientate and polarise the cell through the formation of a uropod upon stimulation with fMLF.

Polymorphonuclear neutrophils (A) untreated; B) treated for 2 minutes and C) treated for four minutes with 10nM fMLF, an immune cell chemoattractant, prior to fixation and staining. The blue asterisk in all image panels shows the location of the MTOC, red selected areas in B and C show the microtubule filled uropod, and green arrows indicate direction of movement. Adapted from (Eddy, Pierini et al. 2002).

1.3.2.2. Generation of force for cellular outgrowth and pseudopodia formation

Neuronal cells rely on the polymerisation and force generated by microtubules and their associated motor proteins for migration and outgrowth. Axons, the neuronal outgrowths that carry electrical signals away from the cell body to the synapses, are filled with bundles of microtubules. Initial neurite outgrowth is not reliant upon microtubule polymerisation; treatment with vinblastine, which inhibits microtubule growth but does not depolymerise existing microtubules, does not have any adverse effects on neuronal outgrowth (Lu, Fox et al. 2013). Microtubule sliding, as opposed to polymerisation, is thought to be the major generator of force required for neuronal outgrowth and is facilitated by the heavy chain of conventional kinesin, or kinesin-1 (Lolly, Kim et al. 2010). RNAi depletion of endogenous kinesin heavy chain (KHC) results in a more static microtubule network, with significantly less sliding observed compared to wild type cells, and KHC homozygous null embryos present with significantly shorter and disordered axons than control cells (Lolly, Kim et al. 2010, Lu, Fox et al. 2013).

3D migration of cells is also in part dependent on microtubule force. Pseudopodia, cellular outgrowths / extensions, are common to many cells during the migratory process, and are key to migration and invasion. Growth and elongation of these “limbs” are reliant on microtubules; treatment with microtubule stabilisers and destabilisers alike result in shorter overall pseudopodal length, eliminate existing pseudopodia, and significantly reduce the invasive abilities of cells (Kikuchi and Takahashi 2008, Martins and Kolega 2012, Lee, Wu et al. 2015).

1.3.2.3. Microtubules as regulators of actin dynamics through RhoGTPase activity

Rho GTPases are a family of signal transducers that regulate, amongst other things, actin dynamics by facilitating the exchange of GTP for GDP (reviewed in (Haga and Ridley 2016)). Guanine nucleotide exchange factor H1 (GEF-H1) is a Rho GTPase whose activity is regulated by its binding to the microtubule lattice (Ren, Li et al. 1998). In its bound state, GEF-H1 is inactive; depolymerisation of microtubules with nocodazole and colchine increase activation of GEF-H1, while stabilisation with Taxol has no impact on GEF-H1 activity (Krendel, Zenke et al. 2002). Upon microtubule depolymerisation, the newly active GEF-H1 catalyses the release

of GDP from RhoA, allowing for its activation by binding with GTP (Haga and Ridley 2016). Active RhoA, in turn, interacts with the actin cytoskeleton and promotes polymerisation of stress fibres and focal adhesions, and aids in the formation of lamellipodia and cell migration (Liu, Chrzanowska-Wodnicka et al. 1998). Depletion of GEF-H1 by siRNA significantly reduces stress fibre assembly and cell contractility, while an overexpression of GEF-H1 induces contractility (Krendel, Zenke et al. 2002, Chang, Nalbant et al. 2008). The regulation of GEF-H1 is crucial to normal cellular physiology as GEF-H1 mutants that are unable to bind to the microtubule lattice have been implicated in oncogenesis (Brecht, Steenvoorden et al. 2005).

1.3.2.4. Transport of cargo required for migration

One of the many functions of microtubules is the provision of tracks for the intracellular transport of cargo, facilitated by the host of motor proteins associated with the microtubule network. Much of this cargo is necessary for the regulation of actin dynamics, focal adhesion dynamics and energy production (Garcin and Straube 2019, Schaks, Giannone et al. 2019). mRNAs encoding actin regulatory proteins such as the Arp2/3 complex and profilin, and the transcript for the β-actin protein are transported along the microtubule to the site of actin polymerisation, where they undergo localised translation and posttranslational modification, allowing for a steady supply of β-actin for rapid actin polymerisation (Mingle, Okuhama et al. 2005, Johnsson and Karlsson 2010).

Mitochondria, also, are transported by microtubules. Cytoskeletal dynamics and cell migration are extremely energetically demanding processes; the localisation of mitochondria to the site of cell migration offers a constant supply of the energy required for these processes. Different types of cells will localise mitochondria to different places during the process of migration. Lymphocytes preferentially transport mitochondria to the uropod, a microtubule-containing protrusion at the rear of the cell that generates force and provides stability to the migrating cell (Campello, Lacalle et al. 2006, Hind, Vincent et al. 2017). In cancer cells such as ovarian adenocarcinoma, mesothelioma and HeLa's, mitochondria are trafficked to the leading edge of the cell. Treatment with both nocodazole and Taxol result in the disruption of mitochondrial trafficking, while perturbations of the actin network have no effect (Cunniff, McKenzie et al. 2016).

1.4. Microtubule regulatory proteins

As microtubules are so heavily involved in a range of cellular processes, it is no surprise that any perturbation in microtubule dynamics can lead to a host of diseases, such as microcephaly, infertility and cancer (Breuss, Heng et al. 2012, Fife, McCarroll et al. 2014, Yang, Yin et al. 2020). As an organism ages, the amount of microtubule polymerisation occurring in cells decreases, as does cellular metabolic activity, resulting in a decrease in the available energy required for the faithful regulation and maintenance of dynamic microtubules (Yu, Pessino et al. 2012). Aged cells are therefore more likely to undergo abnormal spindle formation and subsequent aberrant chromosomal disjunction during anaphase, potentially setting into motion a series of unfortunate events that will lead to cancer. **Table 1** outlines the various microtubule regulatory proteins discussed in this section.

Table 1) Microtubule regulatory proteins and their modes of function

Name	Type of microtubule regulatory protein	Mode of action
Eg5	Promoter	Reduces critical concentration of tubulin
TPP1	Promoter	Inhibits HDAC6 to indirectly promote polymerisation
MAP4	Promoter	Promotes microtubule rescue
TAU	Stabiliser	Binds to and stabilises neuronal microtubules
MAP6	Stabiliser	Protects microtubules against cold temperature stress
MCAK	Destabiliser	Uses ATP turnover to remove tubulin dimers and depolymerise the microtubule
Stathmin	Destabiliser	Sequesters tubulin monomers and promotes catastrophe

1.4.1. Microtubule growth promotors

Microtubule promotors can act in myriad ways to aid polymerisation. Eg5, a kinesin-5 motor protein, is known to facilitate spindle elongation during mitosis, but has an additional function of promoting microtubule nucleation (Chen, Cleary et al. 2019, She, Zhong et al. 2020). Monomeric Eg5 reduces the critical concentration of tubulin from 3.6μM to 2.7μM at 25°C, and, in its dimeric form, preferentially binds to polymers of tubulin rather than free subunits and stabilises tubulin in its straight, more stable conformation (Chen, Cleary et al. 2019). Tubulin Polymerising Promoting Protein 1 (TPPP1), on the other hand, indirectly promotes microtubule polymerisation by inhibiting Histone deacetylase 6 (HDAC6), known to deacetylate microtubules as well as histones (Schofield and Bernard 2013). Acetylated microtubules are more stable than their deacetylated counterparts, and as such, inhibition of HDAC6 promotes microtubule polymerisation by facilitating the stabilisation of the existing polymer(Schofield and Bernard 2013). Microtubule associated protein 4 (MAP4), meanwhile, promotes microtubule polymerisation and rescue. This accessory protein is phosphorylated and inactivate during mitosis, reducing its rescue abilities, as microtubule rescue would prevent chromosome segregation during anaphase (Ookata, Hisanaga et al. 1995). MAP4 overexpression decreases the rate of cell division and mutants lacking the phosphorylation sites block mitosis (Nguyen, Chari et al. 1997, Cassimeris 1999). Depletion of MAP4 using RNAi results in spindle fibres losing their elliptical shape, narrowing and elongating (Samora, Mogessie et al. 2011). In this irregular form, up to 52% of cells show unaligned chromosomes compared to 13% in control cells, and 3D positioning and orientation of the mitotic spindle is more erratic (**Figure 1.6**) (Samora, Mogessie et al. 2011).

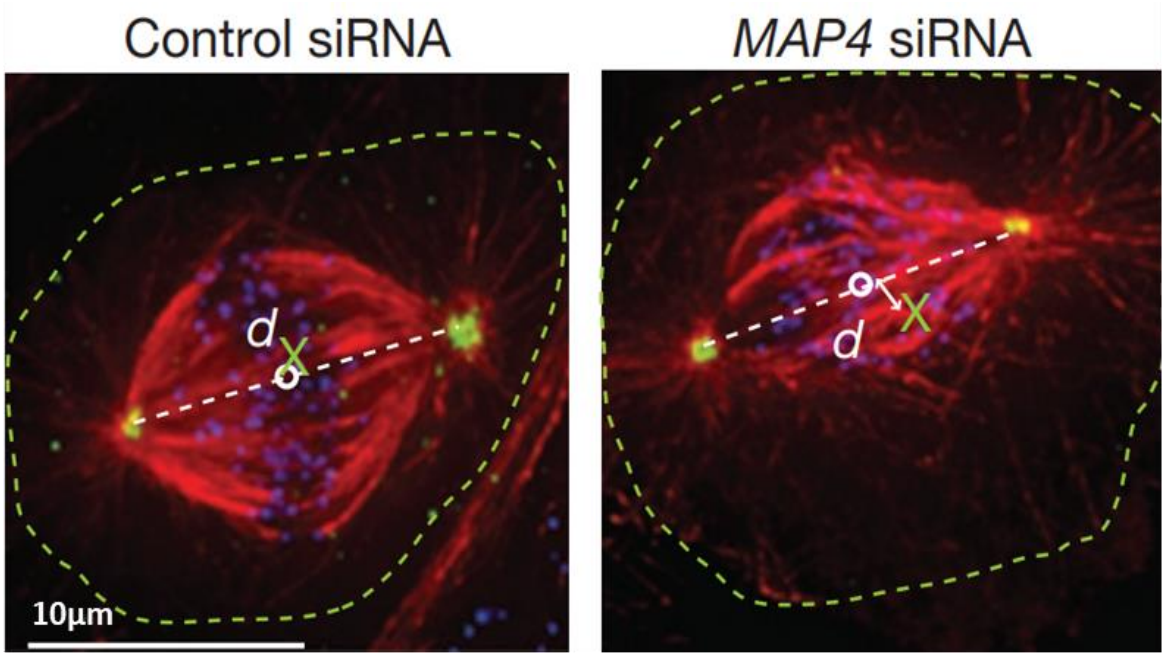

Figure 1.6) MAP4 maintains faithful spindle positioning.

HeLa cells fixed and stained for α-tubulin (red), γ-tubulin (yellow) and CREST (blue). d=distance between the centre of the cell (green X) and the middle of the spindle (white circle). Adapted from (Samora, Mogessie et al. 2011).

1.4.2. Microtubule stabilisers

Microtubule stabilisers confer stability to the microtubule. Stabilisers can be tissue-specific e.g. TAU, a neuronal microtubule stabiliser. TAU promotes tubulin polymerisation below its critical concentration and protects against catastrophe but has no impact on rescue (Trinczek, Biernat et al. 1995, Devred, Barbier et al. 2004). TAU could therefore be classified as both a microtubule promoter and stabiliser. TAU binds to microtubules via a number of short motifs all located between residues 208-324 (Fauquant, Redeker et al. 2011, Kadavath, Hofele et al. 2015). Residues in between these microtubule binding sites have also been picked up by nuclear magnetic resonance (NMR), suggesting that TAU does not bind rigidly to microtubules, but has some variability in its binding conformation, increasing its ability to stabilise the tubules (Kadavath, Hofele et al. 2015).

Microtubule stabilisers can also be expressed in response to stress. Microtubule associated protein 6 (MAP6) is an example of an accessory protein that stabilises microtubules in response to cold temperature-induced stress (Lieuvin, Labbe et al. 1994, Cuveillier, Delaroche et al. 2020). Found exclusively in vertebrates, MAP6 (also known as stable tubule only peptide [STOP]) is expressed in a wide variety of tissue including, but not limited to, brain, heart and lung tissue (Aguezzoul, Andrieux et al. 2003). It has previously been shown that microtubules in HeLa cells which do not endogenously express MAP6 depolymerise when incubated at 4°C, while those in MEF and NIH/3T3 cells with endogenous MAP6 expression do not undergo catastrophe but remain in a stable state, resistant to cold temperature (Bosc, Frank et al. 2001). Exposure to cold stress (4°C) causes MAP6 re-localisation from the cytoplasm to the microtubule in as little as 30s but remains cytoplasmic at 37°C (Delphin, Bouvier et al. 2012). Additionally, MAP6 directly interacts with microtubule ends at temperatures below 25°C and reduces protofilament curling by ~50% (Bosc, Frank et al. 2001, Delphin, Bouvier et al. 2012).

1.4.3. Microtubule destabilisers

Microtubule destabilisers, like promoters, work in different ways. The Kinesin-13 family are microtubule depolymerases that hydrolyse ATP to induce a curved conformation and subsequent removal of tubulin dimers from the microtubule end (Wang and Nogales 2005). Stathmin, on the other hand, is an example of a microtubule destabiliser that does not have nucleotide hydrolysis capabilities, but instead sequesters monomeric tubulin and prevents its polymerisation (Howell, Larsson et al. 1999). Stathmin is of particular interest as it appears to have differing modes of function. At pH 6.8, stathmin slows the rate of microtubule polymerisation by sequestering free tubulin monomers but does not have any effect on preformed microtubules (Howell, Larsson et al. 1999). At a physiological pH of 7.5, however, stathmin has no effect on microtubule elongation rates, but significantly increases the rate of microtubule catastrophe (Howell, Larsson et al. 1999). These differing effects of stathmin rely on properties in the N-terminus (promotion of catastrophe) and C-terminus (sequestration of tubulin) (Rubin and Atweh 2004).

This thesis will describe work carried out on two types of microtubule destabilisers: a peptide, derived from Exchange Factor for ARF6 (EFA6), that sequesters tubulin and inhibits its polymerisation, and MCAK, a nucleotide-hydrolysing microtubule depolymerase.

1.5. EFA6

EFA6, a member of the family of guanine nucleotide exchange factor proteins for the ARF family, negatively regulates axonal growth by inhibiting microtubule polymerisation (O'Rourke, Christensen et al. 2010, Chen, Wang et al. 2011, Qu, Hahn et al. 2019) Four EFA6 proteins exist in mammals (EFA6A, EFA6B, EFA6C and EFA6D), with EFA6A being more commonly known as “pleckstrin and Sec7 domain containing” (PSD) in humans. Only one EFA6 protein is known to exist in *C. elegans* and *D. melanogaster*, though this singular protein does have several isoforms in *D. melanogaster* (reviewed in (Casanova 2007). In all species, *EFA*6 expression is predominantly in brain and central nervous system (CNS) tissue, where it localises to the internal surface of plasma membranes and negatively regulates axonal growth (Casanova 2007, O'Rourke, Christensen et al. 2010, Chen, Wang et al. 2011, Qu, Hahn et al. 2019).

1.5.1. EFA6 function

EFA6 negatively regulates axonal growth. Overexpression of an EFA6 null mutant in Wister rat embryos leads to an increase in the number of growing dendrites during embryonic development, without affecting cell viability (**Figure 1.7**) (Sakagami, Matsuya et al. 2004). In *C. elegans*, depletion of EFA6 prior to the first embryonic mitosis increases the abundance and length of spindle microtubules, with some being up to 6-fold longer than microtubules in control embryos (O'Rourke, Christensen et al. 2010). Severing of posterior lateral mechanosensory (PLM) neurons (axotomy), again in *C. elegans*, results in axonal regeneration beginning with the formation of a growth cone 2-4 hours post axotomy, and growth continuing over the following 24-48-hour period (Wu, Ghosh-Roy et al. 2007, Chen, Wang et al. 2011). In EFA6 deletion mutants, axotomy results in an increase in axonal regrowth compared to wild type, especially in the first 14 hours post axotomy (Chen, Wang et al. 2011). Transgene expression of EFA6 in null mutants rescues the phenotype, and restores PLM regrowth to wild type lengths, while overexpression of EFA6 has the expected effect of reduced axonal regeneration after axotomy (Chen, Wang et al. 2011).

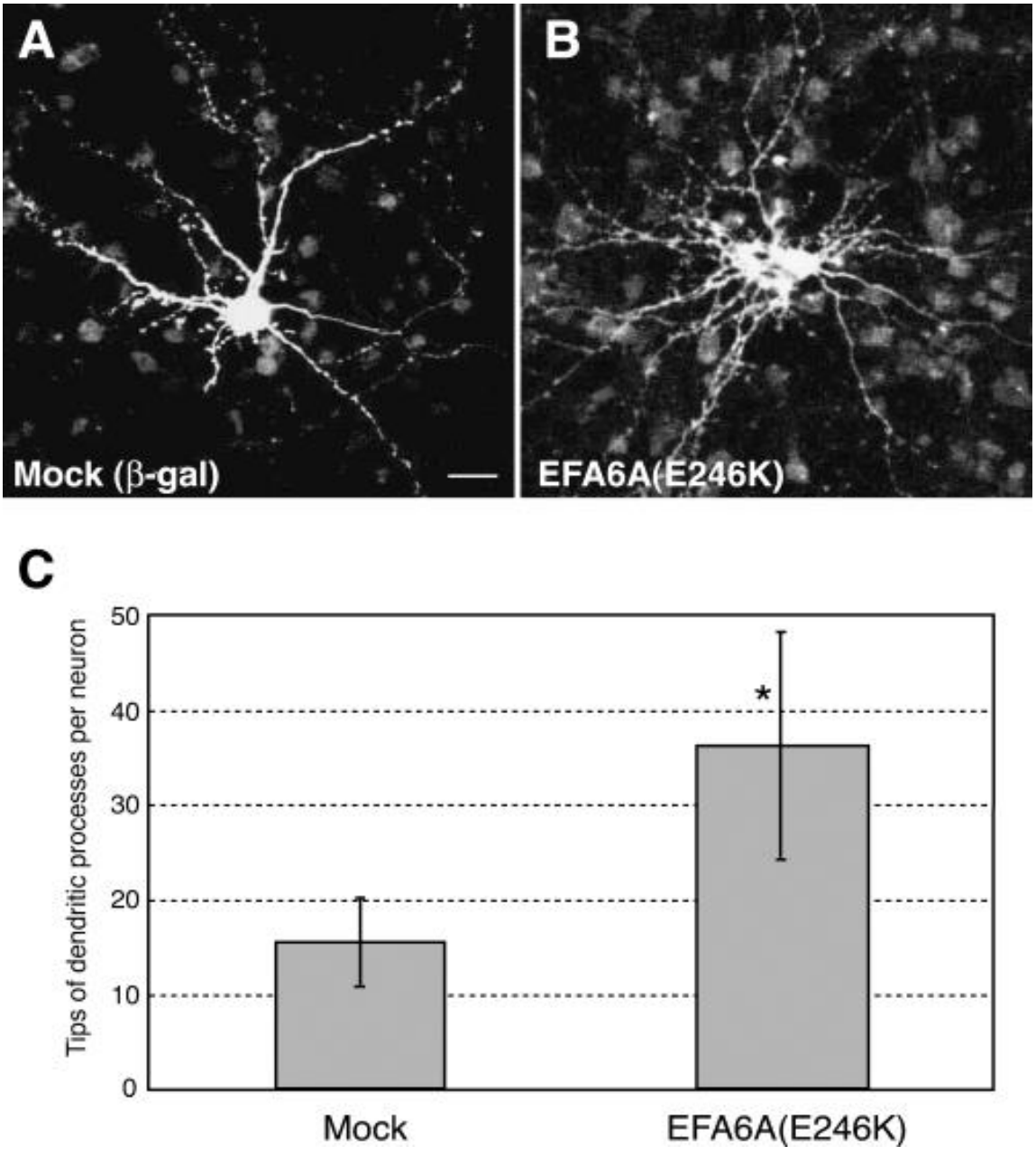

Figure 1.7) An EFA6A null mutant increases dendritic outgrowth.

Primary hippocampal neurons transfected with A) an empty vector and B) GFP-tagged EFA6A null mutant. C) Quantification of the number of dendritic tips in transfected neurons. Scale bar = 10µm. Adapted from (Sakagami, Matsuya et al. 2004).

Using *D. melanogaster* as another model system for studying neuronal development, Qu et al. in 2019 carried out further investigations into the function of EFA6. Using an EFA6:GFP fusion construct, they first demonstrated that, like in *C. elegans*, EFA6 localises throughout the *D. melanogaster* CNS, showing again that this is a neuronal protein (Qu, Hahn et al. 2019). Knockdown of endogenous EFA6 using RNAi results in an approx. 20% increase in axonal length, while overexpression of EFA6 results in up to 50% decrease in axonal length, again, like in *C. elegans*, showing that this protein is a negative regulator of axonal growth (**Figure 1.8**) (O'Rourke, Christensen et al. 2010, Qu, Hahn et al. 2019). To examine whether EFA6 was causing this shortening of axons by regulating microtubule length, mouse fibroblasts were used as a cell system for further investigations into microtubule dynamics. Transfection of fibroblasts with EFA6:GFP results in approximately 70% of cells having perturbed microtubule physiology, compared to ~10% in GFP only cells (Qu, Hahn et al. 2019). Furthermore, the use of EB1:GFP to label the growing end of microtubules shows that during axonal outgrowth from growth cones, microtubules in wild type fibroblasts stop growing when reaching the membrane, while those in EFA6 knockdown fibroblasts extend to the plasma membrane and in some cases, begin to curve under the membrane as they continue to extend (Qu, Hahn et al. 2019). Transfection of *H. sapiens* PSD fused to GFP into fibroblasts has little effect on the microtubule network and is less well characterised than its fly and worm counterparts (Qu, Hahn et al. 2019).

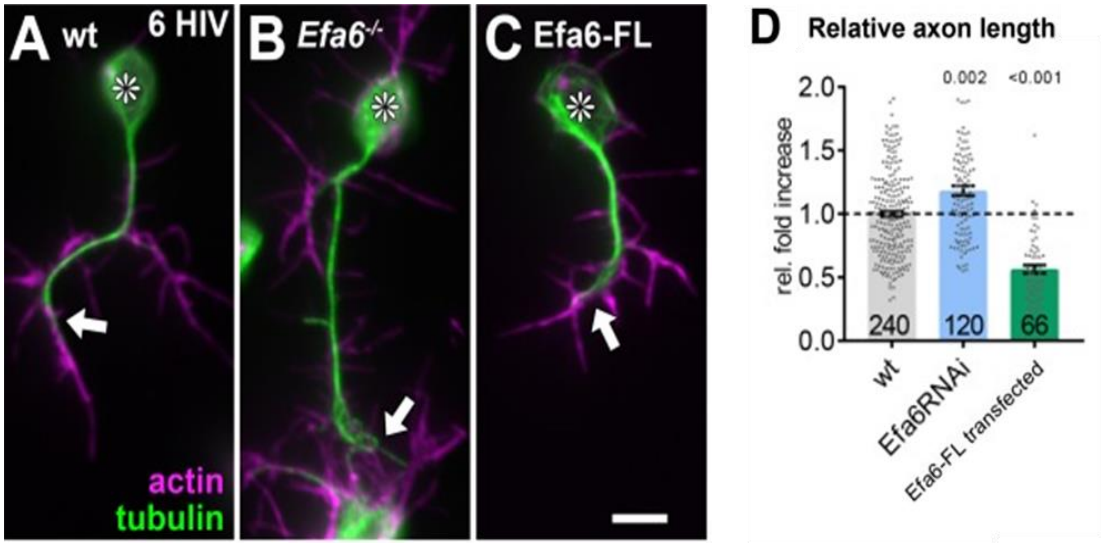

Figure 1.8) EFA6 is a negative regulator of axonal growth in neurons.

A-C) *D. melanogaster* neurons stained for actin (magenta) and tubulin (green). A = wild type control neurons, B= EFA6 null neurons and C= neurons transfected with EFA6-Fl. White arrows indicate axon tips, scale bar - 10µm. D) Relative axonal length in each condition quantified and plotted. Dotted line represents average length of control neurons, with the knockdown and overexpression conditions expressed as a fold change relative to wild type. Adapted from (Qu, Hahn et al. 2019).

1.5.2. EFA6 localisation

EFA6 localises to the internal surface of neuronal plasma membranes (Sakagami, Matsuya et al. 2004, Casanova 2007). Membrane association is dependent on the C-terminus; a GFP:EFA6 truncation construct that lacks the C-terminus (GFP:EFA6-N150) is not membrane associated but, upon axonal trauma, does re-localise to the site of injury within seconds (Chen, Chuang et al. 2015). On the other hand, a GFP:EFA6 construct lacking the N-terminus (GFP:EFA6-FLΔN150) is membrane associated, but does not re-localise upon axonal injury (Chen, Chuang et al. 2015). Transfection of fibroblasts with low levels of EFA6 results in membrane localisation of the protein, however at higher levels of expression, EFA6 is cytoplasmic as well as membrane associated, suggesting that membrane localisation might become saturated with increasing levels of EFA6 (Qu, Hahn et al. 2019).

1.5.3. EFA6 structure

The EFA6 protein family does not have high sequence homology, however, the overall domain organisation is well conserved. Within the C-terminus, a plecstrin homology domain (PH domain) is present, thought to be responsible for the protein's subcellular localisation to the plasma membrane (Macia, Partisani et al. 2008). The N-terminus is much more variable and is very poorly conserved. *D. melanogaster* EFA6 contains a PDZ domain within the first 88 residues of the protein, involved in protein-protein interactions, but this motif is not present in either *C. elegans* EFA6 nor in *H. sapiens* PSD (Chen, Chuang et al. 2015). However, several studies have identified a short motif, ~18 residues in length, within the N-terminus of *D. melanogaster* EFA6, *C. elegans* EFA6 and *H. sapiens* PSD1 that is well conserved (O'Rourke, Christensen et al. 2010, Chen, Chuang et al. 2015, Qu, Hahn et al. 2019). Identification and subsequent analysis of this domain has led to the elucidation of its function, namely the inhibition of microtubule polymerisation, which has led to its naming as the microtubule elimination domain, or MTED (**Figure 1.9**).

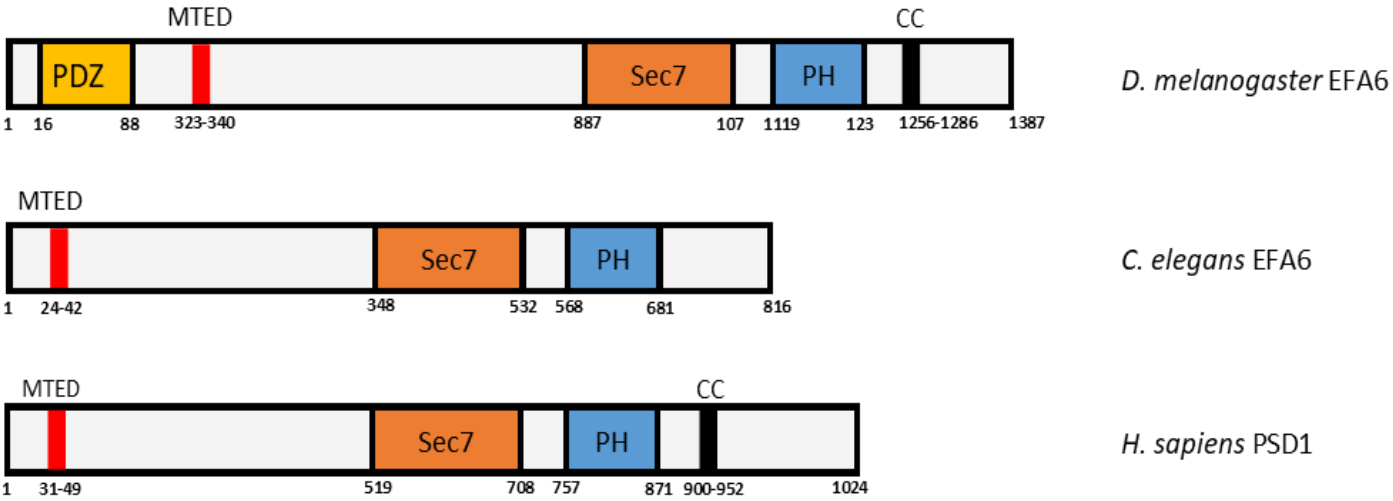

Figure 1.9) An 18 amino acid motif that inhibits microtubule polymerisation is common to *D. melanogaster* and *C. elegans* EFA6 and *H. sapiens* PSD1.

Ribbon diagrams showing the structure of the *D. melanogaster* and *C. elegans* EFA6 and *H. sapiens* PSD1 proteins. The MTED motif is the only N-terminal structure common to all three proteins, highlighted in red. All three proteins contain Sec7 and PH domains, while *D. melanogaster* EFA6 and *H. sapiens* PSD1 contain a coiled coil region (CC) in the C-terminus.

1.6. MTED

In 2010, O'Rourke, Christensen and Bowerman identified an 18-residue motif as the sole conserved domain in the N-terminus of the EFA6 protein across arthropods, nematodes and lophotrochozoa, but make no further mention of it in subsequent investigations (O'Rourke, Christensen et al. 2010). In 2015, Chen et al. identified this motif as being responsible for 1) EFA6 localisation to the site of axonal trauma, and 2) the inhibition of microtubule growth within the axon in *C. elegans* (Chen, Chuang et al. 2015). In 2019, Qu et al. carried out a comprehensive study of *D. melanogaster* EFA6, and again identified this N-terminal 18-residue motif as necessary for the inhibition of microtubule polymerisation in the growing axon and showed that when transfected into fibroblasts, an MTED-GFP DNA construct inhibited microtubule polymerisation throughout the cell (Qu, Hahn et al. 2019). Finally, a recent 2024 study showed that an MTED-mScarlet DNA construct inhibited microtubule polymerisation into dendritic spines when transfected into primary hippocampal neurons (Holland, et al., 2024).

While this peptide has been shown several times over to inhibit microtubule polymerisation in a cellular context, little is known about how (or if) the different cellular functions that rely on microtubule dynamics are altered as a result. Additionally, little is known about the structure, mode of function and binding properties of this peptide for tubulin, a gap this thesis, using the *D. melanogaster* MTED peptide (sequence: APRFEAYMMTGDLILNLSRT) aims to fill.

1.7. Kinesin superfamily

The kinesins are a superfamily of microtubule motor proteins. The highly conserved motor domain is the site of nucleotide hydrolysis and is responsible for the microtubule translocating and depolymerising of functions carried out by the kinesins (reviewed in (Hirokawa, Noda et al. 2009)). Kinesins with + end directional motility have N-terminally located motor domains, while – end kinesins have motor domains located in the C-terminal domain (Hirokawa, Noda et al. 2009). The kinesin-13s are characterised by their centrally located motor domains and have no directional bias but reside on microtubule tips and depolymerise them (Helenius, Brouhard et al. 2006).

1.8. MCAK

Discovered in 1995, MCAK is, to date, the best characterised member of the Kinesin-13 family (Wordeman and Mitchison 1995). MCAK is very similar in structure to conventional kinesins, with the exception of the location of the motor domain, which is centrally located in MCAK as opposed to terminally located in translocating kinesins.

1.8.1. MCAK structure

MCAK is made up of an N-terminal domain, a neck linker, a centrally located motor domain and a C-terminal domain (**Figure 1.10**). The N-terminal domain mediates MCAK localisation (Maney, Hunter et al. 1998, Talapatra, Harker et al. 2015). Mutations in various serine residues in MCAK's N-terminal domain reduce its affinity for microtubules, possibly due to slight alterations in conformation. Cross-linking of MCAK and microtubules has identified a series of residues in the N-terminus which directly bind to α-tubulin and acidic patches on β-tubulin (Moore, Rankin et al. 2005, McHugh, Zou et al. 2019).

MCAK's C-terminal domain is responsible for motor dimerization. In the tail, a coiled coil structure interacts with itself and weakly associates two MCAK monomers together. However, the ability of the C-terminus to bind to two motor domains and stabilise their head-to-head orientation is thought to create the strongest dimerization interface (Hertzer, Ems-McClung et al. 2006, Ems-McClung, Hertzer et al. 2007, Talapatra, Harker et al. 2015). Without the C-terminus, over 90% of MCAK motor domains are monomeric in solution (Talapatra, Harker et al. 2015). Dimerization is necessary for maximal depolymerase activity as although monomers are still functional, they have a greatly reduced microtubule binding and catalytic activity (Maney, Wagenbach et al. 2001, Moores, Yu et al. 2002).

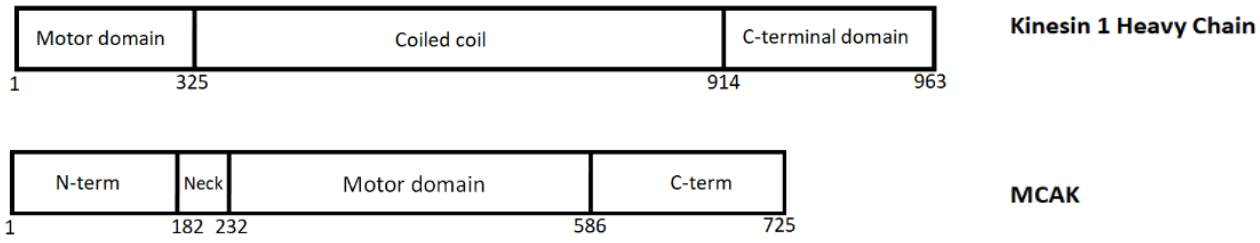

Figure 1.10) Comparison of the domain organisation of Kinesin 1 and MCAK

Translocating kinesins such as Kinesin 1, also known as conventional kinesin, have terminally located motor domains, as opposed to MCAK, which has a centrally located motor domain.

1.8.2. MCAK ATPase cycle

MCAK predominantly binds ATP in solution. Upon interaction with the microtubule lattice, ATP is hydrolysed to ADP, resulting in a non-specific diffusive interaction of MCAK with the microtubule lattice (Friel and Howard 2011). When MCAK encounters the microtubule ends, ADP is released from its binding site on the motor domain and quickly replaced with ATP, allowing MCAK to tightly bind to the terminal GDP-bound tubulin subunit, stabilise its curved conformation and remove it from the microtubule (Friel and Howard 2011).

1.8.3. MCAK localisation

1.8.3.1. To centromeres and kinetochores

MCAK localisation at kinetochores is dependent on shugoshin 2 (Sgo2) and Aurora B kinase (Andrews, Ovechkina et al. 2004, Lan, Zhang et al. 2004, Huang, Feng et al. 2007, Tanno, Kitajima et al. 2010). Sgo2 is a centromeric protein that prevents cohesin breakdown until metaphase, ensuring accurate chromosome segregation (Huang, Feng et al. 2007, Tanno, Kitajima et al. 2010). Human Sgo2 (hSgo2) associates directly with MCAK only when phosphorylated by Aurora B (Tanno, Kitajima et al. 2010). In cells lacking hSgo2, MCAK is undetectable at kinetochores but its presence at centromeres is unaffected (Tanno, Kitajima et al. 2010). MCAK levels are consistent between the control cells and those depleted with hSgo2 such that hSgo2 is not a regulator of MCAK expression, but rather is necessary only for its localisation at kinetochores (Tanno, Kitajima et al. 2010).

1.8.3.2. To microtubule ends

Conventional kinesins translocate along microtubules using ATP hydrolysis. This is not the case for Kinesin-13's, with no translocating activity being observed amongst them (Hunter, Caplow et al. 2003, Helenius, Brouhard et al. 2006). Instead, these kinesins diffuse along the microtubules to the ends, where they are catalytically active. Wordeman suggested that diffusion along the lattice may be biased in an ATP-dependent manner, but directional bias was disproved by Helenius et al. in 2006 when they tracked MCAK movements along the microtubule and "at no time" noted any bias in the direction of MCAK movement (Wordeman 2005, Helenius, Brouhard et al. 2006). Diffusion to MT ends occurs rapidly, and other factors, such as the end-binding proteins (EB) are involved in MT end localisation of MCAK. Helenius et al. observed that MCAK molecules scan approx. 0.79µm of the microtubule and concluded that if an MCAK dimer associates to the microtubule within .25µm of the end, it will diffuse to the end within 100-ms of their determined "frame acquisition time"(Helenius, Brouhard et al. 2006). Additionally, the high association rate of MCAK to microtubules (2.2 MCAK dimers per second) can in part account for the rapid diffusion rate (Helenius, Brouhard et al. 2006).

1.8.4. MCAK function

1.8.4.1. At kinetochores

At kinetochores, MCAK prevents aberrant spindle attachment and ensures correct chromosomal segregation. Previous studies have shown that MCAK corrects merotelic attachments in the lead up to mitosis, but the sheer abundance of these attachments suggest that it does not work alone (Cimini, Moree et al. 2003, Kline-Smith, Khodjakov et al. 2004). Additionally, increased levels of MCAK result in a decrease in tension between sister centromeres, while a reduction in MCAK leads to an increase in tension (Wordeman, Wagenbach et al. 2007). Both states alter chromosome segregation fidelity, although more dramatically for MCAK depletion – increased tension between the centrosomes leads to uncoordinated and inaccurate separation (Wordeman, Wagenbach et al. 2007). A lack of MCAK activity at kinetochores results in chromosomal attachment defects, segregation defects and increased distance between sister centromeres, all of which prevent accurate mitotic completion and can result in lagging chromosomes post segregation (Huang, Feng et al. 2007, Ohi, Burbank et al. 2007, Illingworth, Pirmadjid et al. 2010, Domintz, Wagenbach et al. 2012).

1.8.4.2. Microtubule end recognition and depolymerisation

MCAK's depolymerization ability comes from, in part, a small number of structural differences in its motor domain, compared to conventional kinesin, particularly loop 11 and the α4-helix, both of which are longer than their counterparts in conventional kinesin (Shipley, Hekmat-Nejad et al. 2004). Point mutations in the α4-helix decrease MCAK's depolymerisation abilities by over 80% and decrease MCAK's ATPase activity in the presence of microtubules (Patel, Belsham et al. 2016). These mutations inhibit MCAK's ability to differentiate between the microtubule lattice and microtubule ends, resulting in a decrease in MCAK's end residence time and a loss of microtubule end-stimulated ADP dissociation (Friel and Howard 2011, Patel, Belsham et al. 2016). The increased length of MCAK's Loop 11 is also of importance; deletion of individual residues in Loop 11 results in an inhibition of microtubule depolymerisation regardless of the amino acid deleted, suggesting that the longer length of Loop 11 is more

important for microtubule depolymerisation than the exact amino acid sequence of the structure (Wang, Cantos-Fernandes et al. 2017).

1.8.5. MCAK in cancer

Dysregulated or mutant MCAK leads to defects in spindle fibre formation and chromosome segregation during mitosis, which can subsequently lead to aneuploidies and chromosome instability, a hallmark of cancer. Overexpression of MCAK has been associated with several cancers, including breast, gastric and glioblastomas (Perour, Jeffrey et al. 1999, Nakamura, Tanaka et al. 2007, Shimo, Tanikawa et al. 2008, Bie, Zhao et al. 2012).

In these cancers, MCAK is overexpressed in proliferating cells compared to healthy tissue from the same patients (Nakamura, Tanaka et al. 2007, Bie, Zhao et al. 2012). When overexpressed MCAK is knocked down in breast cancer cell lines T47D and HBC5, cells become multinucleated and are unable to undergo accurate cytokinesis, leading to cell death. The rate of cell growth is subsequently significantly reduced compared to control cells, where no reduction of growth occurs (Shimo, Tanikawa et al. 2008). Similarly, when MCAK is transfected into the gastric cancer cell line AZ521, the rate of proliferation increases compared to control cells (Nakamura, Tanaka et al. 2007). Additionally, metastasis and invasion of cancerous gastric cells into lymph nodes is significantly higher for cells overexpressing MCAK compared to cells with normal expression levels (Nakamura, Tanaka et al. 2007). Perhaps the most interesting association between MCAK/KIF2C expression levels and oncogenesis is seen in glioblastomas. As glioblastomas progress from grade I through to grade IV, MCAK expression increases significantly (Bie, Zhao et al. 2012). Also, the change in expression levels of MCAK are statistically significant enough to use as prognostic markers for survival time, and increased MCAK expression has been associated with poorer survival outcomes as the glioma grade increases (Bie, Zhao et al. 2012). What lends further strength to the association between MCAK overexpression and increased cell proliferation is the fact that MCAK is negatively regulated by p53 (Shimo, Tanikawa et al. 2008, Do Youn Jun, Park et al. 2017). In $p53^{(-/-)}$ colorectal adenocarcinoma cells, MCAK expression is twice as high as $p53^{(+/+)}$ cells, and ectopic introduction of p53 into the $p53^{(-/-)}$ glioblastoma cell line U373MG leads to a reduction in MCAK expression (Shimo, Tanikawa et al. 2008, Do Youn Jun, Park et al. 2017). Genetic analysis has also shown that the proximal promoter for MCAK contains three p53 response elements (p53-REs), two of which are thought to be necessary for p53-mediated repression of MCAK.

1.9. Aims

The work described in this thesis investigates two microtubule destabilisers with differing modes of action: MTED, a peptide that binds to heterodimeric tubulin and inhibits its polymerisation, and MCAK, a motor protein that uses ATP hydrolysis to catalytically depolymerise microtubules. I hypothesise that studying two microtubule regulatory proteins that fall into the same category of destabiliser, but with differing modes of function, will increase our understanding of these types of proteins and better inform our future attempts at manipulating these classes of proteins for use in therapy.

The aims of this thesis are as follows:

Chapter 3:

1. Investigate MTED's microtubule inhibition abilities.
2. Determine the necessity of individual residues within the peptide using a series of microtubule growth assays.
3. Characterise the binding reaction by measuring the peptide's affinity for the tubulin subunit.

Chapter 4:

1. Determine the impact of this peptide on cytoskeletal microtubules using a reporter gene fusion construct.
2. Investigate how other functions of microtubules, namely cell proliferation, are altered as a result of peptide expression.
3. Determine whether the peptide can enter cells unaided, and what impact it has on cytoskeletal microtubules.

Chapter 5:

1. Express and purify a mutant MCAK protein from insect cells.
2. Measure the depolymerisation abilities of this mutant protein to further understand the regulation and depolymerisation of wt MCAK.

Chapter 2) Materials and methods

2.1. DNA manipulations

Table 2) A list of plasmids used in this study

Plasmid name	Shorthand name	Description	Resistance marker	Source
pFasBac-MCAK-h6	MCAK-h6	MCAK with a C-terminal 6xHistidine tag	Ampicillin	In-house
pFasBac-MCAK-Anc13-h6	MCAK-Anc13-h6	MCAK-Anc13 with a C-terminal 6xHistidine tag	Ampicillin	In-house
pCMV-MTED-GFP	MTED-GFP	The MTED DNA sequence, followed by a 42 base linker, followed by the GFP DNA sequence	Ampicillin	Dr Ines Hahn from the laboratory of Dr Andreas Prokop of the University of Manchester
pCMV-Scrambled-GFP	Scrambled-GFP	The Scrambled DNA sequence, followed by a 42 base linker, followed by the GFP DNA sequence	Ampicillin	Self, created in-house

2.1.1. DNA purification

All plasmid DNA was purified from overnight bacterial cultures using the QIAPREP SPIN miniprep or midiprep kits (Qiagen; #12123). Plasmid DNA was eluted from the column in 50µl or 500µl sterile water depending on downstream applications. DNA was quantified using a Nanodrop 2000 spectrophotometer (Thermo Fisher Scientific) and stored at -20°C until further use.

2.1.2. Restriction digestion

Plasmid and gBlock DNA (IDT) was digested to obtain the necessary DNA fragments needed for DNA manipulation. All restriction enzymes and buffers were supplied by New England Biolabs (NEB). Typical restriction digestion reactions contained 10 units of each necessary enzyme, ~500ng-3µg of plasmid DNA to be digested (depending on downstream applications of DNA), 10x reaction buffer to a final concentration of 1x, made up to a final 20µl volume with sterile water. Restriction digests were incubated at the required temperatures for 2-16 hours depending on downstream applications of DNA.

2.1.3. Agarose gel electrophoresis

50x Tris acetate EDTA (TAE: 242.g Tris; 57.2ml glacial acetic acid; 100ml 500mM EDTA; pH8, made up to 1L with deionised water) was diluted 1/50 with deionised water to make 1x TAE buffer. All agarose gels contained 0.8% w/v agarose (Sigma-Aldrich; #05066) dissolved in 1x TAE by boiling and a gel stain (SYBR™ Safe, Invitrogen; #S33102), added once the gel solution had cooled. DNA samples were stained with 6x Purple Loading Dye (NEB; #B7024S) to a final concentration of 1x. A 1Kb DNA ladder (NEB; #N0468S) was loaded for size reference. Gels were run at 80 volts for ~60 minutes. Gels were imaged using a ChemiDoc™ MP Imaging System (Bio-Rad) and the necessary DNA fragments were gel extracted following the procedure provided by GenElute™ Gel Extraction Kit (Sigma-Aldrich; #NA1111). Extracted DNA was eluted in 30µl sterile water and stored at -20°C until further use.

2.1.4. DNA ligations

The desired DNA segments were ligated together using T4 DNA ligase (NEB; #M0202S) in 1x T4 DNA ligase buffer (NEB, supplied with T4 DNA ligase). Each ligation reaction contained ~120ng vector DNA, ~280ng insert DNA and 200U T4 DNA ligase, made up to 20µl with deionised water. All ligations were incubated overnight at 15°C before being transformed into competent bacteria (section 2.2.2) and mini/midi-prepped accordingly.

2.2. Bacterial cell culture

Table 3) A list of bacterial strains used in this study

Strain	Purpose	Source
DH10BAC	Transformation with pFasBac DNA constructs for use in insect cells	Prepared from in-house stocks
DH5α	Transformation with mammalian DNA constructs for use in HeLa cells	Prepared from in-house stocks

2.2.1. Liquid cell culturing

For all liquid cultures, 5-50ml Luria-Bertani broth (LB) (made in-house; 10g tryptone; 5g yeast extract; 10g NaCl, made up to 1L in deionized water and autoclaved at 120°C for 25 minutes) (depending on whether the culture was for a mini- or midi-prep) was supplemented with 100µg/ml Ampicillin (Sigma-Aldrich; #A9393) or 50µg/ml Kanamycin (Sigma-Aldrich; #BP861), depending on plasmid requirements. All cultures were incubated overnight at 37°C, 220rpm in a shaking incubator. LB-agar plates were used for growth on solid medium and, depending on requirement, contained antibiotics at the same concentrations used for liquid growth.

2.2.2. Transformation of DH5-α cells

DNA was transformed into DH5-α competent *Escherichia coli* following a standard heat-shock transformation procedure. Briefly, ~50µl competent bacteria were mixed with ~200ng DNA and incubated on ice for 30 minutes. Reactions were heat-shocked at 42°C for 30 seconds and incubated on ice for a further two minutes. 1ml Super Optimal broth with Catabolite repression (SOC: 20g Tryptone, 5g yeast extract, 0.5g NaCl, made up to 1L in deionized water, made in-house) was added to each reaction and incubated at 37°C, 220rpm for one hour. Cultures were spun at 8000g for 2 minutes to pellet the bacteria. The supernatant was discarded, and pellets were resuspended in 50µl LB broth. Transformed cells were spread onto LB agar plates containing 100µg/ml Ampicillin or 50µg/ml Kanamycin as necessary and incubated at 37°C overnight. Liquid cultures (containing appropriate antibiotics) were inoculated with colonies for overnight growth and plasmid miniprepping/midiprepping the next day.

2.2.3. Transformation of DH10BAC cells

pFasBac vectors containing the gene(s) of interest were transformed into DH10Bac cells. ~200ng of pFasBac DNA was mixed with 50µl DH10Bac cells and incubated on ice for 30 minutes, then heat-shocked at 42°C for 45 seconds. Cells were incubated on ice for a further two minutes before 1ml SOC was added to each transformation reaction. Transformants were incubated at 37°C for at least four hours at 175rpm. Cultures were then spun at 5000g for one minute, the supernatant discarded, and the pellet resuspended in 100µl LB broth and spread

onto selection plates containing LB agar, 30µg/ml kanamycin, 10µg/ml gentamycin, 10µg/ml tetracycline, 100µg/ml X-gal and 40µg/ml Isopropyl β- d-1-thiogalactopyranoside (IPTG). Plates were incubated at 37°C for at least 48 hours. Discernible white colonies were re-streaked onto fresh DH10Bac plates with appropriate antibiotics to ensure they were true white colonies.

2.2.4. Creation of glycerol stocks

~1ml liquid bacterial culture containing the plasmid of interest was diluted with glycerol to create a final concentration of 15% glycerol and stored at -80°C.

2.3. Mammalian cell culture

2.3.1. HeLa cell culturing

In-house stocks of HeLa cells were thawed from liquid nitrogen (LN2) and left to recover for ~72 hours in a T25 flask in Dulbecco's Modified Eagle Medium (DMEM, Gibco; #6429), supplemented with 10% Foetal Bovine Serum (FBS, Gibco; #F7524), 2% Penicillin / Streptomycin (P/S, Gibco; #15140122) and 50µg/ml gentamycin (Sigma-Aldrich), referred to as DMEM onwards unless stated otherwise. For passaging, cells were washed with phosphate buffered saline (PBS, Gibco; #10010023), incubated with ~1ml Trypsin in Ethylene Diamine Tetraacetic Acid (EDTA) (Gibco, #10779413; 10x solution, diluted 1/10 in PBS) for ~5 minutes, then diluted ¼ in DMEM and seeded into fresh T25 flasks. Cells were then split ¼ every four days for regular culturing, and incubated at 37°C, 5% CO_2.

2.3.2. Freezing cells

HeLa cells were grown to ~70% confluency in T25 flasks. The day of freezing, cells were trypsinised, collected in a 15ml centrifuge tube and centrifuged at 500g for 5 minutes at room temperature. The supernatant was discarded, and cells were resuspended in DMEM + 10% dimethyl sulfoxide (DMSO; Sigma-Aldrich; #D2650) and aliquoted into 1.5ml cryovials. Vials were put into an appropriate cell freezing device, such as a Mr Frosty with ~100ml 100% isopropanol and stored at -80°C overnight to allow for freezing at 1 degree per minute. Cryovials were transferred to LN_2 the next day for long term storage.

2.3.3. Transfection

24 hours prior to transfection, HeLa cells, in DMEM supplemented with 10% FBS but without any antibiotics, were seeded at a known concentration onto ethanol-sterilised coverslips in individual wells in a 6 well dish and left to adhere overnight at 37°C, 5% CO_2. The following day, cells were transfected according to the Lipofectamine™ 3000 Reagent Protocol by Thermo Fisher Scientific. A brief outline of this protocol for a 6 well plate is seen in **Table 4**. Lipofectamine™ 3000 and P3000™ transfection reagent were supplied by Thermo Fisher Scientific (#L3000008), Opti-MEM media was supplied by Gibco (#31985062).

Table 4) Lipofectamine™ 3000 transfection protocol. Adapted from Thermo Fisher Scientific

Timeline	Step	Reagent	Volume
Day 0	Seed cells at a known concentration	HeLa cells	0.5 x10^6/ml; 1ml per well
Day 1	Dilute Lipofectamine™ 3000 in Opti-MEM (2x tubes)	Lipofectamine™ 3000	5µl
		Opti-MEM	125µl
Day 1 (continued)	Prepare master mix of DNA, P3000™ and Opti-MEM	DNA	5µg
		P3000™	10µl
		Opti-MEM	250µl
Day 1 (continued)	Add DNA/P3000™/Opti-MEM master mix to Lipofectamine™ 3000	DNA mastermix	130µl
		Lipofectamine™ 3000	130µl
Incubate for 10-15 minutes at room temperature			
Day 1 (continued)	Add DNA-lipid complex to cells in a dropwise fashion and incubate at 37°C, 5% CO_2	DNA-lipid complex	260µl
Incubate for 6 hours at 37°C, 5% CO2			
Day 1 (continued)	Change media	DMEM supplemented with 10% FBS, 2% P/S and 10µg/ml gentamycin	2ml per well
Day 2-4	**Visualisation / further analysis**		

2.3.4. Peptide stocks

Lyophilised peptide was sourced from Genosphere Biotechnologies. All peptides were dissolved in 100% DMSO at a concentration of 1-3mM, depending on downstream applications, and stored at 4°C. Peptides with an N-terminal fluorophore were created by the direct addition of fluorescein (332Da) to the amine side chain, while C-terminal fluorescent peptides were created by adding a lysine to the C-terminus of the peptide, and the fluorescein tag added to the amine side chain of the lysine. For simplicity, the (K) denoting the lysine prior to the C-terminal fluorophore is not shown in the name of the peptide, as it is not part of the original peptide sequence. A description of all peptides used in this study is seen in **Table 5**.

Table 5) A list of all peptides and their sequences used in this study

Peptide name	Sequence
MTED	APRFEAYMMTGDLILNLSRT
Scrambled	MITAPREFDYLNLRAGLSMT
R3A	APAFEAYMMTGDLILNLSRT
E5A	APRFAAYMMTGDLILNLSRT
Y7A	APRFEAAMMTGDLILNLSRT
T10A	APRFEAYMMAGDLILNLSRT
D12A	APRFEAYMMTGALILNLSRT
I14A	APRFEAYMMTGDLALNLSRT
S18A	APRFEAYMMTGDLILNLART
R19A	APRFEAYMMTGDLILNLSAT
K-MTED-R	KRKKKGKGLGKKKRDPCLRKYK APRFEAYMMTGDLILNLSRTRRRRRQRRR
K-Scrambled-R	KRKKKGKGLGKKKRDPCLRKYK MITAPREFDYLNLRAGLSMTRRRRRQRRR
K-MTED-R-Fl	KRKKKGKGLGKKKRDPCLRKYK APRFEAYMMTGDLILNLSRTRRRRRQRRR-Fl
K-Scrambled-R-Fl	KRKKKGKGLGKKKRDPCLRKYK MITAPREFDYLNLRAGLSMTRRRRRQRRR-Fl
MTED-Fl	APRFEAYMMTGDLILNLSRT-Fl
Fl-MTED	Fl- APRFEAYMMTGDLILNLSRT
MTED-AA-Fl	APRFEAYMMTGDLILNLSRTAA-Fl

2.3.5. Peptide treatment

24 hours prior to treatment with peptide, HeLa cells were seeded at a known concentration onto ethanol-sterilised coverslips in individual wells in a 6 well dish and left to adhere overnight at 37°C, 5% CO_2. The following day, peptide was diluted to the desired concentration in DMEM and filter-sterilised using a 0.22µm filter. To ensure the peptide was not lost during filtration, a microtubule growth assay was carried out with filtered material, and the presence of microtubule inhibition activity showed that the peptide is not lost during filtration. Cells were washed with PBS then incubated with peptide-containing media for 24 hours at 37°C, 5% CO_2, before further analysis.

2.3.6. Immunohistochemical staining

HeLa cells were seeded onto ethanol-sterilised coverslips in individual wells in a 6 well plate and left to adhere overnight at 37°C, 5% CO_2. The following day, the media was removed, and cells were fixed using 4% paraformaldehyde in PBS (PFA, Sigma-Aldrich; #158127) for 20 minutes at room temperature. The fixative was removed, and cells were washed 3 times for five minutes with PBS + 0.1% Triton-X100 (PBST). Cells were then incubated with the appropriate primary antibody (Sigma-Aldrich; #T9026 Monoclonal anti-α-tubulin antibody, clone DM1A, ascites fluid, produced in mouse), diluted 1:1000 in PBS for 2 hours at room temperature, covered. The primary antibody was then removed, and cells were washed 3 times for five minutes with PBST. Cells were then incubated with the appropriate secondary antibody (Thermo Fisher, A-21123; Alexa Fluor654^{TM} Goat anti-Mouse), diluted 1:200 in PBS for 2 hours at room temperature, protected from light. The secondary antibody was then removed, and cells were washed 3 times for five minutes with PBST. Hoechst stain (Thermo Fisher, Hoechst 33342), diluted to 1:10000 in PBS, was added to cells for 5 minutes at room temperature, protected from light to stain DNA. The dye was then removed, and cells were washed 3 times for five minutes with PBST. A drop of 90% glycerol in DABCO, an aqueous mounting medium, was dropped onto the centre of a glass microscope slide, and the coverslip was inverted and placed onto the drop. The edges of the coverslip were sealed with clear nail varnish and the stain was left to develop at 4°C, in the dark, overnight, before imaging the

following day. Imaging was carried out on a Zeiss880C confocal microscope, and images were analysed using ImageJ.

2.3.7. Proliferation assay

Cells were seeded at a known concentration into individual wells of a 6-well plate 24 hours prior to transfection and left to adhere overnight at 37°C, 5% CO_2. The next day, cells were transfected with the desired constructs or treated with the desired peptides and incubated overnight at 37°C, 5% CO_2. 24 hours later, on day 1 of the proliferation assay, the media was removed from all cells and kept in a 1.5ml Eppendorf tube. All cells were washed with 1ml PBS, which was removed and added to the media sample. Cells were then trypsinised and added to a separate 1.5ml tube. All samples were centrifuged at 500g for 5 minutes. The supernatant was discarded, and all cell pellets were resuspended in 500µl DMEM. 10µl of the trypsin sample was removed for counting, and the rest re-seeded into a fresh 6-well dish. The number of cells in each sample was determined using a CellDrop BF cell counter on the default settings. The assay was repeated every 24 hours for 96 hours.

2.3.8. Trypan blue viability assay

Cells were seeded at a known concentration into individual wells of a 6-well plate 24 hours prior to peptide treatment and left to adhere overnight at 37°C, 5% CO_2. The next day, cells were treated with 3mM of the desired peptide and incubated for a further 24 hours at 37°C, 5% CO_2. A trypan blue assay to measure cell viability was then carried out in exactly the same way as described in section 2.3.7. Prior to counting, 0.4% Trypan blue (Gibco; #11538886) was added to each sample at a 1:1 ratio and incubated at room temperature for ~3 minutes. The % viability of cells was then determined using a CellDrop BF counter on the Trypan blue setting. The assay was repeated every 24 hours for 72 hours. Peptide was only added 24 hours prior to beginning the assay and was never reapplied.

2.4. Insect cell culture

2.4.1. *Spodoptera frugipera* (Sf9) cell culturing

Sf9 cells were thawed from in-house liquid nitrogen (LN_2) stocks into T25 tissue culture treated flasks (Eppendorf) and incubated at 27°C in Insect-Xpress medium (Lonza) supplemented with 10% FBS, 2% P/S and 50µg/ml gentamycin (referred to as Xpress from here onwards unless stated otherwise). Cells were left to adhere and recover for seven days, with the media being changed at day three. On day seven, cells were transferred to suspension culture in a 25ml suspension flask in Xpress. Cells were then maintained at a concentration of 0.5 x 10^6 cells/ml in Xpress.

2.4.2. Sf9 cell transfection to generate P1 baculovirus

pFasBac vectors are high protein expression vectors designed for use in insect cells, while DH10Bac bacteria contain the necessary machinery to replicate these particular vectors. DH10Bac cells were transformed with the pFasBac plasmids of interest as described in 2.2.3. The day of transfection, Sf9 cells were seeded at a known concentration into individual wells of a 6 well dish and left to adhere for one hour at 27°C. While cells were adhering, bacmid DNA was isolated from liquid cultures of DH10Bac cells using the ZR BAC DNA miniprep kit (Zymo research; #D4049). A brief outline of the transfection protocol, as well as the reagents used, is seen in **Table 6**.

Table 6) Transfection protocol for Sf9 cells

Timeline	Step	Material	Volume/concentration
Day -2	Transform DH10Bac cells with pFasBac vectors of interest	pFasBac-MCAKh6	200ng
		pFasBac-MCAK-Anc13h6	200ng
		DH10Bac cells	50µl
Day 0	Seed cells at a known concentration and incubate at 27°C for one hour	Sf9 cells	$1x10^6$/ml; 2ml per well
Day 0 (continued)	Extract Bacmid DNA from DH10Bac cells	ZR BAC DNA miniprep kit	DNA eluted in 250µl H_2O
		Liquid cultures	
Day 0 (continued)	Prepare DNA for transfection	Bacmid DNA	3µg
		Xpress media	500µl
Day 0 (continued)	Prepare transfection reagent	Escort IV transfection reagent	5µl
		Xpress media	500µl
Day 0 (continued)	Add DNA mixture to transfection mixture	DNA/ Xpress mixture	500µl
		Escort IV/Xpress mixture	500µl
Incubate DNA/transfection mixture at room temperature for 45 minutes			
Day 0 (continued)	Wash Sf9 cells	Xpress media	1ml
Day 0 (continued)	Add DNA/Transfection mixture to Sf9 cells	DNA/Transfection mixture	1ml
Incubate at 27°C for 5 hours			
Day 0 (continued)	Change media on cells	Xpress media supplemented with 2% FBS, 2% P/S and 50µg/ml gentamycin	2ml
Incubate at 27°C for five days			
Further visualisation / analysis			

2.4.3. P1 virus generation

Five days after transfection, the transfected cell suspension was harvested and centrifuged for five minutes at 340g at room temperature. The supernatant, containing the baculovirus "P1 virus" was decanted, wrapped in tin foil to protect from light and stored at 4°C.

2.4.4. Baculovirus Infected Insect Cell (BIIC stocks) generation

1ml of P1 virus was used to infect 50ml of Sf9 cells in suspension at a concentration of 0.5 x 10^6 cells/ml. The culture was incubated for 24 hours at 27°C, 185rpm in a shaking incubator. Cell diameter was then measured using MOXI^{TM} Z automated cell counter (Avantor). Cells infected with the P1 virus would grow in size as the virus replicated inside them, before lysing to release the virus into the culture medium. To harvest infected cells prior to lysis, the diameter of cells was measured and compared to uninfected (control) cells. Once the diameter of infected cells was at least 1µm greater than control cells, the culture was spun at 450g for five minutes, and the pellet was resuspended in 2.5ml Xpress (serum free) with 10% DMSO and 2% P/S. 200µl was aliquoted into cryovials and frozen at -80°C overnight before being transferred to LN_2 for long term storage.

2.5. Protein purification

2.5.1. Protein expression

125µl of BIIC stock (2.4.4) was used to infect 400ml Sf9 cells in suspension at a concentration of 1 x 10^6 cells/ml and incubated for ~70 hours at 27°C, 185rpm in a shaking incubator. Cells were then spun at 450g for 10 minutes. The pellet was resuspended in lysis buffer (50 mM HEPES pH 7.5; 150 mM NaCl; 5 % glycerol; 0.1 % Tween 20; 1 mM $MgCl_2$; 1 mM EGTA) at 2ml/g pellet weight. A LN_2 resistant bowl was filled with LN_2 and a sieve placed inside to catch pearls. The cell culture was then slowly dropped into the LN_2 to form pearls, which were collected and stored at -80°C.

2.5.2. 2-step protein purification

All proteins of interest were purified using cation exchange and nickel exchange columns. Pearls were resuspended in lysis buffer (50 mM HEPES pH 7.5; 150 mM NaCl; 5 % glycerol; 0.1 % Tween 20; 1.5 mM $MgCl_2$; 3 mM EGTA [1mM dithiothreitol [DTT]); 0.5mM MgATP and 1x concentration Leupeptin (Sigma-Aldrich; #L8511), Pepstatin A (Sigma-Aldrich; P5318) and phenylmethylsulfonyl fluoride (PMSF; Thermo Fisher; #36978) were added fresh after addition of lysis buffer to pearls]) at 2ml/gram of pearl weight by rocking incubation at 4°C for approx. 30 minutes, until solution was fully resuspended and homogeneous. A 20µl sample for an SDS-PAGE gel was taken at this stage. Lysate was spun at 20,000rpm for one hour to clear it. During this time, the cation exchange column was prepped with 5ml water, 5ml cation exchange buffer (CEB) (20mM HEPES/KOH pH7.5 and 1.5mM $MgCl_2$) with 1M NaCl and 5ml CEB with 150mM NaCl. A 20µl sample of the cleared lysate was taken and the lysate was loaded onto the cation exchange column. A 20µl sample was taken of the flow through. The column was washed with CEB supplemented with 200mM NaCl. A 20µl sample was taken of the exchange wash. The protein was eluted from the column with 20ml CEB supplemented with 500mM NaCl. A 20µl sample was taken of the eluate. The cation exchange column was then washed with CEB supplemented with 1.5M NaCl and again with H_2O. A 20µl sample was taken of the end wash. The column was then stored in 20% ethanol at 4°C.

A nickel-affinity column was washed with 5ml H_2O and 5ml nickel-affinity buffer (Ni buffer) (50mM Tris/HCl pH7.5, 300mM NaCl, 1mM $MgCl_2$ and 10% glycerol). The eluate was loaded onto the column. A 20µl sample was taken of the Ni flow through. The column was then washed with Ni buffer with 80mM imidazole. A 20µl sample was taken of the Ni wash.

The protein was then eluted with Ni buffer with 300mM imidazole into 10 1ml fractions into 1.5ml low-binding tubes (Nerbeplus). A quick Bradford assay (5µl fraction sample + 250µl Bradford reagent (Bio-Rad) was done to identify the protein-containing fractions. These fractions were pooled together, aliquoted at 125µl and snap-frozen in LN_2 before being stored at -80°C. The Ni column was washed with H_2O before being stored in 20% ethanol at 4°C.

2.5.3. SDS-PAGE

A pre-cast 4-12% gradient SDS-PAGE gel (Genscript; #M00652) was run to determine the purity of the protein purification process. Each sample collected during the protein purification process was mixed with 2x protein loading dye (Bio-Rad; #1610373) and 25µM DTT and boiled at 98°C for 10 minutes. ~Half of each sample was then loaded onto the gel at run for 50 minutes at 150V in pre-mixed MOPS running buffer (Genscript; #M00138). The gel was then stained by rolling incubation with InstaBlue (Novus Biologicals) for ~25 minutes and viewed on a light source.

2.5.4. Determination of protein concentration (Bradford assay)

A Bradford assay was done to determine the concentration of the purified protein(s). Powdered bovine serum albumin (BSA, Sigma-Aldrich) was made up to an initial concentration of 2mg/ml in H_2O and serial diluted to a final concentration of 0.015mg/ml in a 50µl volume. 200µl Bradford reagent was added to each sample, and 200µl was added to a separate solution of 50µl H_2O, which acted as the blank measurement. The absorbance of each sample was measured using a spectrophotometer with the absorbance set to 595nm. The absorbance value of each sample was plotted against its concentration on an x,y scatterplot, and a line of best fit was generated, along with an equation of the line in the format y = mx +c; where y represents the absorbance value and x represents protein concentration. The concentration of the protein was measured in exactly the same way, except that the protein was serial diluted in Ni buffer with 300mM imidazole, as this was the buffer it was eluted in. 50µl of Ni

buffer with 300mM imidazole was used as the blank measurement. The absorbance values were measured and a value less than 1 but greater than the blank value was used for the y value in the equation of the line to determine the protein concentration (**Figure 2.1**)

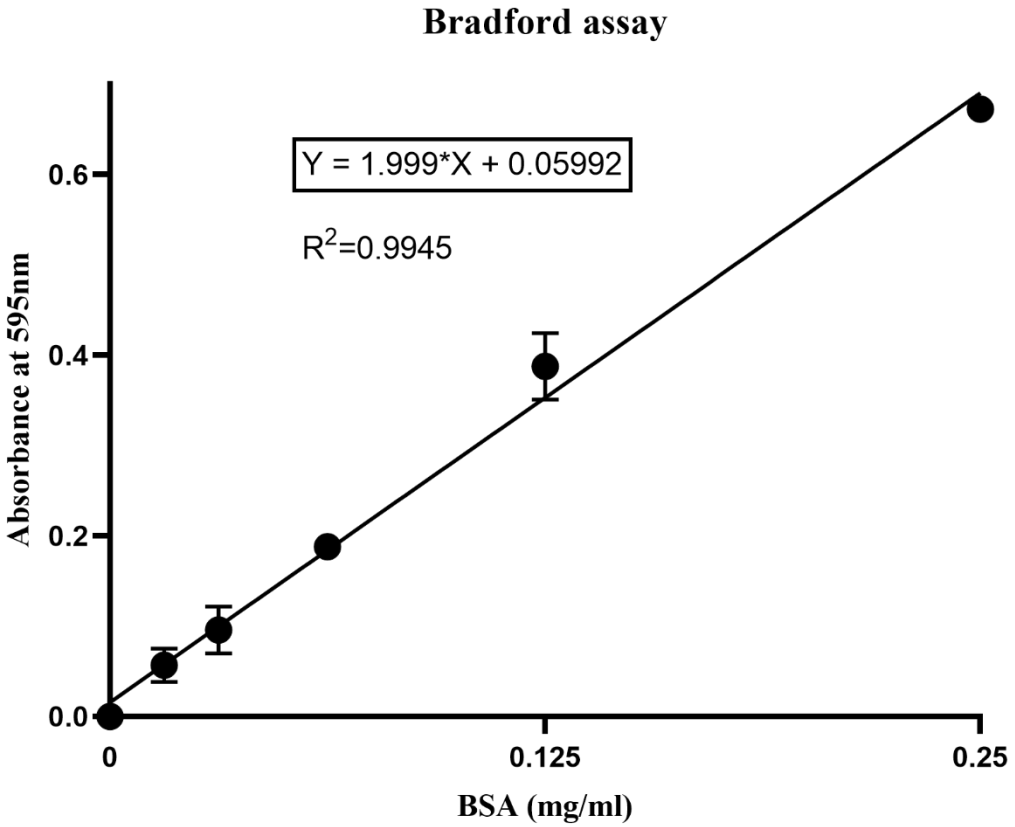

Figure 2.1) XY scatterplot of the absorbance of BSA at 595nm.

Error bars represent one standard deviation, n=3, where n is the number of biological repeats. Outlined box contains the equation of the line used for future protein concentration measurements.

2.5.5. Buffer exchange of proteins

A protein desalting spin column (Thermo Fisher Scientific; #89893) was inverted a few times to resuspend the slurry, then put into a 1.5ml centrifuge tube and spun at 1500g for one minute to remove the excess liquid. 400µl of exchange buffer was added to the column and spun at 1500g for 1 minute to remove excess liquid. The addition of exchange buffer and spinning was repeated 5 times, with the liquid being removed after each spin. The column was then transferred to a new 1.5ml centrifuge tube and 120µl of the protein sample was added to it. The column was spun at 1500g for 2 minutes and the buffer exchanged protein was eluted into the tube. This protein was then aliquoted into low binding tubes, snap frozen and stored at -80°C.

2.6. Tubulin preparations

2.6.1. Cycling tubulin

Work carried out in the Friel lab prior to the commencement of this thesis involved the purification of tubulin from pig brain pellets according to an in-house protocol, which yielded a purified tubulin concentration of ~4mg/ml. This was then aliquoted into 4ml samples and stored at -80°C until further use. ~4ml purified porcine tubulin was recovered from -80°C storage and thawed on ice. A polymerisation mixture was made up while the tubulin was thawing according to **Table 7**, and the tubulin was added to this mixture once thawed. Polymerisation was allowed to occur for 1 hour at 37°C, and the resulting microtubule-containing solution was centrifuged through a 60% glycerol solution in BRB80 (BRB80 made up at 5x: 400mM PIPES, 5mM EGTA, 5mM $MgCl_2$, 5mM DTT, to pH6.8 with KOH, made up to 1L in deionised water. Diluted 1/5 in deionized water to make 1xBRB80) at ≥20,000g, 37°C for 1 hour. The supernatant was discarded, and the resulting pellet washed with room temperature BRB80, before incubation on ice with as little 0.1% (v/v) β-mercaptoethanol in BRB80 needed to cover the pellet for 20 minutes. The pellet was then resuspended and centrifuged at ≥20,000g, 4°C for 15 minutes. The supernatant was collected and aliquoted into 10µl or 50µl low binding tubes, snap frozen with LN_2 and stored at -80°C.

Table 7) Polymerisation mixture for cycling tubulin.

Reagent	**Concentration**
Glycerol	30%
BRB80	1x
GTP	1mM
$MgCl_2$	4mM
Porcine tubulin	~4ml, @ 4mg/ml
dH_2O	Up to 10ml

2.6.2. Determination of cycled tubulin concentration

One aliquot of tubulin was thawed on ice for 5 minutes, then serial diluted to concentrations ranging from 1:20 to 1:160 in BRB80. The absorbance of each sample was measured at 280nm using a spectrophotometer, and the concentration was calculated using the equation $A=\varepsilon cl$, where A = absorbance, ε (extinction coefficient of the dye) = 115000, c= concentration and l = path length.

2.6.3. Alexa 647 labelling of tubulin

Tubulin was labelled using an amine reactive dye, i.e. dyes that conjugate to exposed lysines on the α/β subunit. ~4ml purified porcine tubulin was recovered from -80°C storage and thawed on ice. A polymerisation mixture was made up while the tubulin was thawing according to **Table *7***, and the tubulin was added to this mixture once thawed. After a 5-minute incubation on ice, the polymerisation mixture, with the added tubulin, was incubated at 37°C for one hour. The resulting microtubule-containing solution was gently layered onto a high-pH cushion buffer (100mM NaHEPES, pH 8.6, 4mM $MgCl_2$, 1mM EGTA, 60% glycerol) and centrifuged at 50,000rpm for one hour at 37°C. The supernatant was discarded, and the pellet was washed with pre-warmed labelling buffer (100mM NaHEPES, pH 8.6, 4mM $MgCl_2$, 1mM EGTA, 40% glycerol), before resuspension in 200µl labelling buffer. A 10-fold molar excess of the desired dye (Alexa Fluor™ 647 Hydroxylamine, Thermo Fisher; A30632;) was added to the resuspended tubulin solution (assuming a tubulin recovery of ~70%) and labelling was allowed to occur for 40 minutes at 37°C. The labelled tubulin solution was then layered onto 500µl low pH cushion buffer (60% glycerol in BRB80) and centrifuged at 100,000rpm for 20 minutes at 37°C. The supernatant was discarded, and the resulting pellet washed with pre-warmed BRB80. The pellet was then incubated in the minimal volume of ice-cold BRB80 necessary to submerge it for 30 minutes at 4°C before resuspension and centrifugation at 80,000rpm for 10 minutes at 4°C. The supernatant was collected and BRB80, $MgCl_2$ and GTP were added to final concentrations of 1x, 4mM and 1mM respectively, before incubation on ice for 3 minutes, then 37°C for 2 minutes. Glycerol was then added to a final concentration of 33% before a further 30-minute incubation at 37°C for tubulin polymerisation. The microtubule-containing solution was gently layered onto 500µl low pH cushion and centrifuged at 100,000rpm for 20 minutes at 37°C. The supernatant was discarded, and the pellet was washed with pre-warmed

BRB80, before incubation with 200µl ice-cold BRB80 for 30 minutes. Pellets were then resuspended and centrifuged at 80,000rpm for 10 minutes at 4°C, before the supernatant was collected, aliquoted and stored at -80°C for future use. The concentration of tubulin (in mg/ml) was calculated using the equation (A_{280} – (Abs dyemax * CF)) / 1.15, where dyemax is the Lambda max of the dye and CF is the correction factor of the dye at a 280nm absorbance. For Alexa Fluor 647, these values were 650 and 0.03, respectively. The degree of labelling (DOL) was then calculated using (Abs dyemax * 110,000) / Tub. Conc. in mg/ml * Dye extinction coefficient. For Alexa 647, the extinction coefficient used was 239000.

2.6.4. Buffer exchange of tubulin

Tubulin was buffer exchanged from BRB80 into BRB40 (1xBRB80 diluted ½ with deionised water, supplemented with 0.5mM EGTA, 0.5mM $MgCl_2$, 0.5mM DTT to ensure only the concentration of PIPES was being diluted) using Thermo Fisher Scientific Slide-A-Lyzer Dialysis cassettes (66330). A 0.5 – 3ml capacity dialysis cassette was added to a beaker containing BRB40 for 2 minutes to allow the membrane to hydrate. Using a needle and syringe, the tubulin sample was gently introduced between the membranes, taking care not to puncture the membrane. Excess air was removed, and the cassette was incubated in the target buffer for 2 hours at 4°C. The beaker was then emptied and refilled with fresh BRB40, and the cassette was incubated in this for a further 2 hours at 4°C. The beaker was then emptied and refilled with fresh BRB40 for a final time, and the cassette was incubated in this overnight at 4°C. Tubulin was then gently extracted using a needle and syringe, aliquoted into low-retention tubes and stored at -80°C until further use.

2.7. Growing microtubules

2.7.1. Taxol stabilised microtubules

Fluorescently labelled, Taxol stabilised microtubules were grown by adding 3.2µl H_2O, 2.6µl 100mM $MgCl_2$, 2.6µl 25mM GTP and 1.6µl BRB80 to 50µM 25% rhodamine labelled tubulin. After incubation at 37°C for 30 minutes, BRB80 + 10µM Taxol was added to stabilise the microtubules post-polymerisation.

2.7.2. GMPCPP stabilised microtubules

Fluorescently labelled, GMPCPP stabilised microtubules were grown by incorporating GMPCPP, a non-hydrolysable GTP analogue into the growing microtubule in place of GTP. 10µM 25% rhodamine labelled tubulin was mixed with BRB80, 100mM $MgCl_2$ and 5µl GMPCPP in the above order, put on ice for five minutes then incubated at 37°C for two hours. Microtubules were then diluted with 200µl BRB80 and spun at 10 psi (90,000rpm) through a 40% glycerol + BRB80 solution using a Beckman Airfuge for 10 minutes. The supernatant was discarded, and the pellet was resuspended in 200µl BRB80.

2.8. Treatment of microscope coverslips

2.8.1. Silanisation

22mm x 22mm and 18mm x 18mm square coverslips were submerged in 100% acetone and sonicated for 20 minutes, then 100% methanol and sonicated for 20 minutes, then nanopure water to soak. Coverslips were then submerged in 1M potassium hydroxide (KOH) and sonicated for 1 hour, then washed three times with nanopure water. Coverslips were then again soaked in 100% acetone and sonicated for 20 minutes, then 100% methanol and sonicated for 20 minutes, then nanopure water. Coverslips were then submerged in 5M KOH and sonicated for 1 hour, then washed three times with nanopure water, then blow dried with nitrogen (N_2) gas. Coverslips had to be completely dry before proceeding in order to prevent a precipitate forming during the next step. In a fume hood, coverslips were submerged in trichloroethylene (TCE). 125µl of dimethyldichlorosilane (silane) was carefully measured in a fume hood using a needle and syringe to avoid agitating the bottle and added to the TCE. The needle was gently moved around while adding the silane to distribute it evenly. Coverslips were left to soak in this solution for one hour. They were then washed in 100% methanol three times and sonicated for 5, 15 and 30 minutes respectively before being blow dried with N_2 and stored at room temperature.

2.8.2. Poly-L-Lysine coating

22mm x 22mm and 18mm x 18mm square coverslips were sonicated in 1:20 Mucasol:deionised water (Mucasol, Fisher Scientific) for 20 minutes. Coverslips were then rinsed in nanopure water before being sonicated for 10 minutes in 100% ethanol. Coverslips were then rinsed three times in deionised water before being blow dried with N_2 gas. Once completely dry, coverslips were incubated in a 1:10 ratio of 0.1% poly-L-lysine (Sigma-Aldrich; #P8920) to deionized water for at least two hours at room temperature. Following this, coverslips were rinsed in deionised water three times before a 100% ethanol rinse and blow drying with N_2 gas and storage at room temperature.

2.9. Microtubule microscopy assays

2.9.1. Preparation of coverslip channels

Coverslip channels were created using pre-treated coverslips (section 2.8) to allow the microtubules to adhere. A 22mm x 22mm coverslip was placed into the coverslip holder. Four strips of double-sided tape were cut and placed about 3mm apart on the coverslip, and an 18mm x 18mm coverslip was placed on top to create three channels with a volume of ~20ul each (**Figure 2.2**).

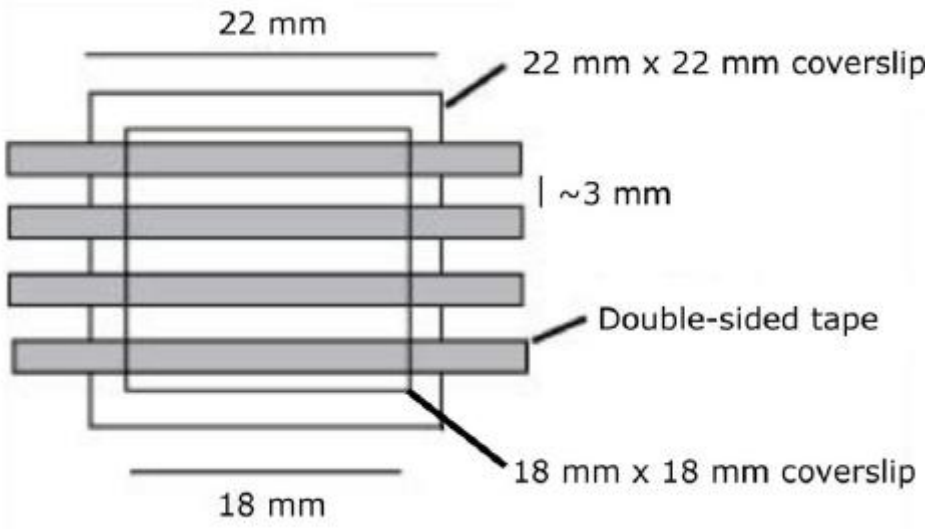

Figure 2.2) Preparation of coverslip channels for microscopy assays.

Double-sided tape was cut into strips and laid across the 22x22mm coverslip, and the 18x18mm coverslip placed on top. Image courtesy of Hannah Belsham, PhD thesis, 2019.

2.9.2. Microtubule growth assay

Fluorescently labelled Taxol stabilised microtubules were grown as per section 2.7.1. In the case of an experiment, 250µM peptide of interest suspended in 25%DMSO was added along with other reagents, and 25% DMSO in BRB80 for the control. Peptide had to be added first to the labelled tubulin to prevent microtubule polymerisation before the peptide had a chance to act. After the 30-minute 37°C incubation, BRB80 + Taxol + 30µm peptide of interest was added to stabilise the microtubules post polymerisation and to ensure the effect of the peptide wouldn't wear off. BRB80 + Taxol with no additional components was added to the control. Poly-lysine coated coverslips were prepared as per section 2.8.2.

One assay was carried out per coverslip channel. Microtubules were diluted 1:10 in BRB80 and added to the coverslip channel. Excess microtubules were removed by flushing the channel with BRB80. Approx. five images were taken of different fields of view of the microtubules.

2.9.3. Image acquisition and data analysis

Microscopy was carried out on a Zeiss200M microscope at the School of Life Sciences imaging facility (University of Nottingham). Using ImageJ, each field of view was thresholded to reduce as much background noise as possible, the highlighted microtubules were selected using the select function, and the area of polymerised tubulin was quantified using the measure function. Jitter plots were generated using the Plots of Data website.

2.9.4. Microtubule depolymerisation assay

Fluorescently labelled GMPCPP stabilised microtubules were grown as per section 2.7.2, and silanised coverslips were prepared as per section 2.8.1.

One assay was carried out per coverslip channel. The assay was built up as follows. β-tubulin antibodies (Sigma-Aldrich; Monoclonal anti β-tubulin antibody, produced in mouse, clone SAP.4G5, ascites fluid; #T7816; 1:200 in BRB80) were added to one side of the channel and a vacuum pump was used to pull the liquid through due to the hydrophobic nature of the silanised coverslips. Antibodies were left to sit in the channel for ~five minutes before being washed twice with BRB80 + 0.2% Tween 20. This solution (and all following) was pulled

through with filter paper. Microtubules were then added to the channel and left to sit for ~ three minutes. Incubation time was varied depending on the density of microtubules when visualised after one minute and the desired final density. Excess microtubules were washed off with BRB80 + 0.2% Tween 20. The assay reaction mixture (1x BRB20 + 75mM potassium chloride [KCl; w/v] + 0.1% Tween 20 [v/v]; 100mM MgATP; BSA [10mg/ml]; BME; d-glucose; glucose oxidase and catalase) was then added to the channel, which was now ready for use. Once the channel was prepped, the protein of interest was diluted down to 40nM in the assay reaction mixture for use. Microtubules were photographed every 2 or 5 seconds, depending on the protein being added, until all the microtubules had disappeared from the field of view. Protein was added after 30 seconds.

2.9.5. Data analysis

Microscopy was carried out on a Zeiss200M microscope at the School of Life Sciences imaging facility (University of Nottingham). Post acquisition, microtubule length over time was measured using Fiji image analysis software. The data generated was inputted into Microsoft excel and exported to Igor Pro (Wavemetrics) to calculate and plot microtubule depolymerisation rates.

2.10. Biochemical assays

2.10.1. Fluorescence polarisation

Cycled tubulin (2.6.1) was recovered from -80°C storage, thawed on ice and serial diluted to concentrations ranging from 100µM – 0.19µM in BRB80 in a 96 well plate. Fluorescently labelled peptide was thawed on ice and diluted to 100nM in BRB80, then incubated with tubulin at a 1:1 ratio to halve the above concentrations. The reaction was incubated for 20 minutes at room temperature, before each sample was transferred to a black 296 well plate using a multi-channel pipette. Using a Pherastar microplate reader, the polarisation of light emitted from the fluorescently labelled peptide in each sample was measured and recorded in a Microsoft Excel spreadsheet, which was subsequently analysed and plotted using Graphpad PRISM.

2.10.2. Isothermal Titration Calorimetry (ITC)

Purified porcine tubulin was buffer exchanged into BRB40 as described in section 2.5.5, then diluted to a concentration of 20µM in BRB40 and kept on ice until further use. Lyophilised peptide was made up to 300µM in the same batch of BRB40 that tubulin had been buffer exchanged into and kept on ice until further use. 300µl of 20µM tubulin was added to the experimental cell, 300µl BRB40 to the reference cell and 70µl of 300µM peptide was loaded into the injection syringe. ITC was then carried out at 37°C, using a microcal PEAQ-ITC machine. 18 injections of peptide into the experimental cell were carried out 150 seconds apart, and the resulting data was analysed using MicroCal PEAQ-ITC analysis software.

2.10.3. Microscale Thermophoresis (MST)

MST was carried out using a Nanotemper Monolith Nt.115 Pico, by Nanotemper™ Technologies. Low retention pipette tips and microcentrifuge tubes, provided by Nerbe Plus were used throughout the assay. Purified porcine tubulin labelled with an Alexa Fluor 647 dye (section 2.6.3) was recovered from -80°C, thawed on ice and centrifuged at >20000g at 4°C for 10 minutes, then transferred to a new tube, diluted to 20nM in BRB80 with 0.1% Tween20

and centrifuged again under the same conditions. The peptide of interest was serial diluted to concentrations ranging from 2.56µM – 0.0781nM in BRB80 with 1.02% DMSO. Tubulin was added to each peptide concentration at a 1:1 ratio to halve the above concentrations, and each peptide-tubulin sample was centrifuged at >20000g at 4°C for 10 minutes, before being transferred to new tubes. Standard treated capillaries provided by Nanotemper™ Technologies were filled by capillary action and loaded into the Nanotemper equipment, with capillary 1 having the highest peptide concentration and capillary 16 having the lowest. The MST was then run at 10% LED and 40% MST power at 21°C, with a 30-second MST on time. Raw data was exported from the MO.Affinity Analysis software provided by Nanotemper™ Technologies to a Microsoft Excel file, which was subsequently analysed and plotted using Graphpad PRISM.

Chapter 3) The MTED peptide binds to the α/β - tubulin heterodimer and inhibits its polymerisation

3.1. Background

D. melanogaster EFA6 is a known negative regulator of axonal growth, acting by inhibiting microtubule polymerisation (Qu, Hahn et al. 2019). Expression of truncation variants of EFA6 in fibroblasts shows that an 18-residue motif in the N-terminal domain, termed the microtubule elimination domain (MTED), is sufficient to inhibit microtubule growth and disrupt the microtubule network (**Figure 3.1**). The N-terminus of EFA6 is not well conserved, with differing lengths and motifs found across species. However, *D. melanogaster* EFA6, *C. elegans* EFA6 and *H. sapiens* PSD1 (an EFA6-like protein) all have an N-terminal 18 amino acid motif involved in microtubule inhibition, with an 89% similarity between the *D. melanogaster* and *C. elegans* MTED motifs (Qu, Hahn et al. 2019).

Transfection of fibroblasts with the MTED motif from *D. melanogaster* shows that only ~25% of microtubules retain a normal morphology and are unaffected by this construct, compared to a ~40% normal microtubule morphology seen in fibroblasts transfected with *C. elegans* MTED (Qu, Hahn et al. 2019). The higher potency of *D. melanogaster* MTED therefore makes it the ideal construct for further investigations.

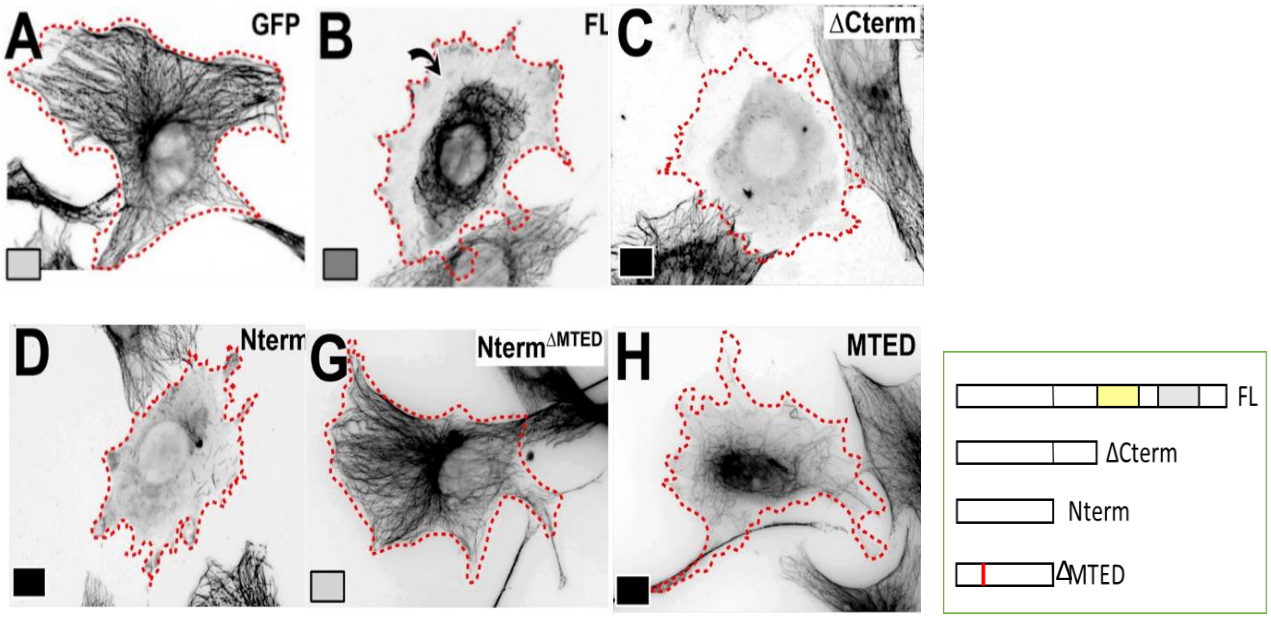

Figure 3.1) The MTED domain is sufficient for microtubule inhibition

Fibroblasts transfected with *D. melanogaster* EFA6 and various truncation constructs. Boxes in the lower right of each image represent the degree of microtubule loss: complete microtubule inhibition (black), intermediate loss (dark grey), no impact (light grey). Dotted red lines show the cell membrane. Legend on the right shows the structure of truncation constructs used (Adapted from (Qu, Hahn et al. 2019).

To further study the activity of the *D. melanogaster* MTED motif, a peptide with the 18 amino acid *D. melanogaster* MTED sequence, along with the residue immediately preceding and after the motif within the EFA6 protein, was synthesized, (the MTED peptide) to use for biochemical analysis (**Figure 3.2b**). Binding assays using Sepharose beads coated with the MTED peptide showed that beads coated with peptide pulled down unpolymerized, heterodimeric porcine tubulin, while beads with no peptide did not (**Figure 3.2c**) (Qu, Hahn et al. 2019). Furthermore, tubulin was unable to polymerise into microtubules when incubated with the MTED peptide in optimal polymerisation conditions (**Figure 3.2d**).

These results led to the idea that MTED could be developed as a potential therapeutic agent. Indeed, many microtubule-targeting drugs are used as cancer therapeutics and several appear on the World Health Organisation (WHO) list of essential medicines, such as vinca alkaloids, which prevent microtubule polymerisation, and taxanes, which inhibit depolymerisation, both of which lead to a suppression of microtubule dynamics and subsequent mitotic arrest (WHO, 2023).

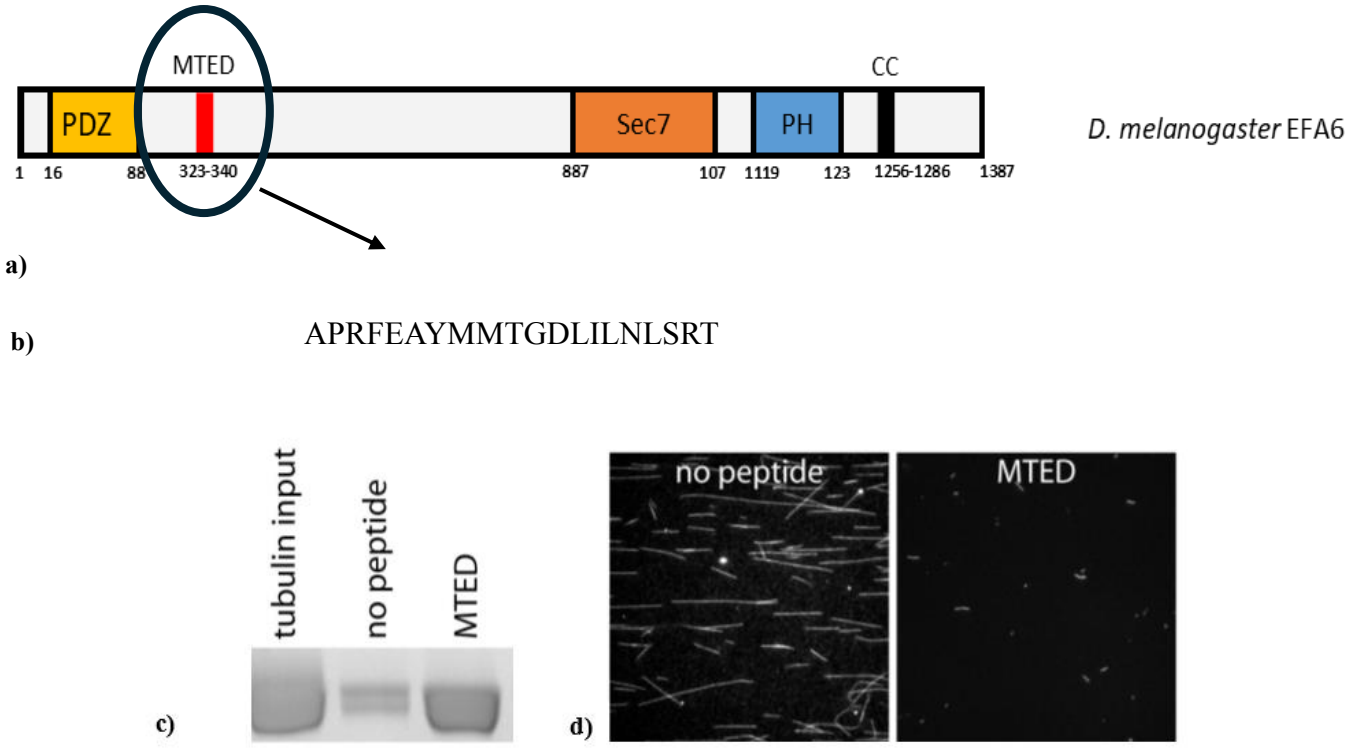

Figure 3.2) An 18 amino acid motif that inhibits microtubule polymerisation in the *D. melanogaster* EFA6 N-terminus.

a) Ribbon diagram showing the structure of the D. melanogaster EFA6 protein with annotated N-terminal motifs. b) The MTED sequence derived from D. melanogaster. c) Pull down of porcine brain tubulin using Sepharose beads coated with no peptide or the MTED peptide, d) microtubules grown in the absence of peptide and in the presence of the MTED peptide. Adapted from (Qu, Hahn et al. 2019).

3.2. Aims

To determine whether the MTED peptide had potential to be developed as a therapeutic, I set out the following aims for this chapter:

1) The investigation of individual residues in the MTED peptide to learn more about how the peptide as a whole inhibits tubulin polymerisation
2) To determine what effect, if any, MTED has on preformed microtubules
3) How modifications to the peptide can affect its behaviour
4) The affinity of the peptide for the tubulin heterodimer

Taken together, these results can inform on the optimal conditions necessary for MTED to function as an effective microtubule inhibitor.

3.3. MTED inhibits microtubule polymerisation

To confirm and further investigate the data from Qu et al. (2019), a microtubule growth assay using MTED (APRFEAYMMTGDLILNLSRT) was carried out using purified porcine tubulin labelled with a fluorescent rhodamine dye. To allow for an excess of peptide, 60µM peptide was incubated with 30µM fluorescently labelled tubulin, and the results were imaged on a poly-L-Lysine coated coverslip using wide-field fluorescent microscopy. A scrambled peptide (MITAPREFDYLNLRAGLSMT) was used as a control peptide, and a microtubule growth assay lacking any peptide was also carried out to quantify the polymerisation of tubulin in the absence of any peptide.

In the absence of any peptide, microtubules grow and are easily visualised (**Figure 3.3a**), with the amount of polymerised tubulin measuring 862.4±135.9AU; n=19. In the presence of the scrambled peptide control, microtubules grow and are again easily visualised, with tubulin polymerising to 830.2±153.4 AU; n=6. By contrast, few or no microtubules are observed when tubulin is incubated with the MTED peptide. Quantification of the amount of polymerised tubulin per field of view show that tubulin polymerised to 49.6±12.2AU; n=15, statistically significantly lower than tubulin incubated in the presence of the scrambled control, and that of tubulin polymerised in the absence of any peptide ($p<0.0001$, One-way ANOVA).

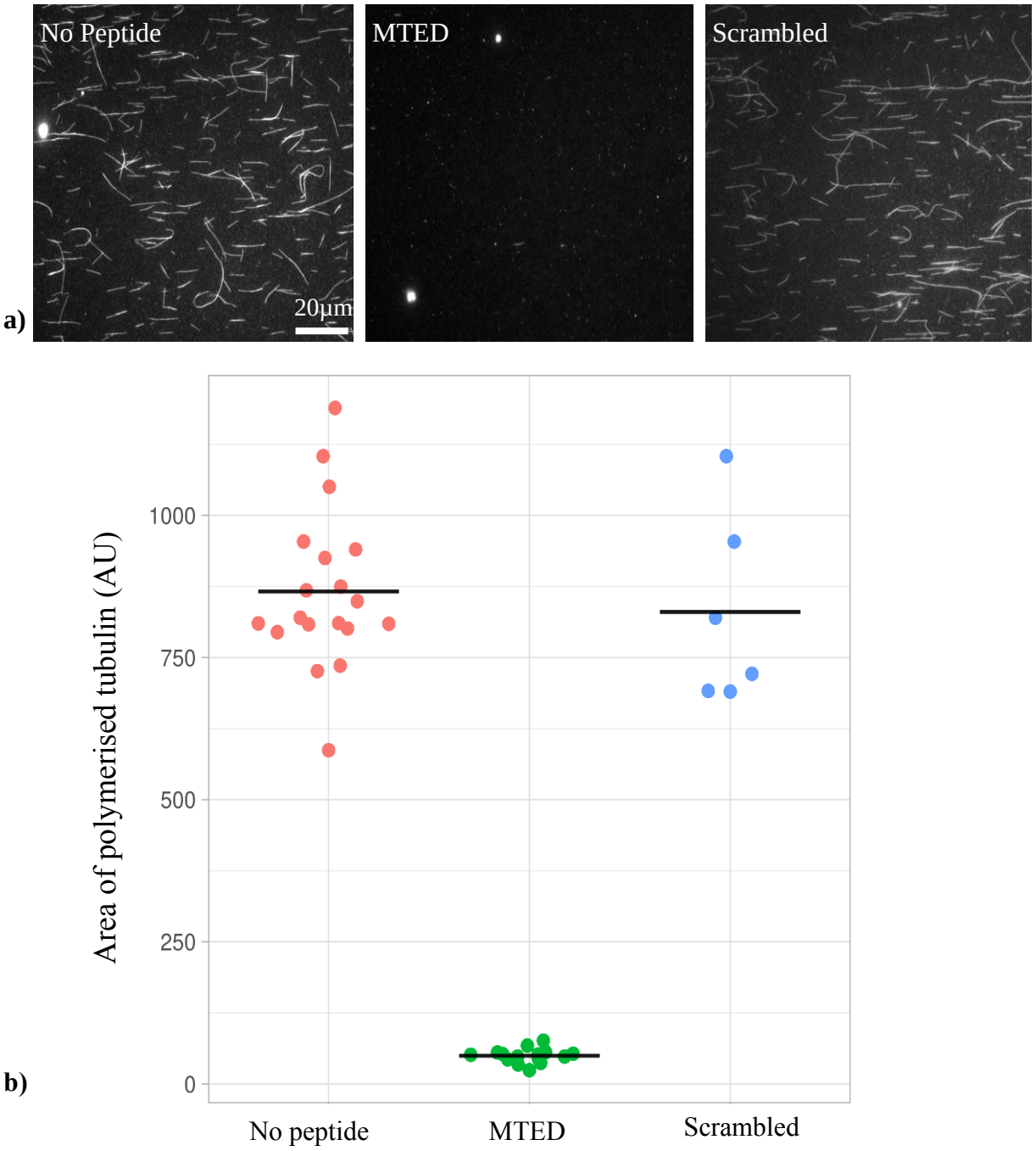

Figure 3.3) The MTED peptide inhibits microtubule growth while a scrambled peptide does not.

a) Representative fields of view showing the results of a microtubule growth assay: in the absence of peptide, in the presence of MTED peptide or a scrambled version of MTED. b) Jitter plot showing the quantified area of tubulin able to polymerise under all three conditions. Horizontal bars denote the mean value for each dataset. Each datapoint represents one field of view. For each condition, n=3, where n is the number of biological repeats.

3.4. Residues toward the C-terminal end of the MTED peptide are less important in microtubule growth inhibition

Having established that the MTED peptide's inhibitory ability is sequence-specific, further studies were carried out to determine which MTED residues were necessary for microtubule growth inhibition. Molecular modelling experiments looking at several hypothetical binding interactions between MTED and tubulin (collaboration with Dr Aditi Borkar of the University of Nottingham, unpublished data) had highlighted certain residues possibly important in the binding between the MTED peptide and tubulin (R3, D12 and R19) and these, along with a selection of charged residues (E5, Y7, T10, I14, S18), were individually substituted with alanine to create eight mutant peptides (**Figure 3.4a**). All modelling was hypothetical as to date, neither the structure nor binding location of MTED to tubulin has been solved.

The inhibition ability of each mutant was determined using a microtubule growth assay and comparing the area of tubulin that polymerised in the presence of each mutant to the wild-type MTED peptide. More microtubule polymerisation occurred in the presence of the R3A, E5A, Y7A, T10A, D12A and I14A peptides relative to wild-type MTED ($p<0.0001$ for all samples compared to MTED, one-way ANOVA), suggesting that these residues are all necessary for microtubule inhibition (**Figure 3.4b**). However, none of these mutations allowed microtubule polymerisation to the same level as in the absence of peptide ($p<0.05$, one-way ANOVA). Only the peptide variants S18A and R19A retained an ability to inhibit microtubule growth comparable to the wild-type peptide (**Figure 3.4**) ($p=0.99$ and >0.99, respectively [one-way ANOVA]).

a) APRFEAYMMTGDLILNLSRT

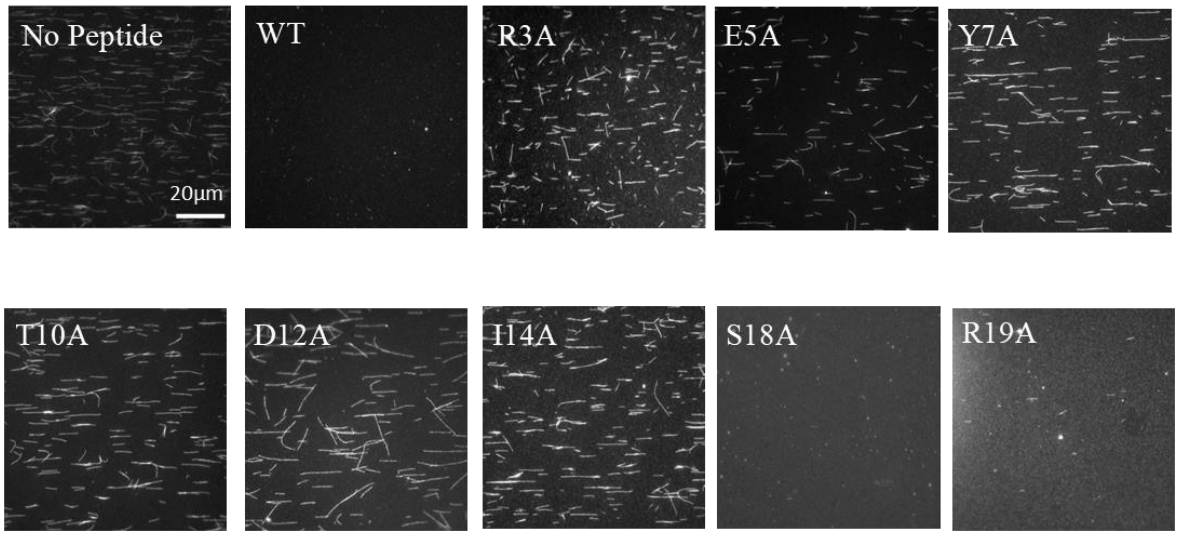

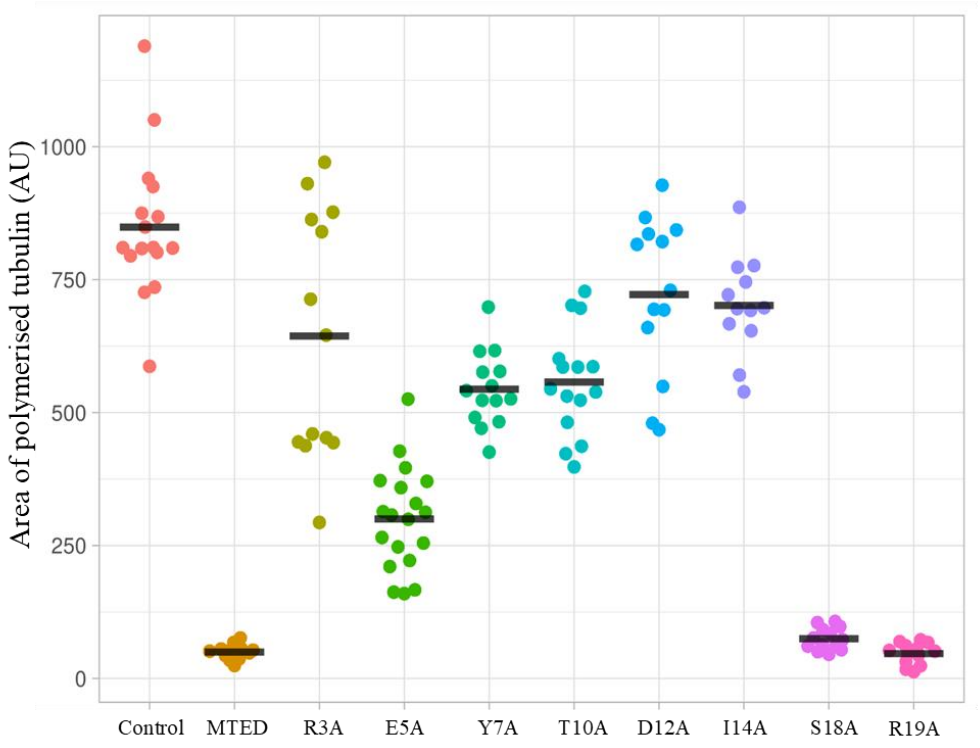

c)

Figure 3.4) All mutated residues apart from S18 and R19 are necessary for microtubule inhibition.

a) The *D. melanogaster* MTED sequence with the residues individually substituted for alanine highlighted in red. b) Representative fields of view showing the results of a microtubule growth assay for all alanine substituted peptides. c) Jitter plot showing the quantified area of tubulin able to polymerise under control conditions and in the presence of each peptide. Each data point represents one field of view. Horizontal bars denote the mean value of each dataset. N=3, where n is the number of biological repeats.

3.5. The MTED peptide does not actively depolymerise microtubules

The MTED peptide binds to tubulin and inhibits its polymerisation (**Figure 3.3**), as shown in the pull down and microtubule growth assays. However, the molecular mechanism of this activity is unknown. What also remains unknown is what effect, if any, the MTED peptide has on polymerised microtubules.

Sequence alignment of the kinesin-13 motor MCAK, a known microtubule depolymerase, with MTED does not show any similarity. This is not entirely surprising as MTED is not big enough to be a motor domain (20aa peptide vs 350aa MCAK motor domain). It is therefore unlikely that MTED has any depolymerisation activity through this mechanism.

To determine whether the MTED peptide can depolymerise preformed microtubules, a depolymerisation assay was carried out. Briefly, GMPCPP-stabilised rhodamine-labelled microtubules were adhered to a coverslip and 50µM MTED peptide added. Microtubules were imaged every 5s and the resultant movies analysed for changes in microtubule length. As a positive control the same assay was performed with the addition of 40nM MCAK, and no added peptide/protein was used as a negative control.

The MTED peptide does not actively depolymerise GMPCPP-stabilised microtubules. The rate of depolymerization in the presence of this peptide was 0.03±0.02µm/min, n=8, not significantly different to the spontaneous depolymerization rate of GMPCPP-stabilised microtubules immobilised on cover glass surfaces at 20°C, which falls in the range of 0.02-0.03µm/min, widely accepted as the spontaneous rate of microtubule depolymerisation (Gell, Bormuth et al. 2010). By contrast, microtubules exposed to 40nM MCAK depolymerise at a rate of 2.43 ± 0.177 µm/min, n=8 (**Figure 3.5**)

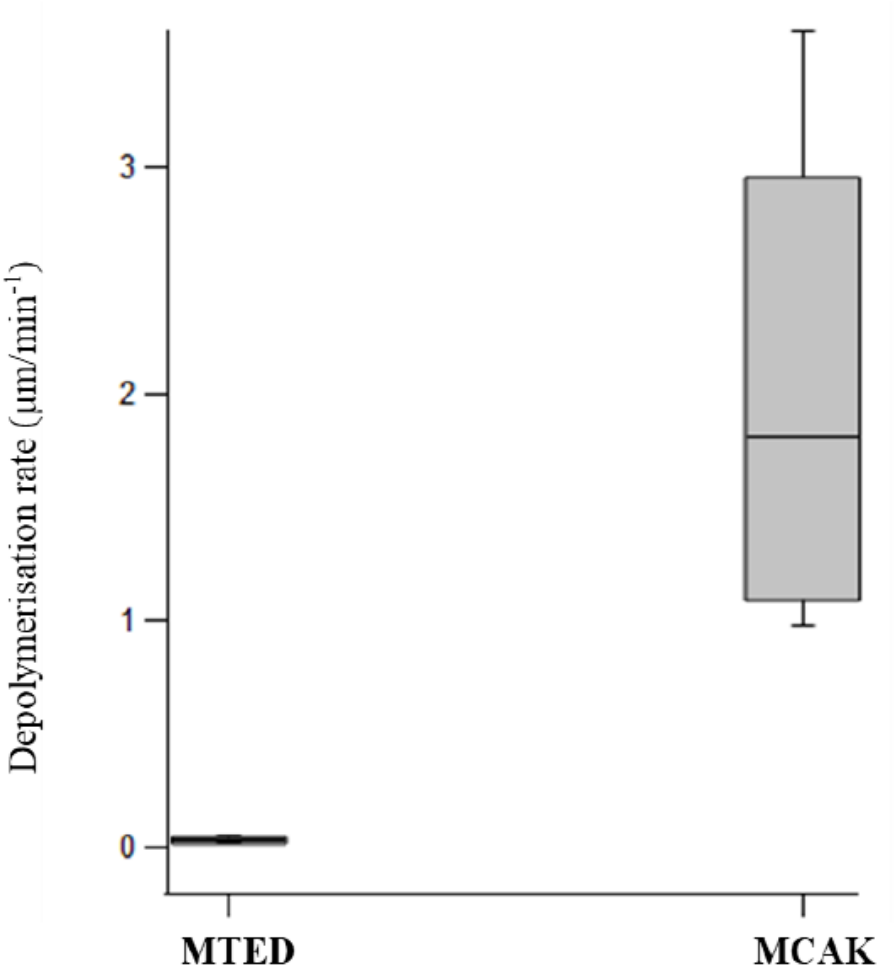

Figure 3.5) MTED has no depolymerisation activity.

Boxplot showing the depolymerisation rates for MTED and MCAK. Error bars represent the range of values, lines through the boxes represent the average depolymerisation rate. N=3, where n is the number of biological experimental repeats.

3.6. MTED does not retain its activity when directly tagged at either terminus

As the MTED peptide has been shown not to have any depolymerisation activity, it is likely that it inhibits microtubule polymerisation by binding to and sequestering unpolymerized tubulin. To understand more about the interaction of the MTED peptide with tubulin, I wanted to measure the affinity of the interaction. A fluorescently tagged version of the MTED peptide was synthesised to use fluorescence polarisation to report on the binding of peptide to tubulin. Briefly, polarised light is used to excite a fluorophore and the degree of polarisation of the emitted light is inversely proportional to the molecular rotation that has occurred between excitation and emission. Since molecular rotation is correlated with the size of the molecule or molecular complex to which the fluorophore is attached, this technique is very useful to measure the interaction of a small, labelled ligand (MTED peptide 2.3kDa) with a larger protein (tubulin 110kDa). A small fluorescent molecule would have low polarisation due its high rotational freedom, compared to when bound to a larger molecule, which would rotate more slowly, resulting in a high polarisation (Lea and Simeonov 2011).

Two labelled peptides were initially created as described in 2.3.4: one with fluorescein directly on the N-terminus (Fl-MTED), and one with fluorescein attached via the side chain of a lysine residue added to the C-terminus (MTED-Fl) (**Figure 3.6a,b) .** To ensure these labelled peptides could bind to tubulin and inhibit polymerisation, microtubule growth assays were carried out. Microtubules were able to grow in the presence of both these peptides (**Figure 3.6c**) indicating that the addition of a fluorophore at either end interfered with the peptide's ability to inhibit microtubule growth, rendering them unsuitable for the fluorescence polarisation assay.

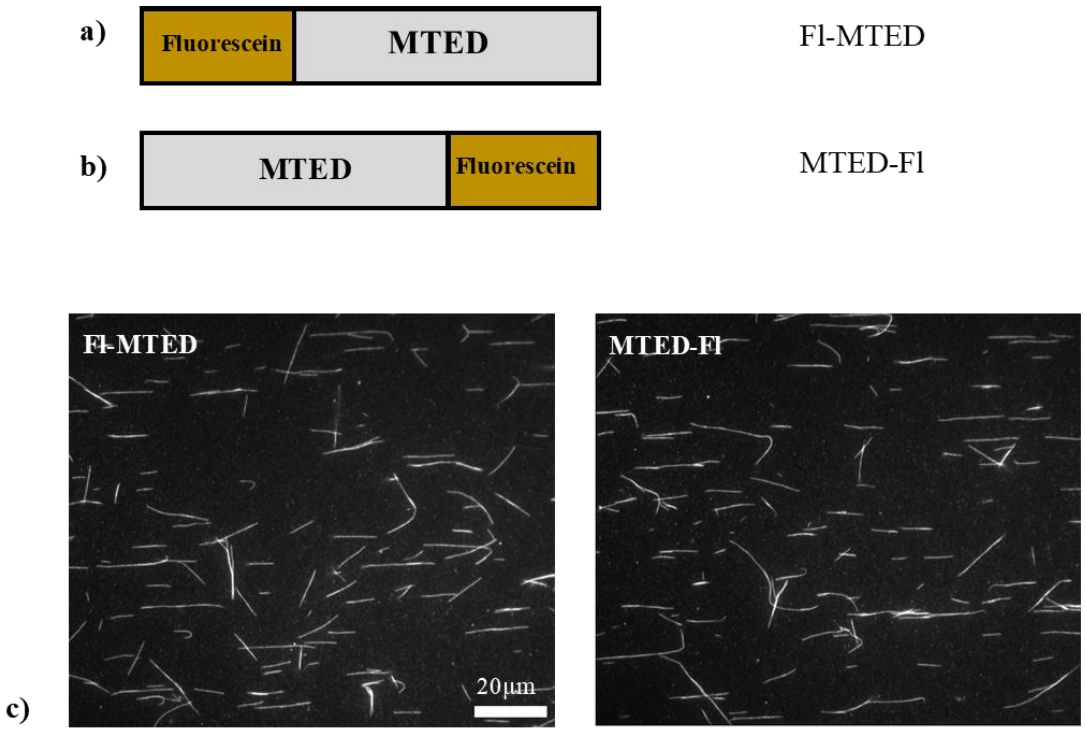

Figure 3.6) MTED cannot inhibit microtubule polymerisation when directly tagged at either terminus.

a-b) ribbon diagrams showing the structure of the fluorescent peptides created for the fluorescence polarisation assay. c) Microtubule growth assay results showing that microtubules grow in the presence of each peptide, making them unsuitable for the assay.

Discussed in detail in Chapter 4, a version of the MTED peptide had already been synthesised in which fluorescein was added to the sidechain of a C-terminal lysine separated from the end of the wild-type peptide by a nine amino acid linker (K-MTED-R-Fl) (**Figure 3.7a**). This fluorescently labelled version of MTED had been shown to inhibit microtubule polymerisation using a microtubule growth assay, indicating that the nine-residue linker between the end of wild-type MTED and the fluorophore was long enough to allow the peptide to remain functional (**Figure 3.7b**). As this peptide was able to bind tubulin and inhibit microtubule growth, it was used as the ligand in a fluorescence polarisation tubulin binding assay. This peptide is twice as large as wild-type MTED but still much smaller than the tubulin heterodimer (6.2kDa compared to 110kDa, respectively) so a large increase in polarisation upon the peptide binding to tubulin was still expected.

Unlabelled tubulin was serially diluted to concentrations ranging from 100µM – 0.19µM in BRB80 with 2mg/ml BSA, then incubated with 100nM fluorescent peptide (K-MTED-R-Fl) in BRB80 with 1% DMSO at a 1:1 ratio, making final concentrations of 50µM – 0.095µM tubulin, 1mg/ml BSA, 50nM K-MTED-R-Fl and 0.5% DMSO. Light polarisation was measured using a Pherastar microplate reader. An additional run of 50nM K-MTED-R-Fl in the absence of tubulin was carried out as a control to determine the behaviour of the fluorescently labelled peptide in its unbound state. No change in polarisation was observed when K-MTED-R-Fl was added to tubulin and attempts made using GraphPad PRISM to fit the data to the binding equation $Y = Bmax*X/(K_d + X)$, where X = ligand concentration, K_d is the binding constant and Bmax is the maximum binding, resulted in a straight line, similar to K-MTED-R-Fl in the absence of tubulin (**Figure 3.8**). It is unlikely that this peptide is not binding to tubulin as it has been shown to do so in a microtubule growth assay. It is more likely that the nine amino acid linker between the end of the MTED peptide and the fluorophore is so long that the rotational freedom of the fluorophore is unaffected by the binding state of the peptide.

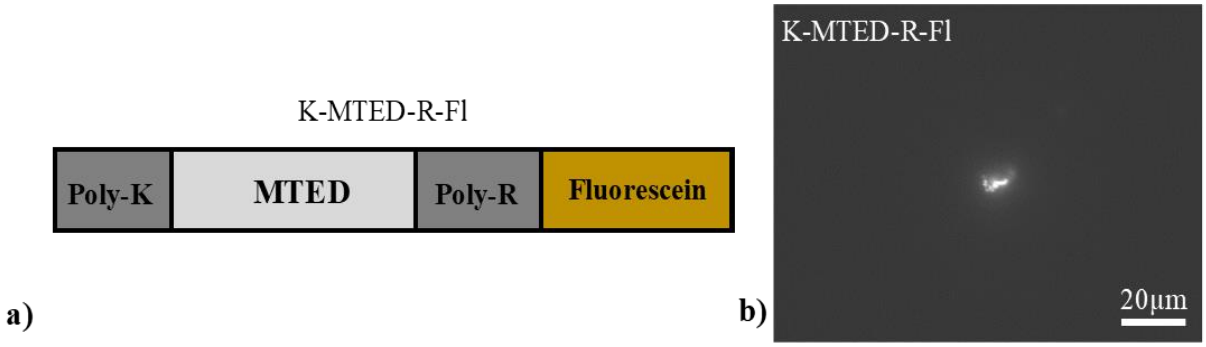

Figure 3.7) The nine amino acid poly-R linker is long enough for MTED to retain its inhibition abilities.

a) ribbon diagram showing the structure of the K-MTED-R-Fl peptide, and b) a microtubule growth assay carried out with the peptide showing that tubulin is unable to polymerise, and instead forms an aggregate.

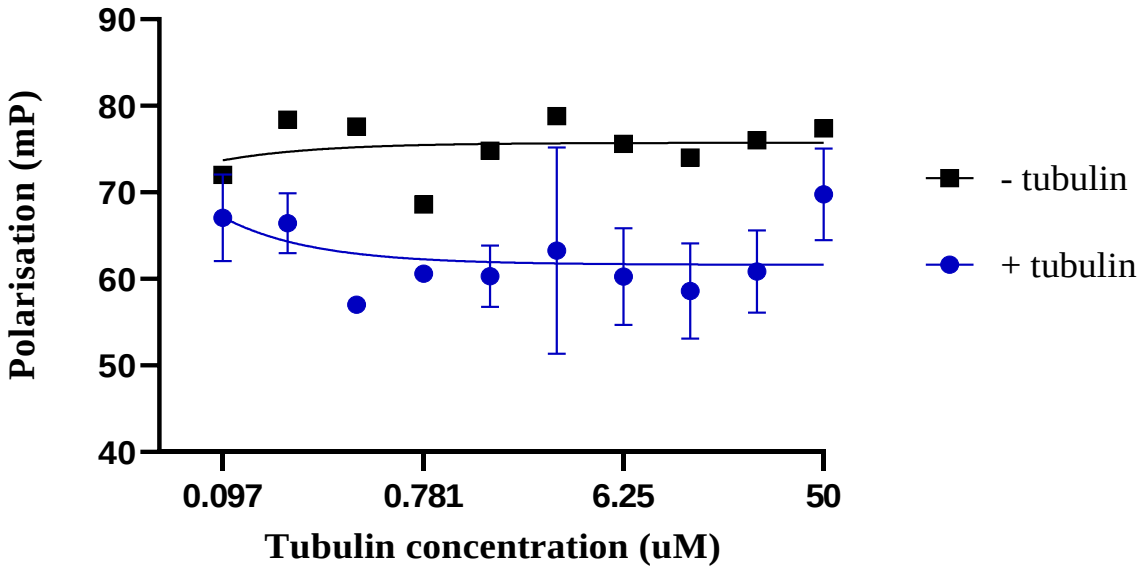

Figure 3.8) No change in light polarisation occurs when K-MTED-R-Fl is incubated with tubulin.

Measurement of the degree of polarised light emitted from the K-MTED-R-Fl peptide incubated in the presence and absence of tubulin. Lines running through the datasets denote a binding curve fitted to the equation $Y = Bmax*X/(K_d + X)$. Error bars for peptide in the presence of tubulin (blue) represent one standard deviation. n=1 for K-MTED-R-Fl in the absence of tubulin, and n=2 for K-MTED-R-Fl in the presence of tubulin, where n=the number of biological experimental repeats.

3.7. A two amino acid linker is too short to restore MTED's inhibition abilities

A further attempt was made to create a fluorescently labelled peptide that could inhibit microtubule growth whilst having a sufficiently short linker to report on tubulin binding via fluorescence polarisation. It was previously shown that residues toward the C-terminus of MTED are not involved in microtubule growth inhibition (**Figure 3.4**). Therefore, a two amino acid (alanine) linker was added to the C-terminus of MTED followed by the fluorophore attached to the sidechain of a lysine (MTED-AA-Fl) (**Figure 3.9a**). The rationale was that this may distance the fluorophore enough from the end of the wild-type peptide that it wouldn't interfere with tubulin binding but be close enough to report on tubulin binding. Unfortunately, when the inhibition abilities of this peptide were tested with a microtubule growth assay, the presence of microtubules indicated that this peptide also did not retain its activity when tagged(**Figure 3.9b**), rendering it unsuitable for the fluorescence polarisation assay.

It is likely that the 3 amino acid linker used here is the longest linker that would allow the rotational freedom of the fluorophore to be influenced by the peptide binding to tubulin, a critical requirement for fluorescent polarisation. Therefore, due to this and time constraints, no further attempts were made to generate a peptide suitable for a fluorescence polarisation binding assay.

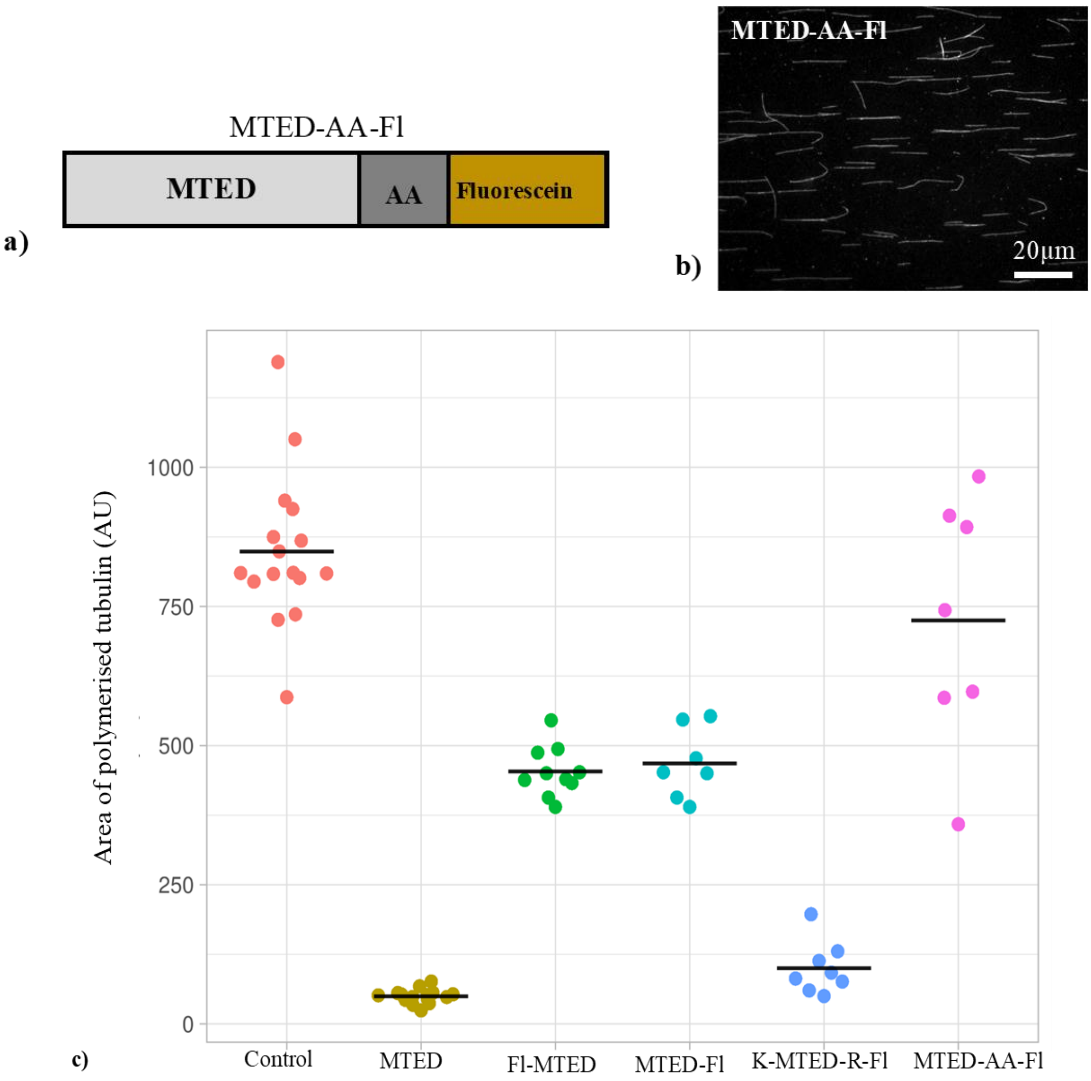

Figure 3.9) No fluorescently tagged MTED construct is suitable for fluorescence polarisation.

a) Ribbon diagram showing the structure of the MTED-AA-Fl peptide and b) Microtubule growth assay using the same peptide. c) Jitter plot showing the area of tubulin that was able to polymerise in the presence of the wt MTED peptide and all fluorescent variations of the peptide. Horizontal bars denote the mean value of each dataset.

3.8. Isothermal Titration Calorimetry

Another technique that could report on the binding interactions of two partners was Isothermal Titration Calorimetry (ITC), and I next tried this method to measure the affinity of the MTED peptide for the tubulin heterodimer.

ITC is a technique that measures the change in temperature that occurs when a protein binds to a ligand and uses this information to report on the binding affinity of the two partners. The greatest advantage of this technique is that the assay is label free i.e. no fluorescent tag is needed. While this would allow for the wild type MTED peptide to be used, there were two limitations to this assay. Firstly, DMSO is unsuitable for use in ITC as it is known to create false heat peaks, or mask those created by the protein-protein interaction (Boudker and SeCheol 2015). Secondly, an absolute buffer match between the peptide and ligand is necessary to ensure any changes in temperature are a result of binding activity between the two partners, and not due to changes in buffer composition.

Previous work in the Friel lab has shown that the MTED peptide is insoluble in many BRB based buffers and does not retain its activity for longer than 24 hours when dissolved and stored in H_2O at any temperature. Therefore, our typical protocol for making stock solutions of MTED and related peptides is to dissolve the peptide in 100% DMSO and keep stocks at 4°C for long term storage.

Although MTED can be dissolved and remain functional for ~24 hours in H_2O, it was not considered as a possible buffer for ITC as H_2O is unlikely to be a suitable buffer for tubulin. Therefore, I wanted to find a suitable BRB-based buffer for ITC that both MTED and tubulin could be dissolved into and remain active. I did a ½ dilution of BRB80 with H_2O to make BRB40, and dissolved 1mM MTED peptide into this buffer and carried out a microtubule growth assay to determine whether the peptide remained functional and bound to tubulin in this buffer. The microtubule growth assay was carried out as described in Methods 2.9.2 with the omission of DMSO. 25% BRB40 in the absence of peptide was used for control conditions instead.

Under control conditions of the assay, the area of tubulin that polymerises is significantly greater than in the presence of the MTED peptide ($p<0.0001$, t-test), showing that the MTED peptide remains functional in BRB40 and thus is a suitable buffer for ITC (**Figure 3.10**).

In preparation for ITC, existing stocks of tubulin in BRB80 were dialysed into BRB40, and the MTED peptide was then dissolved into this same buffer at a concentration of 1mM.

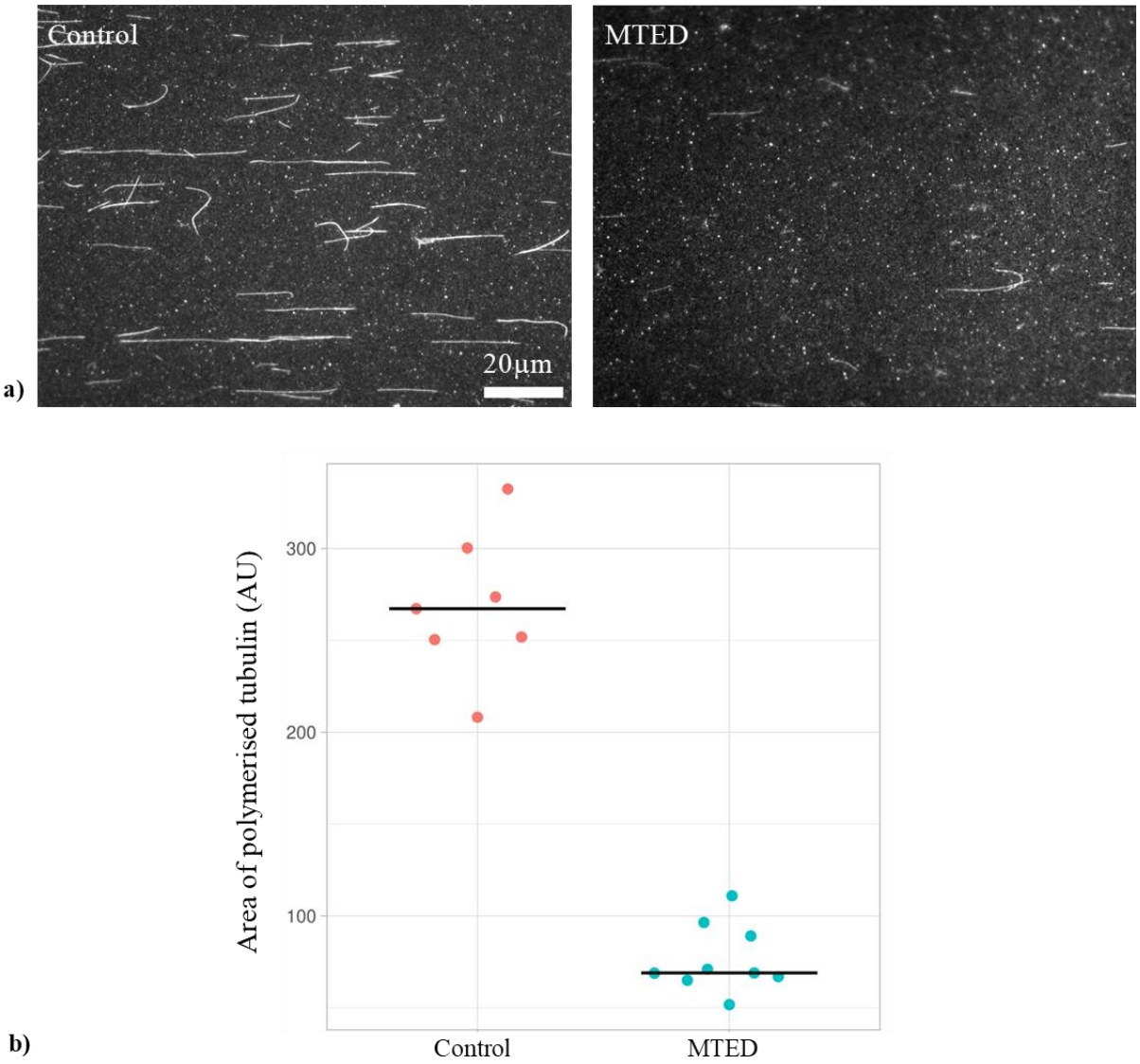

Figure 3.10) MTED inhibits microtubule polymerisation when dissolved in BRB40.

a) representative fields of view of a microtubule growth assay when MTED in dissolved in BRB40. b) Jitter plot of the area of tubulin able to polymerise under control conditions and in the presence of the MTED peptide. Horizontal bars denote the mean value of each dataset.

ITC was carried out as described in Methods section 2.10.2. The reference cell contained BRB40, 20µM tubulin in BRB40 was added to the experimental cell and 300µM MTED in BRB40 was in the injection syringe. Injections occurred every 150 seconds, and the change in temperature was recorded. An additional run with BRB40 in the reference cell, 20µM tubulin in the experimental cell and BRB40 with no peptide in the syringe was carried out as a control.

The power differential (DP (µW)), or the amount of power required to keep the temperature between the reference and experimental cells the same, changed very little over the course of the experiment, and was almost identical between the control and MTED runs (**Figure 3.11a**). Additionally, normalisation of the data shows very little change in enthalpy (ΔH), or the change in the energy of the reaction when MTED is added to tubulin, and again looks very similar between the control and experimental samples (**Figure 3.11b**). A K_d of 0.0001 ± 35µM was determined by the MicroCal PEAQ-ITC analysis software, which had an error far too large for the value to be considered valid. As well as this, MTED did not stay in solution for the duration of the assay, as physical examination of the solution in the syringe showed a white precipitate.

Taken together, this data suggests that no binding is occurring between MTED and tubulin, most likely due to MTED coming out of solution. Further investigations to find a buffer compatible with the assay would have taken up time and resources that were not available to me at the time, and so ITC was not continued.

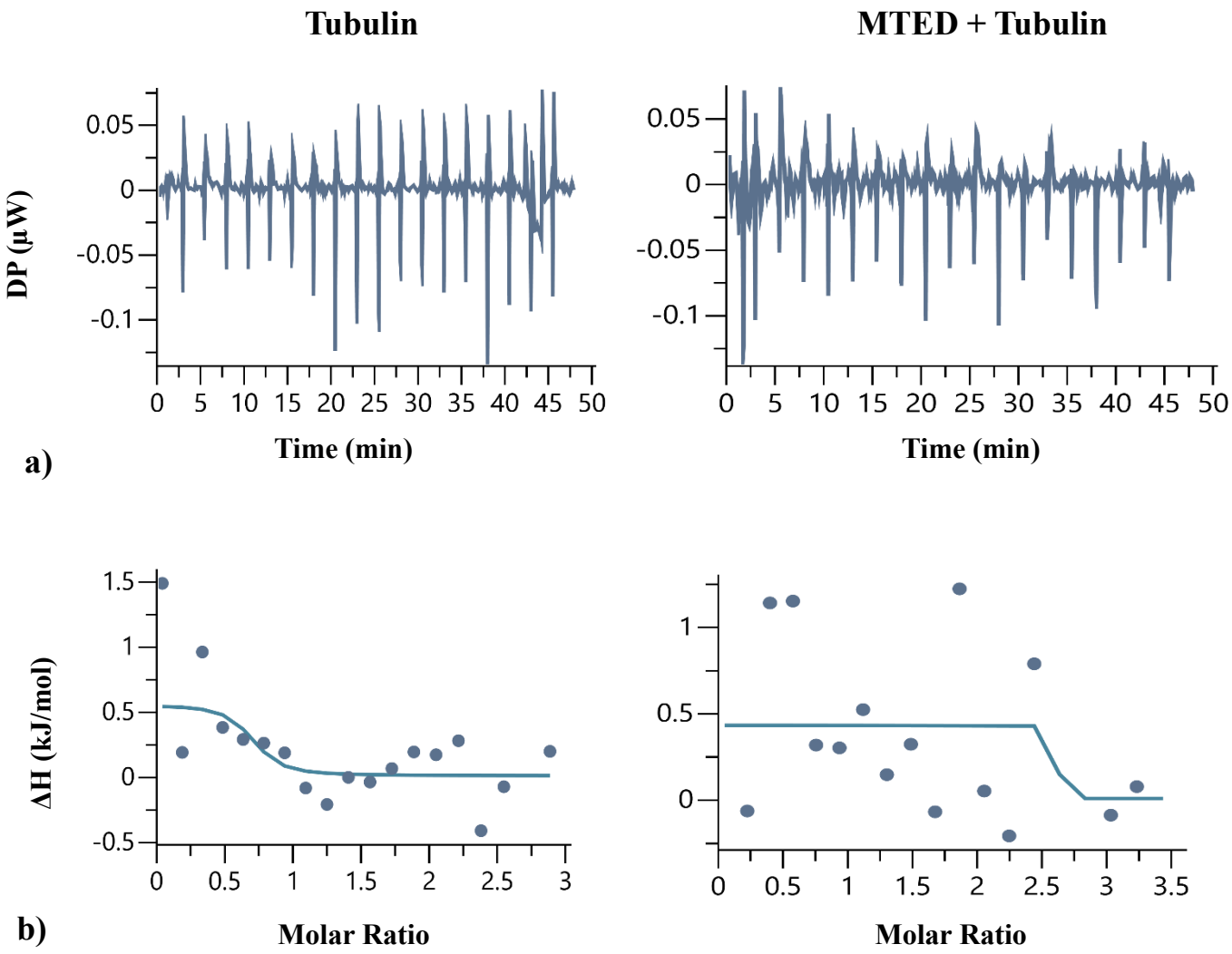

Figure 3.11) No binding is observed between the MTED peptide and tubulin during ITC.

a) Graphs showing the power differential between the reference and experimental cells for tubulin in the absence and presence of the MTED peptide. b) Normalisation of the heat change registered when buffer without and with MTED is added to tubulin.

3.9. Microscale Thermophoresis is compatible with MTED

The technique Microscale Thermophoresis (MST) was then attempted to quantify the affinity of the interaction of the MTED peptide with tubulin. This technique measures the change in the intensity of fluorescent signal of a labelled molecule when bound to an unlabelled partner, under the influence of a laser-induced temperature change and uses this data to report on the binding interaction between the two partners.

This assay had several advantages over fluorescence polarisation and ITC. Buffer match was not essential, up to 5% DMSO could be used in the assay buffer, and it was independent of molecular weight changes. The addition of DMSO prevented the need to dissolve lyophilised MTED peptide anew each time the assay was run, saving both time and resources, and ensured that MTED remained in solution and fully functional throughout the assay. Additionally, the independence in molecular weight change meant that in this case, tubulin could be fluorescently labelled, as the existing fluorescent MTED peptides were incompatible with the in-house Nanotemper (all fluorescent MTED peptides were tagged with fluorescein, with an excitation/emission wavelength of 495/520nm, while the Nanotemper Monolith NT.115 Pico only reads light with an excitation/emission wavelength of 649/670).

Labelling MTED with a fluorophore compatible with the in-house Nanotemper was not an option. The labelling kit provided by Nanotemper™ Technology had a molecular weight cut-off of 5kDa, over twice the size of the MTED peptide, and synthesising a new peptide with a compatible fluorophore would take months. Labelling tubulin, on the other hand, would take one day, and an optimised protocol for this already existed. Tubulin was therefore labelled with an Alexa 647 dye.

Next, the optimal concentration of tubulin, as well as the required materials and conditions for the assay were determined. An initial test concentration of 200nM tubulin was far too high, as the fluorescent signal was oversaturated (**Figure 3.12a**). After multiple attempts with lower concentrations, the optimal concentration was found to be 10nM. However, the concentration of fluorescent molecule was not consistent between the capillaries, with the fluorescent signal increasing with each capillary (**Figure 3.12b**). This was rectified by using low-retention tips and tubes for the assay, to ensure an even distribution of tubulin throughout the capillaries. Finally, tubulin was seen to bind to the internal surface of the capillary and creating uneven

fluorescent peaks (**Figure 3.12c**), so 0.05% Tween 20 was added to the buffer to prevent non-specific binding. The final conditions were therefore determined as 10nM tubulin in BRB80 + 0.5% DMSO + 0.05% Tween 20, all prepared with low binding apparatus (**Figure 3.12d**).

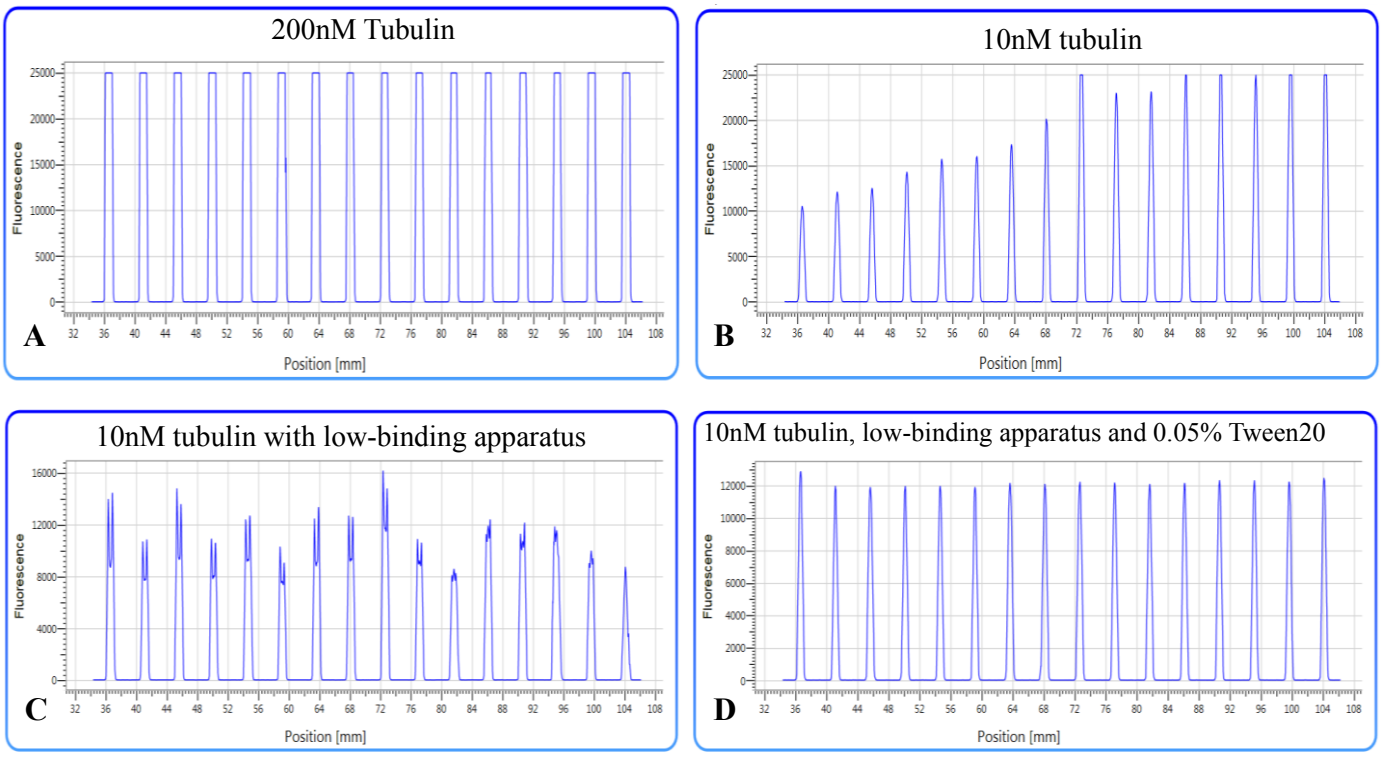

Figure 3.12) Determination of tubulin concentration and conditions for consistent fluorescence signals.

Capillary scans showing the fluorescent signal produced by tubulin under different conditions and the process of determining the optimal tubulin concentration along with the apparatus and buffer composition required for an even fluorescent signal throughout the capillaries. Position (mm) on the x-axis refers to the position of each capillary within the Nanotemper™ Monolith NT. 115 Pico equipment. Capillary 1 is at 36mm, capillary 2 at 40mm… capillary 16 is at 104mm.

The elimination of tubulin aggregates was the final and most difficult challenge, as the Nanotemper™ is very sensitive to the presence of aggregates of the fluorescently labelled protein. Several attempts at running tubulin showed that the only way to reduce the aggregation as much as possible was to centrifuge the tubulin sample for 10 minutes at >20000g at 4°C immediately after thawing, after dilution and after peptide addition (**Figure 3.13**). A simplified schematic of this process is outlined in **Figure 3.14**.

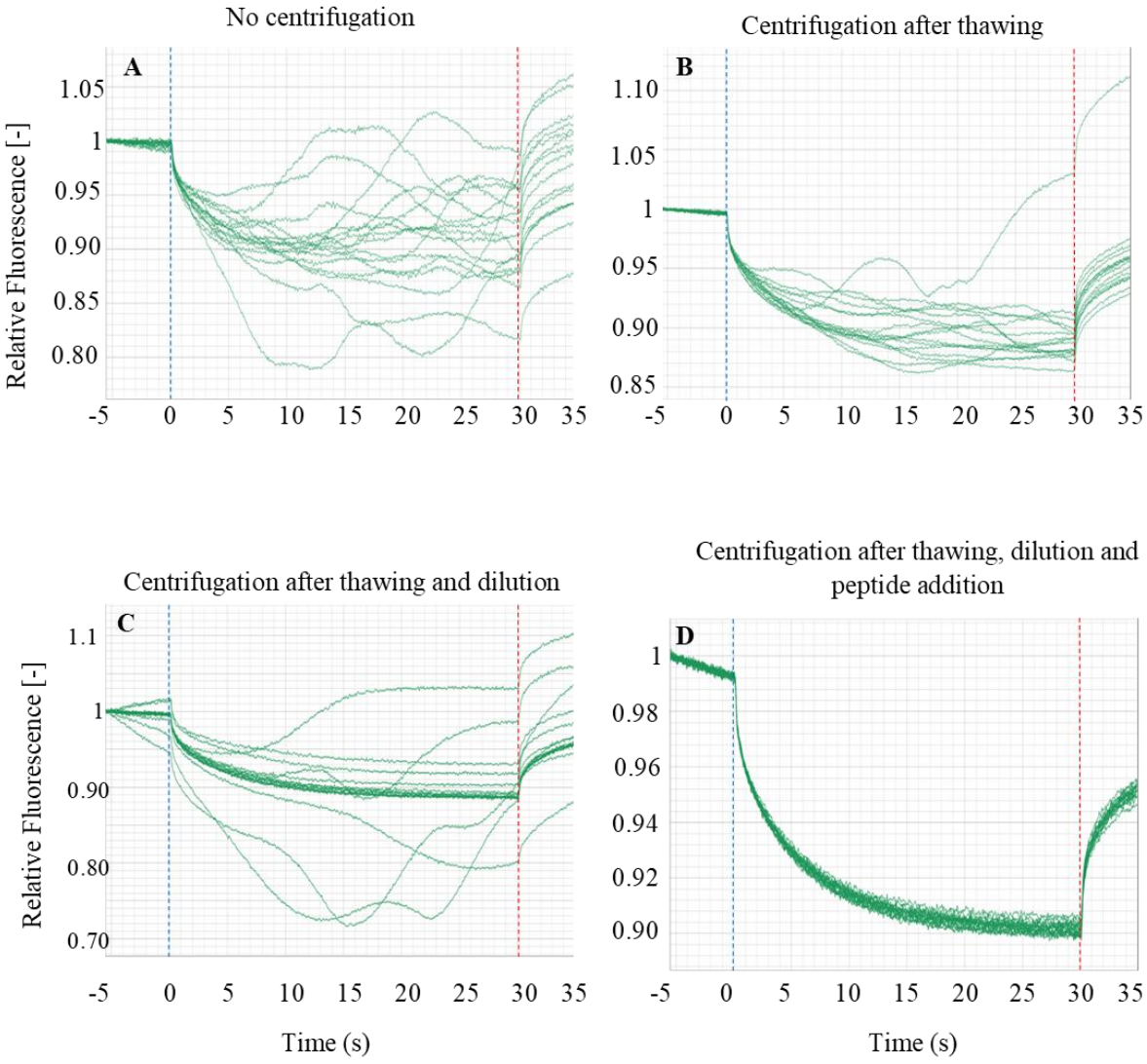

Figure 3.13) Tubulin requires centrifugation to remove aggregates.

Irregular MST traces showing the presence of tubulin aggregates in A) without centrifugation, B) centrifugation after thawing and C) centrifugation after thawing and dilution. D) Smooth, consistent MST traces showing that all tubulin aggregates are removed by centrifuging tubulin after thawing, dilution, and peptide addition. Blue dotted lines at 0 seconds indicate the MST start time, when the ionising laser is activated and the red dotted line at 30 seconds indicates the MST off time, when the laser is turned off.

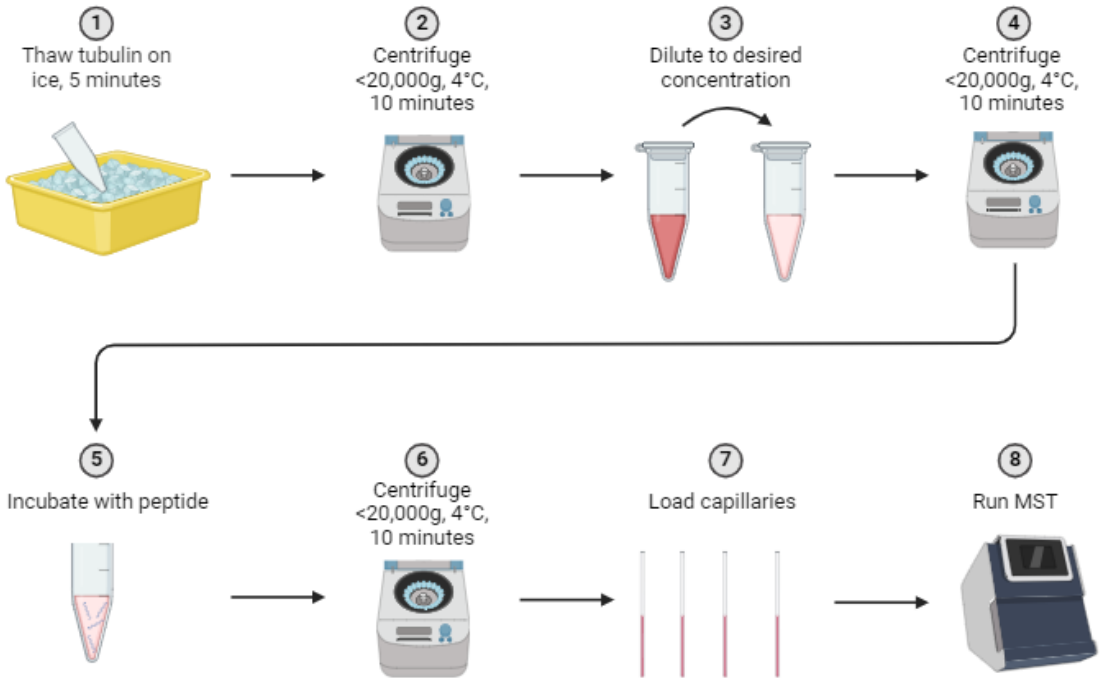

Figure 3.14) Simplified schematic outlining the process of sample preparation for MST.

The preparation of fluorescently labelled tubulin for MST requires several rounds of centrifugation and handling all at 4°C to ensure it is aggregate-free.

3.10. The MTED peptide has a strong affinity for the tubulin heterodimer

Once the optimal assay conditions had been determined, the experiment was carried out. The MTED peptide was serial diluted to concentrations ranging from 3.56µM – 0.078nM in BRB80 + 0.5% DMSO, then incubated with 20nM fluorescently labelled tubulin in BRB80 + 0.1% Tween20 at a 1:1 ratio, thereby halving the above concentrations. Capillaries were loaded by capillary action and the MST was run at 40% MST intensity, 10% LED intensity. The scrambled peptide was run under the exact same conditions.

The MTED peptide shows binding. A non-linear regression curve was fit to the data by GraphPad PRISM using the equation $Y = Bmax*X/(K_d + X)$ and a K_d of 6.43 ± 5.14nM was determined, indicative of a strong binding reaction. The scrambled peptide, on the other hand, does not bind to tubulin. Neither the MST analysis software nor GraphPad PRISM were able to generate a K_d, and the non-linear regression curve fitted by GraphPad PRISM was a horizontal line (**Figure 3.15**).

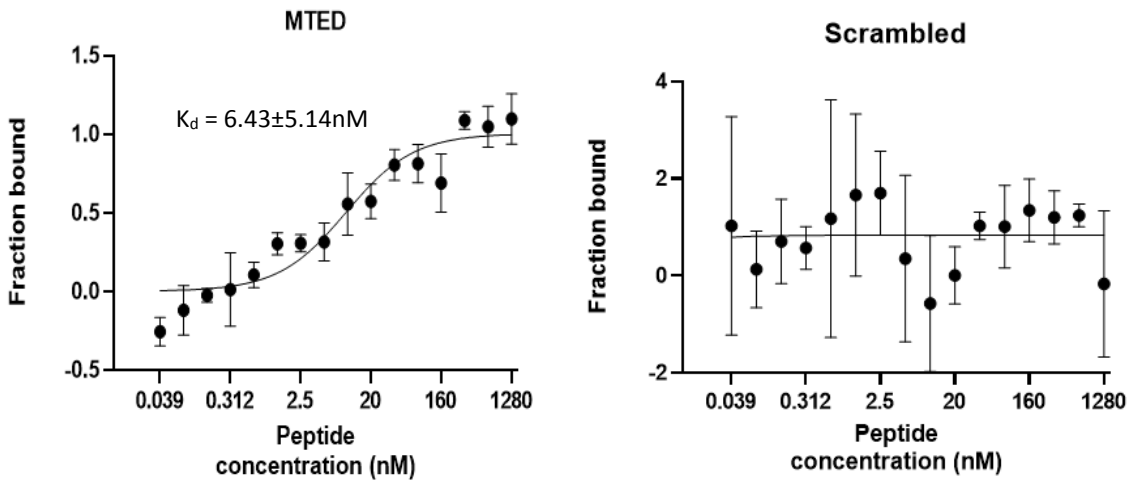

Figure 3.15) Graphs showing the non-linear regression curves fitted for the MTED and Scrambled peptides.

Binding is seen between the MTED peptide and tubulin, while no binding is seen between the scrambled peptide and tubulin. Error bars represent one standard deviation, n=3 for each peptide, where n is the number of biological repeats.

3.11. Discussion

3.11.1. Summary and limitations

MTED is an 18-residue motif derived from EFA6 that binds directly to the α/β-tubulin subunit and inhibits its polymerisation. Investigations into the role of selected residues, based on previous modelling data, showed that S18 and R19 are not involved in microtubule inhibition, as peptides with alanine substitutions at these positions retained microtubule inhibiting activity. Interestingly, however, when a fluorophore, attached to the side chain of a lysine, is directly added to the C-terminus, the peptide loses its microtubule inhibition activity, and even a 2 amino acid alanine linker is insufficient to restore it.

The solubility of this peptide has proved quite difficult, as although it is initially soluble at low concentrations (~1mM) in H_2O and BRB80, the peptide precipitates out of solution within hours at room temperature and does not retain its activity for longer than 24 hours when stored at 4°C. While 100% DMSO allowed for concentrations up to 3mM, this buffer was not ideal for assays such as ITC, where the use of DMSO is known to create false heat signatures and/or mask those created by the protein : ligand interaction (Boudker and SeCheol 2015).

Using MST, the dissociation constant of MTED for tubulin was determined to be 6.4 ± 5.1nM, indicative of strong binding. Limitations existed with this method as well, however, as MST relies on a fluorescent partner. As the in-house Nanotemper only read light in the far-red spectrum, all fluorescent MTED constructs, tagged with fluorescein, were unsuitable. While the assay was successful using tubulin labelled with Alexa647, the resultant signal change may not have been as large as I would have liked. Binding of a small ligand (MTED is 2.3kDa) to a fluorescent protein as large as tubulin (110kDa) is likely to produce a much smaller signal change than the other way around. Had MTED been labelled, it is likely that the signal change in fluorescence upon binding to tubulin would have been much greater and may have resulted in a smaller error. Nonetheless, the fact that the scrambled peptide shows no binding to tubulin further validates this result.

While the resultant K_d suggests that the MTED peptide has a strong affinity for the tubulin subunit, the binding parameters have yet to be determined. Additionally, although the necessity of select residues within the peptide have been examined, it has not been

determined to what degree these residues are involved in microtubule inhibition. As the microtubule growth assay is carried out at a 2:1 ratio of peptide to tubulin, it is likely that the peptide is present in excess. Therefore, while it is evident that residues (R3, E5, Y7, T10, D12 and I14) are necessary for microtubule inhibition, as microtubules polymerise in their absence, it is not known whether the critical concentration of MTED is altered as a result of the loss of these residues. Ideally, the K_d of MTED and each of the mutants for tubulin would inform on the minimal concentration of peptide necessary to inhibit tubulin polymerisation, and the microtubule assay redesigned with these values.

ITC is another area that, with more time and resources, could be further explored as a technique to characterize the binding reaction between MTED and tubulin. At the time of study, MTED's solubility was the limiting factor when it came to ITC. A limited supply of lyophilised peptide was available at the time and so, while it may have been possible to dissolve small amounts of peptide (~100μM) into a range of buffers such as PBS or HEPES, its ability to remain in solution and inhibit microtubule polymerisation would have required numerous microtubule growth assays and ITC trial runs. The behaviour of tubulin in these buffers was another unknown factor that would have required its own investigations.

3.11.2. Future work

One solution to the problem posed by the limited supply of lyophilised peptide is to create DNA constructs encoding the MTED peptide and expressing and purifying recombinant protein. Once optimised, this would allow for a virtually limitless supply of wild type peptide, and, using techniques such as site-directed mutagenesis, alanine-substitution mutants can be created with little effort. Fluorescent labelling of the protein would be much easier as well, as reporter genes such as GFP or red fluorescent protein (RFP) can be added, in frame, to the C-terminus of the protein, provided they are separated from the peptide by a~9 residue linker.

Additionally, it may be worth measuring the length of individual microtubules that polymerise in the presence of all alanine mutants that fail to inhibit polymerisation and comparing this data to the length of microtubules grown in the absence of any peptide. At the moment the presence of microtubules when incubated with mutant peptides (excluding S18A and R19A) is enough to say that these peptides fail to inhibit microtubule polymerisation. However, if

mutant peptides lead to shorter (but still present) microtubules, it is possible that inhibition is still taking place to some degree. Determination of the K_d of each of the mutant peptides for tubulin, along with the data regarding microtubule length may give a better idea of the inhibition abilities of each peptide and further inform on the necessity of each of the studied residues.

Chapter 4) MTED-GFP inhibits cell proliferation by inhibiting microtubule polymerisation.

4.1. Introduction

The previous chapter characterised the binding interaction of the MTED peptide with tubulin. Its affinity for the tubulin heterodimer has been determined and its ability to inhibit microtubule polymerisation is a direct result of this binding activity. However, to explore the potential of MTED as a therapeutic, more information is required about the behaviour of MTED in a cellular context.

Microtubule-targeting drugs are currently used as cancer treatments and work by targeting and inhibiting the dynamic nature of microtubules, which in turn, inhibits cell division. Taxol, also known by its generic name of Paclitaxel, is perhaps the most well-known of these microtubule-targeting drugs and was the first to be developed as a chemotherapeutic. Taxol acts by promoting microtubule polymerisation and preventing their subsequent depolymerisation, leading to an inhibition of cell proliferation and cell death (Weaver 2014). Conversely, vinca alkaloids, such as Vinblastine, are a class of microtubule destabilisers that bind to the tubulin heterodimer and prevent its polymerisation (Dhyani, Quispe et al. 2022). While the two classes of drugs have differing modes of action, the result is the same: inhibition of cell proliferation and cell death.

MTED is hypothesised to fall into the latter category of microtubule destabilisers. However, determining whether MTED's cellular effect has therapeutic potential is only half the battle. All drugs, no matter their target, need an efficient delivery system and it is currently unknown whether the MTED peptide can enter cells.

Cell-penetrating peptides (CPPs) are a class of short (<30aa), usually cationic peptides that can enter cells through mechanisms such as, but not limited to, endocytosis or passive translocation (Xie, Bi et al. 2020). NFL-TBS.40-63 is one such peptide. Derived from the light chain of a neurofilament (NFL) containing a tubulin binding site (TBS), this 24-residue peptide has been shown to enter glioblastoma and human neuronal stem cells (hNSCs) by passive translocation in its wild-type state (Berges, Balzeau et al. 2012, Barreau, Montero-Menei et al.

2018) (Lepinoux-Chambaud and Eyer 2019). At a physiological pH of 7.4, the net charge of this peptide is 1.8, likely facilitating its attraction to the negatively charged cell membrane (Berges, Balzeau et al. 2012). While MTED has the advantage of being only 18 amino acids in length, at physiological pH 7.4, it has a net charge of -0.4, meaning that despite its small size, it is unlikely that it could pass unaided through the cell membrane.

If the MTED peptide cannot enter cells, it has been shown that modification of proteins to promote their uptake into the cell is possible. The addition of cationic protein transduction domains (PTDs) on the N and C terminus of a variety of proteins facilitates their rapid uptake into the cell (<6 hours), without any alterations to cell morphology, behaviour or metabolism (**Figure 4.1**) (Dixon, Osman et al. 2016). These extensions add a charge of 20.7 at pH 7.4 to their host protein, meaning that with these PTDs, MTEDs net charge would increase to approx. 20.3, increasing its chances of cellular uptake.

To investigate MTED's behaviour in a cellular context, a pre-existing DNA construct with the MTED sequence tagged with GFP was the ideal starting point. Transfection of DNA into cells is a well-documented and optimised process and the fusion to a reporter gene will easily confirm protein expression. Once the impact of this construct on cellular microtubules and cell proliferation has been determined, further investigations can be carried out using external addition of synthetic peptide.

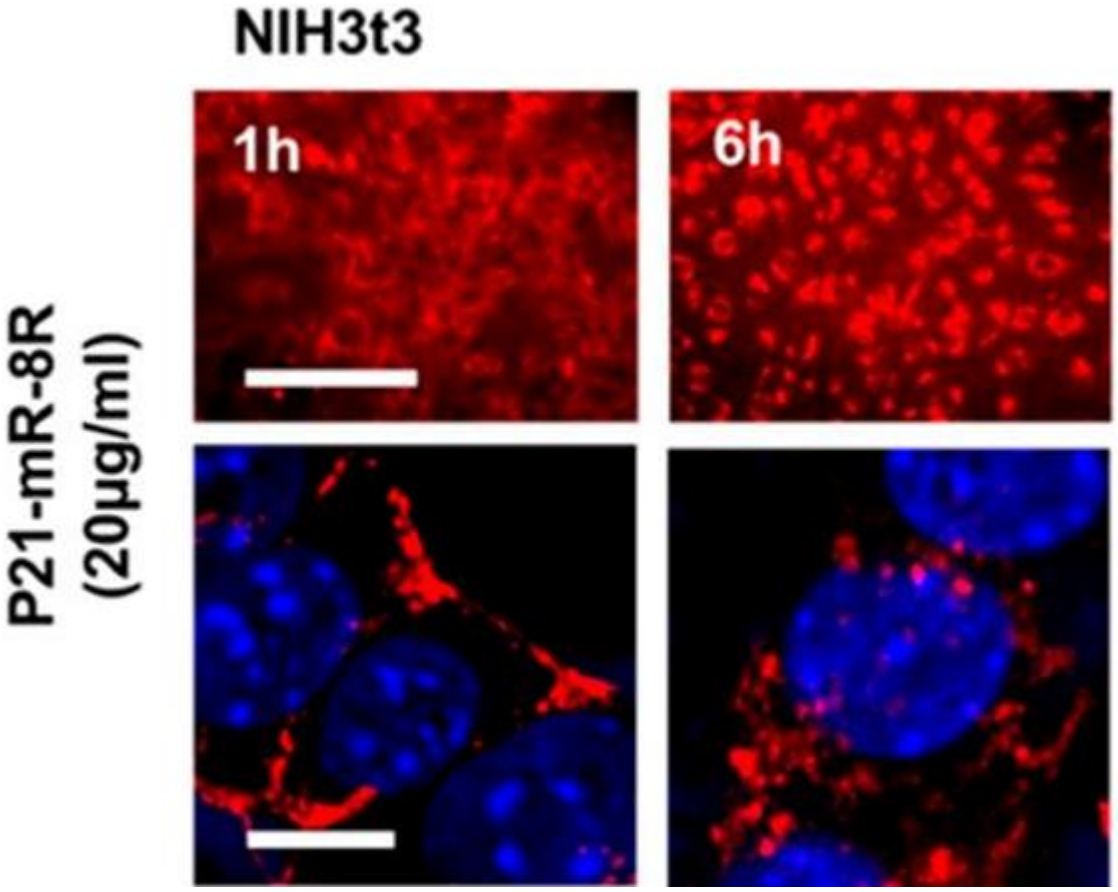

Figure 4.1) PTDs facilitate rapid uptake of cargo.

NIH3T3 cells treated with cargo modified with N- and C-terminal PTDs, imaged 1hr and 6hrs post treatment. Adapted from (Dixon, Osman et al. 2016).

4.2. Aims

To study the impact of the MTED peptide in cells, I set out the following aims for this chapter:

1) The creation of a DNA construct encoding the Scrambled peptide as a control for DNA experiments
2) To determine the impact of these constructs on the microtubule network and morphology of mammalian cells
3) To determine what effect these constructs have on cell division
4) To determine whether the synthetic MTED peptide can directly enter cells
5) What modifications, if any, are necessary to facilitate its entry into cells
6) Once within cells, what effect does synthetic MTED have on the microtubule network, cell morphology and proliferation.

Taken together, these results will inform on MTED's cellular impact and how to target it into cells to make it a candidate for further development as a therapeutic.

4.3. Creation of Scrambled-GFP

An MTED-GFP expression plasmid (Qu, Hahn et al. 2019) was kindly provided by Dr Ines Hahn from the lab of Dr Andreas Prokop, University of Manchester. A suitable control for this plasmid was not available and so a Scrambled-GFP DNA construct was created. A gBlock was designed and ordered from IDT containing the Scrambled MTED DNA sequence, flanked by KpnI and NotI restriction sites, as these were the restriction sites that flanked the MTED-GFP sequence (**Figure 4.2a**). The Scrambled gBlock was digested with 10 units of KpnI and NotI in a single reaction, PCR cleaned and stored at -20°C until further use. 2µg of MTED-GFP was digested with 10 units of KpnI and NotI in a single reaction, and the digest run on a 0.8% (w/v) agarose gel. *In silico* digestion of this plasmid using ApE showed 101bp released leaving a 6097bp vector, which is what was seen on the gel (**Figure 4.2b**). The 6kb band containing the linearised DNA backbone was excised and the DNA extracted from the gel. The digested plasmid and gBlock were combined in a ligation reaction at 4°C overnight and the products of this reaction were transformed into DH5-α bacteria. Single colonies were selected, grown up overnight and plasmid DNA extracted via mini-prep. A diagnostic digest was carried out on the purified plasmid samples using the restriction enzyme StuI, which was predicted to have one cut site in the Scrambled-GFP plasmid and two in the MTED-GFP plasmid. Upon digestion with StuI, the plasmid containing MTED-GFP runs as two bands of the size expected (4327 and 1871bp) when the plasmid is cut twice at the StuI restriction sites (**Figure 4.2c**). By contrast, the samples of plasmid expected to contain Scrambled-GFP all produced a single band at the expected size of the linearized plasmid (6198bp). Two colonies confirmed by diagnostic digest were sent for sequencing for further confirmation of the identity of the plasmid created (**Figure 4.2d**).

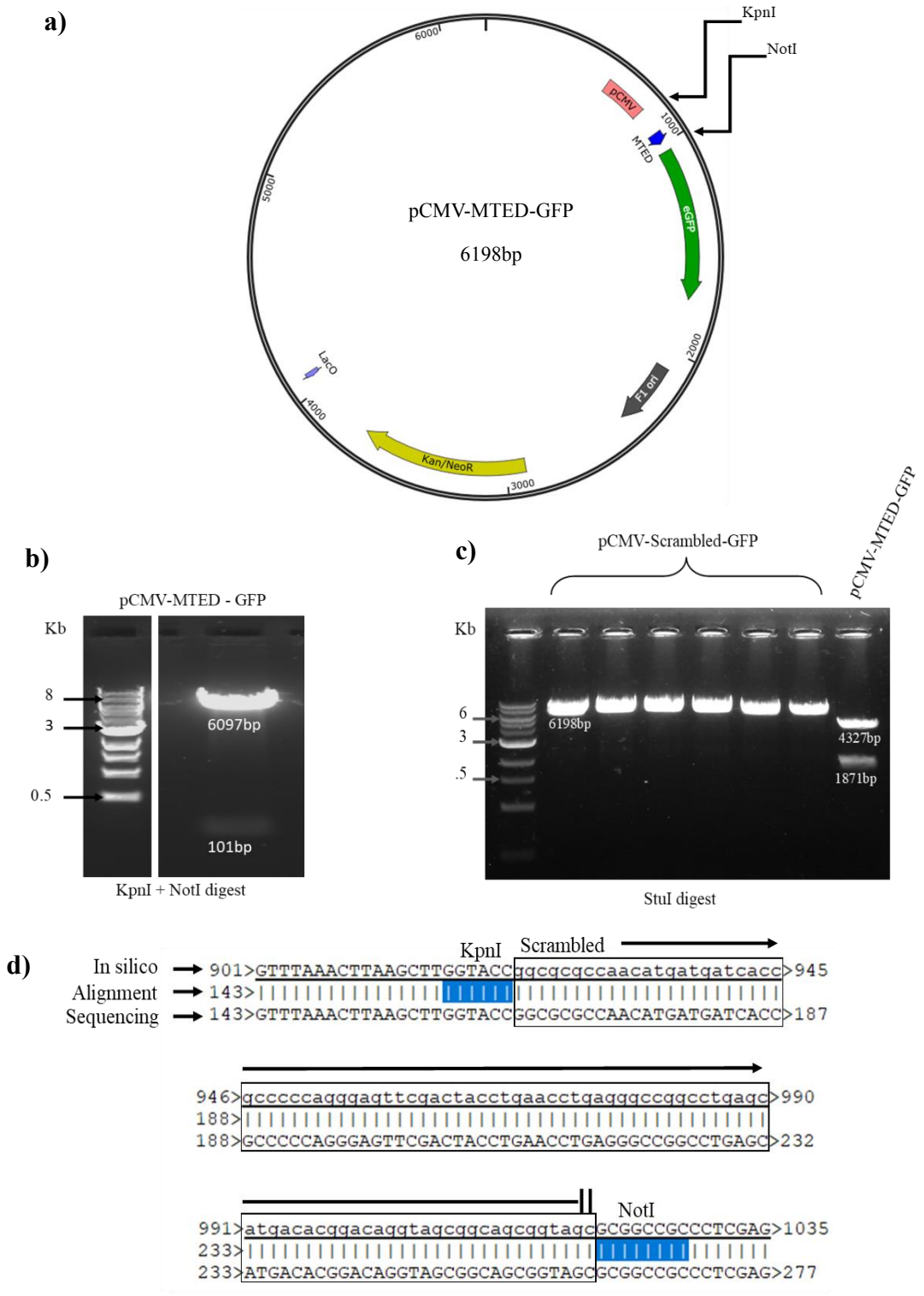

Figure 4.2) Creation of Scrambled-GFP.

a) Plasmid map of Scrambled-GFP created *in silico*, with restriction sites flanking MTED highlighted. b) agarose gel of pCMV-MTED-GFP digested with KpnI and StuI to release the 6kb vector backbone. c) agarose gel of a diagnostic digest of pCMV-Scrambled-GFP with StuI, and pCMV-MTED-GFP in the final lane for comparison. d) in silico alignment of the predicted pCMV-Scrambled-GFP sequence and the true sequence. Restriction sites are highlighted in blue.

4.4. MTED-GFP disrupts the microtubule network

MTED-GFP and Scrambled-GFP were transfected into HeLa cells, which were fixed and stained for α-tubulin. The stain was allowed to develop overnight in the dark at 4°C. Cells were imaged by confocal fluorescence using 1) a TRITC filter for visualisation of the immunohistochemically stained microtubule network and 2) a FITC filter for plasmid GFP expression.

All cells shown to express MTED-GFP had very disordered microtubule networks. No MTED-GFP expressing cells had microtubules that extended radially to the edge of the cell, and instead had condensed networks which predominantly circled the nucleus and defined the cell membrane (**Figure 4.3a**). In contrast, cells expressing Scrambled-GFP had much more structured and spread-out microtubule networks (**Figure 4.3b**). In these cells, individual microtubules were easily discernible when visualised directly on the coverslip using the microscope eyepiece, and at the post-imaging analysis stage using ImageJ. At either stage it was difficult to resolve microtubules in cells expressing MTED-GFP.

4.5. MTED-GFP affects cell morphology

As is evident from **Figure 4.3**, cells expressing MTED-GFP not only had much more irregular microtubule networks but appeared much smaller in size than those expressing Scrambled-GFP. It was possible, however, that while the microtubule network was much smaller in MTED-GFP cells, the cell itself may not have changed in size. Brightfield images were therefore taken of cells expressing either MTED-GFP or Scrambled-GFP to examine cell morphology, and the two dimensional (2D) area of each cell expressing MTED-GFP or Scrambled-GFP, was measured in ImageJ, by thresholding the image, outlining the cell of interest and measuring the area of the cell inside the outline (**Figure 4.4**). As expected, cells expressing MTED-GFP were statistically significantly smaller ($p<0.0001$, t-test), with an average 2D area of 182.47±52.94 μm^2 (n=15 cells), compared to Scrambled-GFP cells, with an average area of 791.81±238.4 μm^2 (n=11 cells). Untransfected cells in the same field of view as MTED-GFP and Scrambled-GFP cells, identifiable by their lack of GFP expression, had an average two-dimensional area of 747.47±313.73μm^2 (n=8 cells), not significantly different to Scrambled-GFP cells ($p=0.739$, t-test), showing that the Scrambled-GFP construct has no effect on cell morphology.

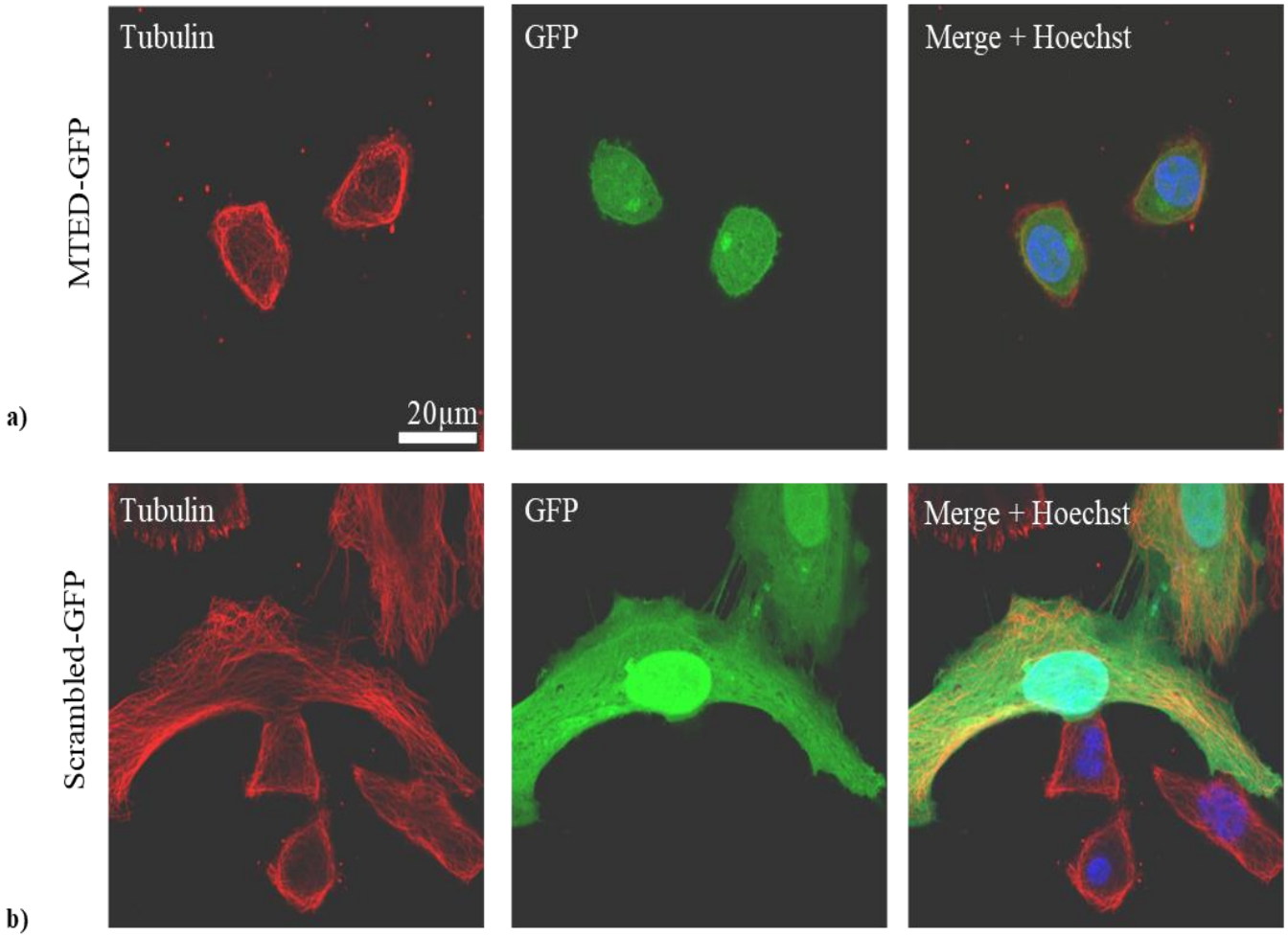

Figure 4.3) MTED-GFP disrupts the microtubule network.

Confocal fluorescent images of HeLa cells transfected with a) MTED-GFP and b) Scrambled-GFP. The microtubule cytoskeleton was stained in all cells, with GFP expression verifying which cells had been successfully transfected and were expressing the construct.

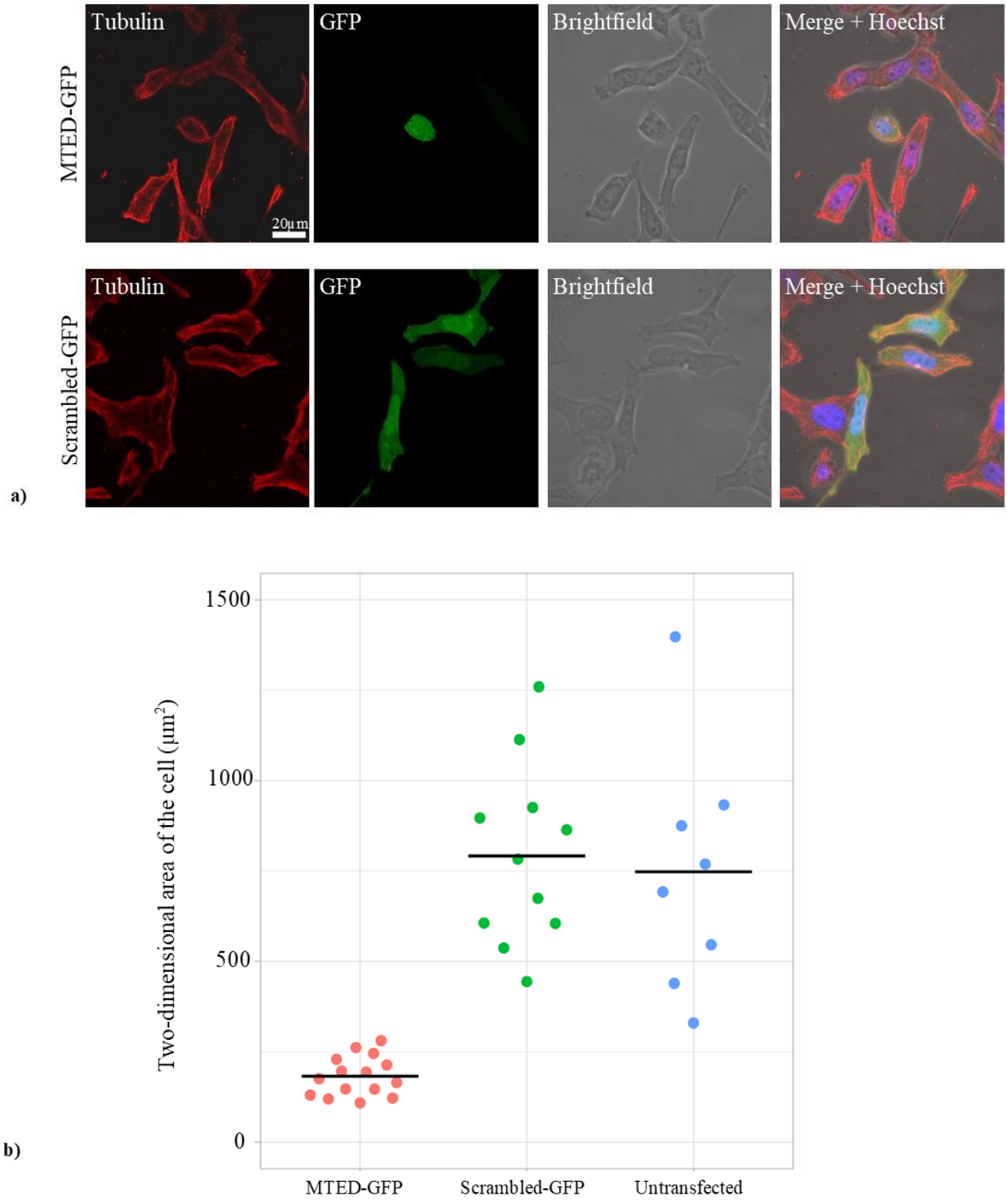

Figure 4.4) MTED-GFP significantly alters cell morphology.

a) Confocal, fluorescent and brightfield images of HeLa cells transfected with MTED-GFP and Scrambled-GFP. The microtubule cytoskeleton was stained in all cells, with GFP expression verifying which cells had been successfully transfected and were expressing the construct. b) Jitter plot showing the quantification of the two-dimensional area of MTED-GFP and Scrambled-GFP expressing cells.

4.6. MTED-GFP inhibits cell proliferation

To determine whether transfecting cells with MTED-GFP impacted cell proliferation, I wanted to carry out a proliferation assay by counting the number of cells over a set time frame. However, previous data (section 4.4) showed that cells expressing MTED-GFP were significantly smaller in terms of measured cell area than those expressing Scrambled-GFP (**Figure 4.4**). When growing in adherent culture, HeLa cells form proteinaceous attachments along the surface of the culture vessel and require the use of a proteinase such as trypsin to break these adhesions to remove cells. Therefore, it is possible that cells expressing MTED-GFP would form fewer attachments to the culture vessel, due to their reduced surface area, and dislodge more easily than cells expressing Scrambled-GFP during routine cell culture. This could result in many MTED-GFP cells being lost during washing prior to the addition of trypsin.

To account for this, when MTED-GFP and Scrambled-GFP expressing cells were counted over a four-day period, cells in the wash and cells removed after trypsinisation were retained and counted separately, ensuring the entire population was accounted for. Cells collected in the post-trypsinisation sample were re-seeded in a fresh culture well and continued to grow until the next time point, when cells were collected and counted in the same way.

The number of cells in each sample (wash and trypsin) were combined to determine the total cell number. The total number of cells in the MTED-GFP-expressing sample was significantly reduced compared to the Scrambled-GFP-expressing sample at the 48h, 72h and 96h timepoints ($p<0.05$ at 48, 72 and 96 hours post transfection, t-test) (**Figure 4.5a**).

Next, I calculated the percentage change in the number of cells between time points over the course of the assay. Cells expressing Scrambled-GFP consistently increased in number by ~40% over each 24-hour period (**Figure 4.5b**). By contrast, in the 24-48 hours post transfection period, cells expressing MTED-GFP decreased in number by 33±14%. The decrease in cell number for the MTED-GFP population compared to Scrambled-GFP was significantly different over the 24-48h period ($p<0.0001$, t-test). However, for the remainder of the assay (48-72- and 72-96-hour time points) there was no significant difference in the percentage change in cell number between the two samples ($p>0.05$, t-test).

a)

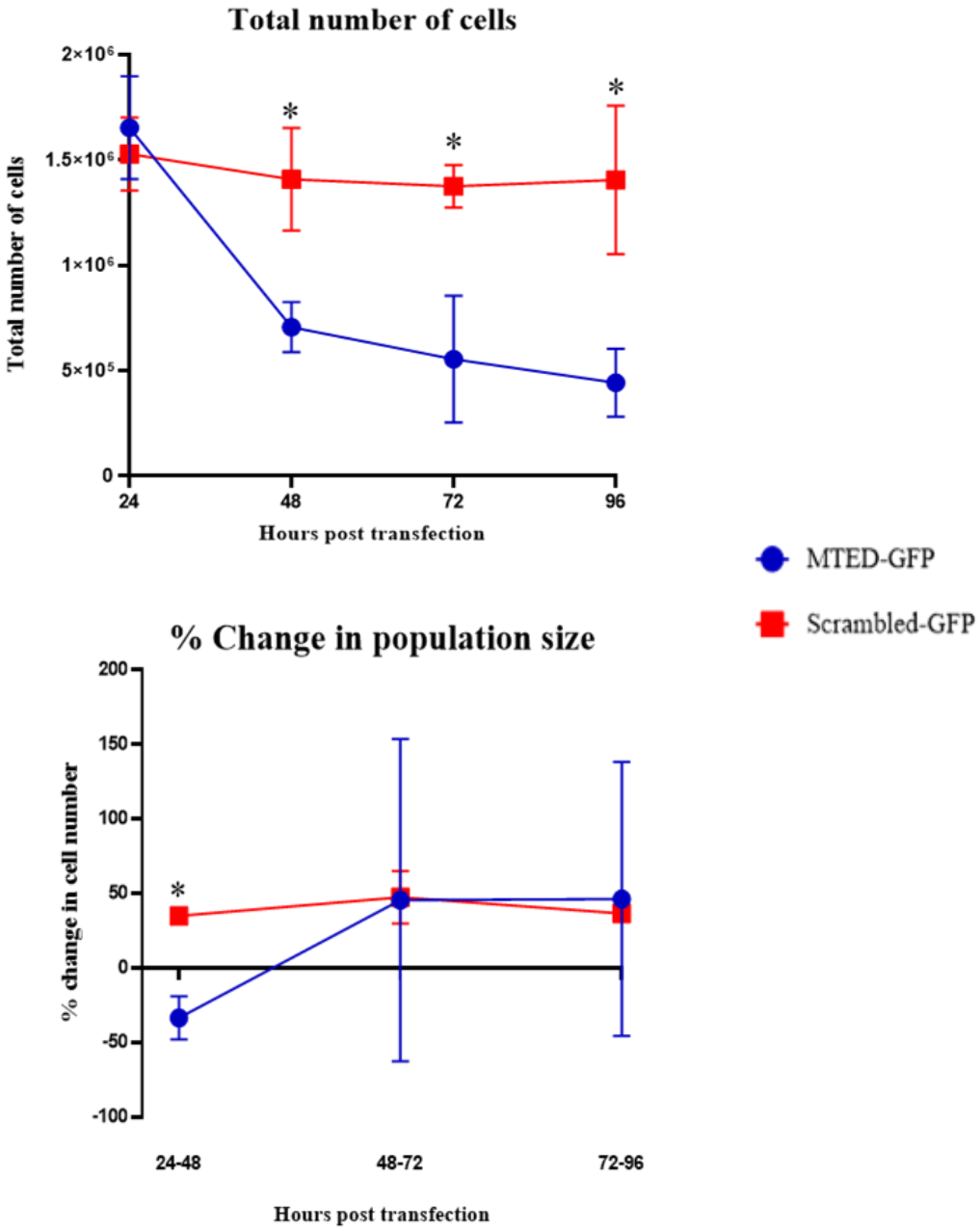

Figure 4.5) MTED-GFP cells are significantly fewer in number compared to Scrambled-GFP.

Graphs showing the total number of cells in the MTED-GFP (blue) and Scrambled-GFP (red) populations over the course of the assay. Asterisks above the data points represent a significant difference between the samples. Error bars represent one standard deviation, n=3 for each sample in each assay.

When the data from detached (washes) and attached (trypsinised) cells were analysed separately, there is no significant difference in the number of cells collected during washing between the MTED-GFP and Scrambled-GFP populations at any time point ($p>0.05$ at all time points, t-test). Similarly, the number of cells collected during trypsinisation is not significantly different between the two populations at the 24-, 48- and 72-hour time points ($p>0.05$ at these time points, t-test). However, 96 hours post transfection, there are significantly fewer cells collected in the trypsin sample from the MTED-GFP population, compared to the Scrambled-GFP population ($p<0.05$, t-test) (**Figure 4.6a**)

When represented proportionally, the MTED-GFP population loses significantly more cells during washing 24- and 48-hours post-transfection, compared to the Scrambled-GFP population ($p<0.05$, t-test). However, for the remainder of the assay, there is no significant difference in the proportion of cells lost during the wash between the populations ($p>0.05$ at the 72- and 96-hour time points, t-test) (**Figure 4.6b**).

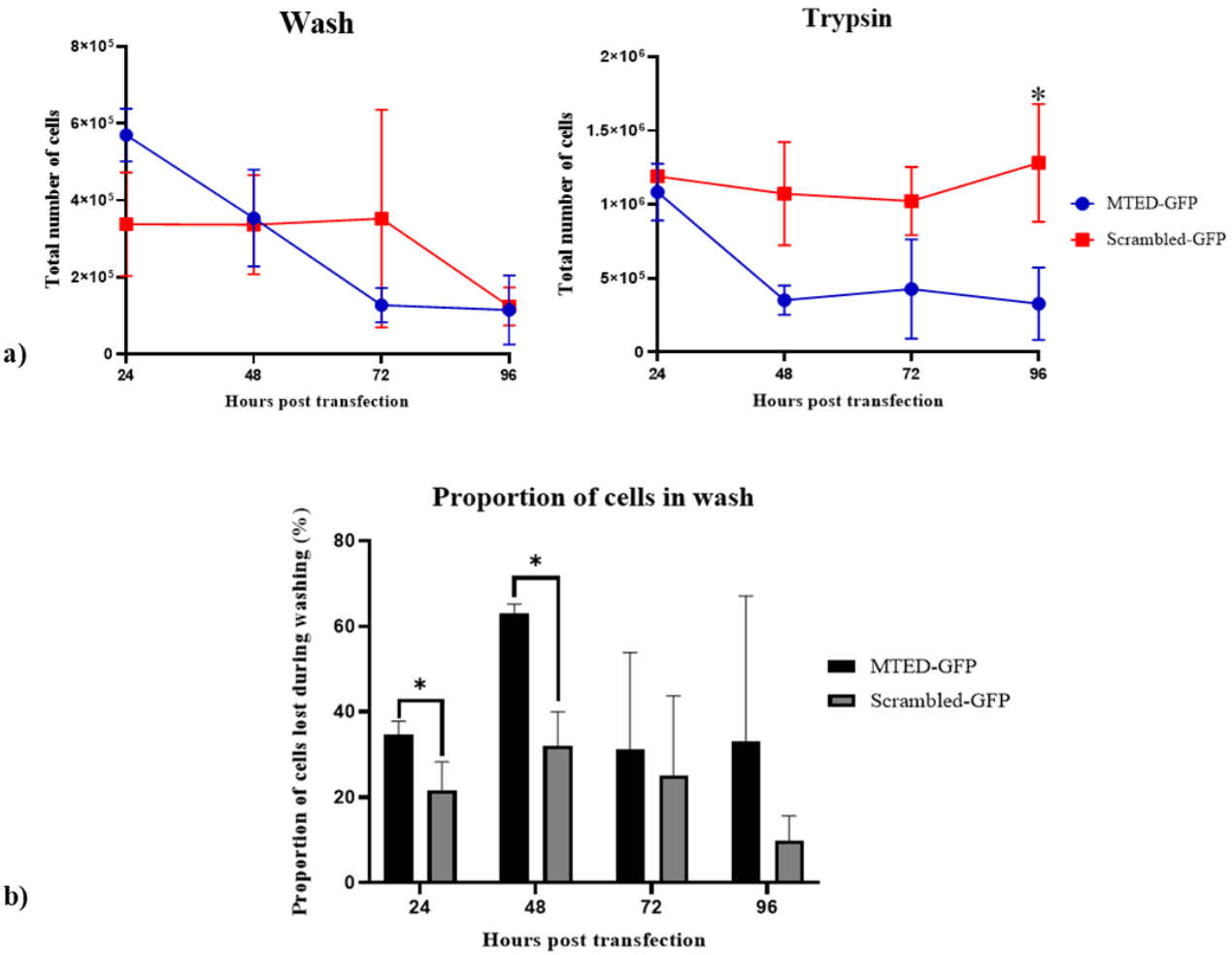

Figure 4.6) MTED-GFP significantly decreases cell adhesion.

Graphs showing the total number of cells in the wash and trypsin samples at each time point of the assay. b) Proportional representation of the number of cells lost during washing in the MTED-GFP and Scrambled-GFP populations. Error bars represent one standard deviation, asterisks represent a significant difference between the data points. n=3 for each sample in each assay.

Figure 4.5 shows that by the 48-hour time point, the total number of cells in the MTED-GFP population is significantly lower than the Scrambled-GFP population and continues to decrease until the end of the assay. This indicates that the MTED-GFP construct is inhibiting cell proliferation, likely as a result of its microtubule inhibition abilities.

To further examine this data, I first measured the proportion of cells expressing each construct 24 hours after transfection using Fluorescence-activated Cell Sorting (FACS). At this time-point, both populations had a similar transfection efficiency of ~30% (**Figure 4.7**). Next, to determine what proportion of cells continued to express each construct at the end of the assay, I repeated FACS at the 96-hour time point. At this stage, the proportion of cells expressing MTED-GFP had dropped to 24%, while 73% of the Scrambled-GFP population were expressing the construct (**Figure 4.7**). Fluorescent images were also taken of each population at the 24- and 96-hour time points for direct visualisation of GFP-expressing cells. MTED-GFP and Scrambled-GFP have a similar proportion of GFP positive cells 24 hours after transfection, which agrees with the FACS data (**Figure 4.8**). At the 96-hour mark, however, many more cells are GFP-positive in the Scrambled-GFP population compared to MTED-GFP, again matching the FACS data.

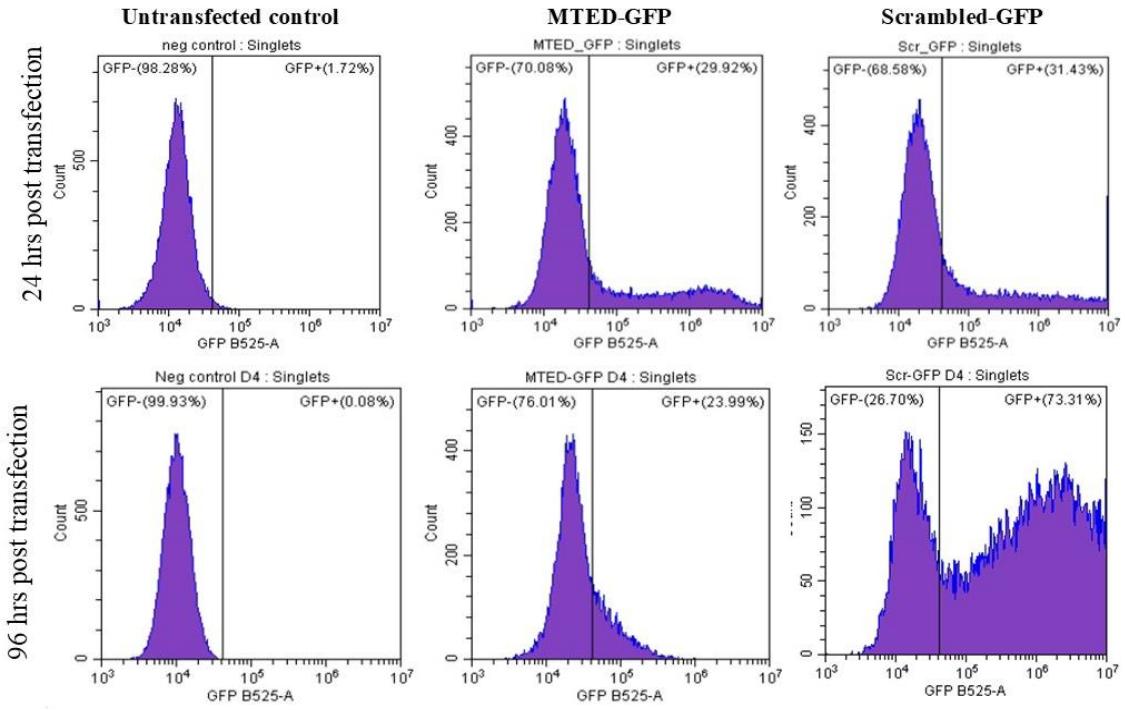

Figure 4.7) MTED-GFP expression decreases within 96 hours.

FACS data showing the proportion of fluorescent cells in an untransfected population, a population transfected with MTED-GFP and Scrambled-GFP 24 and 96 hours after transfection. X axis = intensity of the fluorescent signal; y axis = raw number of cells counted. Graphs generated using Kaluza flow cytometry analysis software.

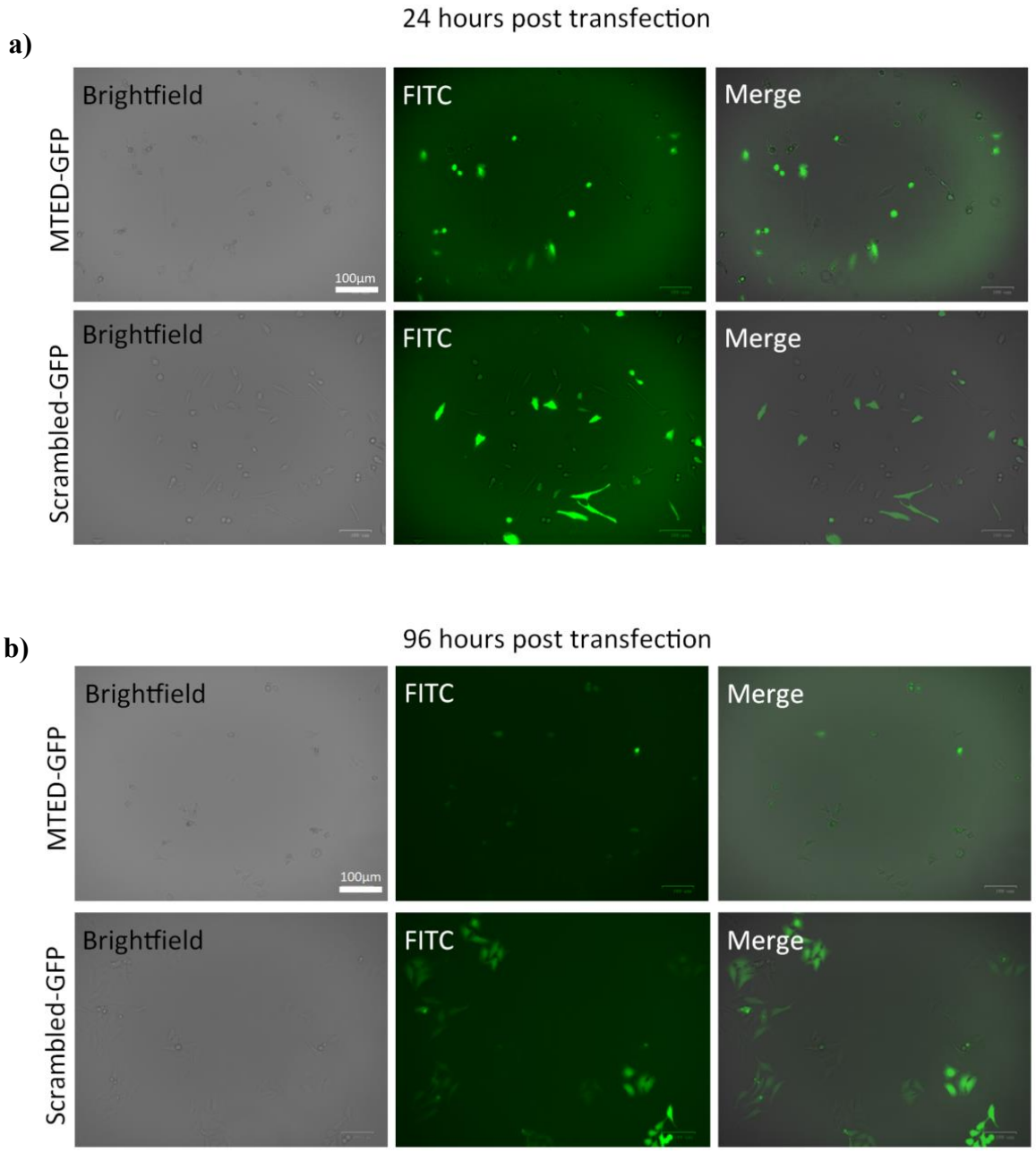

Figure 4.8) MTED-GFP- expressing cells are lost within 96 hours

Brightfield, FITC and Merge images taken of cells expressing MTED-GFP and Scrambled-GFP 24 and 96 hours after transfection to visualise the proportion of cells expressing GFP in both populations over the course of the assay.

In summary, MTED-GFP inhibits cell proliferation as a direct result of its microtubule inhibition abilities. By the 48-hour post transfection time point, the MTED-GFP population is significantly smaller in number compared to the Scrambled-GFP population, as seen in **Figure 4.5a**. This agrees with **Figure 4.5b,** which shows that within these first 48 hours, the MTED-GFP population decreases by 33±14%. For the remainder of the assay, the MTED-GFP and Scrambled-GFP populations proliferate at the same rate. This is likely due to cells expressing MTED-GFP 1) not dividing and 2) being outcompeted by cells that have not taken up the construct and are dividing. This is confirmed by FACS data in **Figure 4.7**, which shows that the proportion of cells expressing MTED-GFP drops from 30% to 24% within 96 hours, while the proportion of cells expressing Scrambled-GFP grows from 30% - 75%. As only 24% of cells in the MTED-GFP population are expressing the construct by the 96-hour time point, the remaining 76% of cells are proliferating at the same rate as those in the Scrambled-GFP population, agreeing again with **Figure 4.5b.**

4.7. The wtMTED peptide cannot enter cells

Expression of MTED in cells via transfection with DNA constructs is an effective way to study the peptide's effect on cytoskeletal microtubules and cell division. Reliable protocols already exist for transfection of cells with plasmid DNA, and the GFP-label allows for visual confirmation of protein expression. However, to develop MTED as a therapeutic, it is necessary to develop a method to deliver the peptide directly into cells. The ability to introduce synthetically generated MTED peptide would eliminate the need for transfection agents, waiting times for plasmid transcription and translation and potentially give better control over the concentration of peptide available to cells.

I first tested whether MTED added externally to cultured cells would be internalised and impact MT growth. It was unlikely that WT-MTED could cross the cell membrane, however, a peptide derived from neurofilament protein has been observed to penetrate glioma cells without any modification (Berges, Balzeau et al. 2012). I first needed to estimate what concentration of peptide should be added to cells that would inhibit microtubules growth. To do this, I carried out microtubule growth assays with varying MTED : tubulin ratios, ranging from 2:1 (the ratio used in previous microtubule growth assays) to 0.5:1. Inhibition was seen at the 2:1 and 1:1 ratios, but at 0.5:1 microtubules were seen, although they were reduced compared to the no peptide control (**Figure 4.9**). Assuming a cellular tubulin concentration of ~24μM (Gard and Kirschner 1987), I decided to use 30μM MTED to allow for an excess of peptide to tubulin.

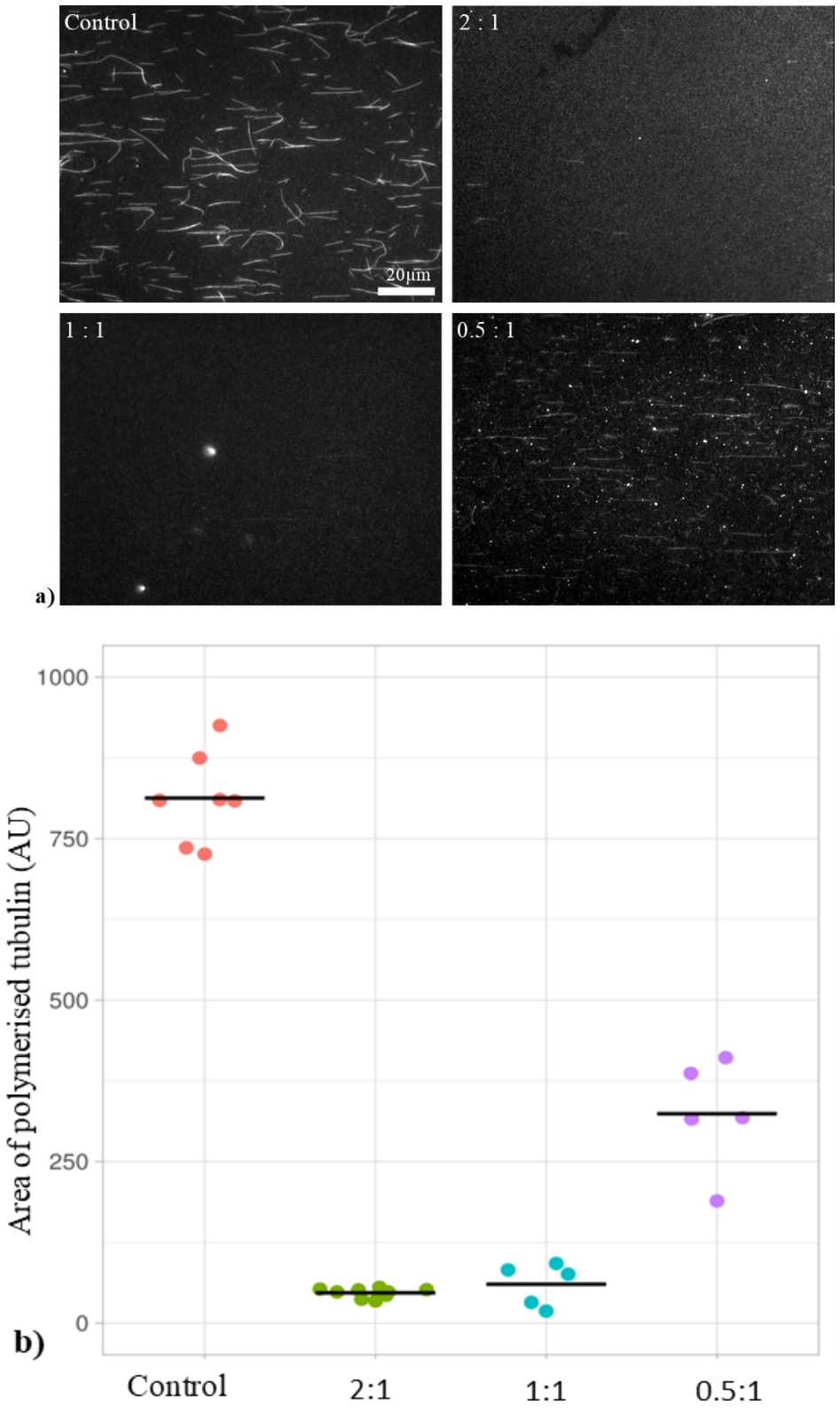

Figure 4.9) MTED inhibits tubulin polymerisation at a 1:1 ratio.

a) fields of view showing the results of a microtubule growth assay carried out in the presence of decreasing concentrations of peptide. Scale bar represents 20µm. b) Jitter plot showing the quantified area of tubulin able to polymerise in the presence of decreasing concentrations of peptide. Horizontal bars denote the mean value of each dataset.

As previously mentioned, the MTED peptide does not retain microtubule growth-inhibiting activity when stored for more than two days in any solvent tested apart from DMSO. Therefore, when adding synthetic peptide directly to cells, some DMSO would also be added. As DMSO is toxic to cells, I determined the highest concentration of DMSO cells could tolerate using a cell survival assay. Cells were incubated with DMSO concentrations ranging from 0 – 2.5% at 37°C, 5% CO_2 overnight. The following day, all cell cultures were washed, trypsinised and incubated with Trypan blue (1:1), and the percentage viability of each of these samples was determined using a CellDrop BF cell counter on the Trypan blue setting. (**Figure 4.10**). In 1% DMSO, 50% of cells remained viable after 24h. Therefore, it was decided that 1% DMSO could be introduced when adding peptide externally to cells. A 3mM stock of MTED was therefore made up in 100% DMSO, allowing MTED to be added to cells at a final concentration of 30µM, with a final DMSO concentration of 1%.

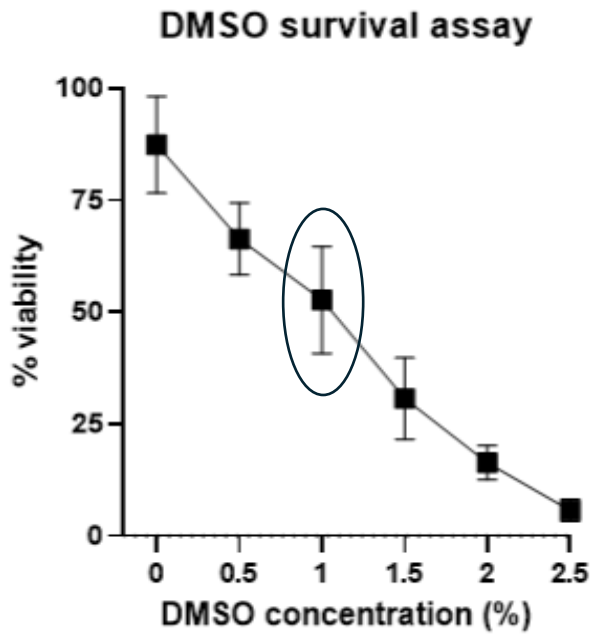

Figure 4.10) Percentage cell viability after treatment with increasing concentrations of DMSO.

The % viability of HeLa cells measured 24 hours after treatment with varying concentrations of DMSO, measured using Trypan blue. The datapoint at 1% DMSO is highlighted as this is the concentration that, based on this data, was used for further assays. Error bars represent one standard deviation: n=3, where n is the number of biological repeats.

Both unlabelled MTED and MTED labelled with fluorescein (MTED-Fl) were added externally to HeLa cells in culture. Despite not inhibiting microtubule growth, MTED-Fl would allow visual confirmation of whether the peptide entered cells.

3mM peptide (dissolved in 100% DMSO) was diluted to 30µM in DMEM (for a final DMSO concentration of 1%) and filter sterilised with a 0.22µm filter. Cells were washed and incubated with peptide-containing media at 37°C, 5% CO_2 overnight. Cells were then fixed and stained for α-tubulin and imaged the day after staining (**Figure 4.11a**).

Cells incubated with the wtMTED peptide did not look morphologically different to the 1% DMSO control population, and there was no obvious observable difference in the appearance of the microtubule network, suggesting this peptide has not entered cells. In the case of MTED-Fl, no internal fluorescent signal was observed in any of the cells, and there was no disruption of the microtubule network. Additionally, there was no significant difference in the 2D area of the cells among all three populations ($p>0.05$, one-way ANOVA), supporting the hypothesis that the wild type peptide cannot enter cells.

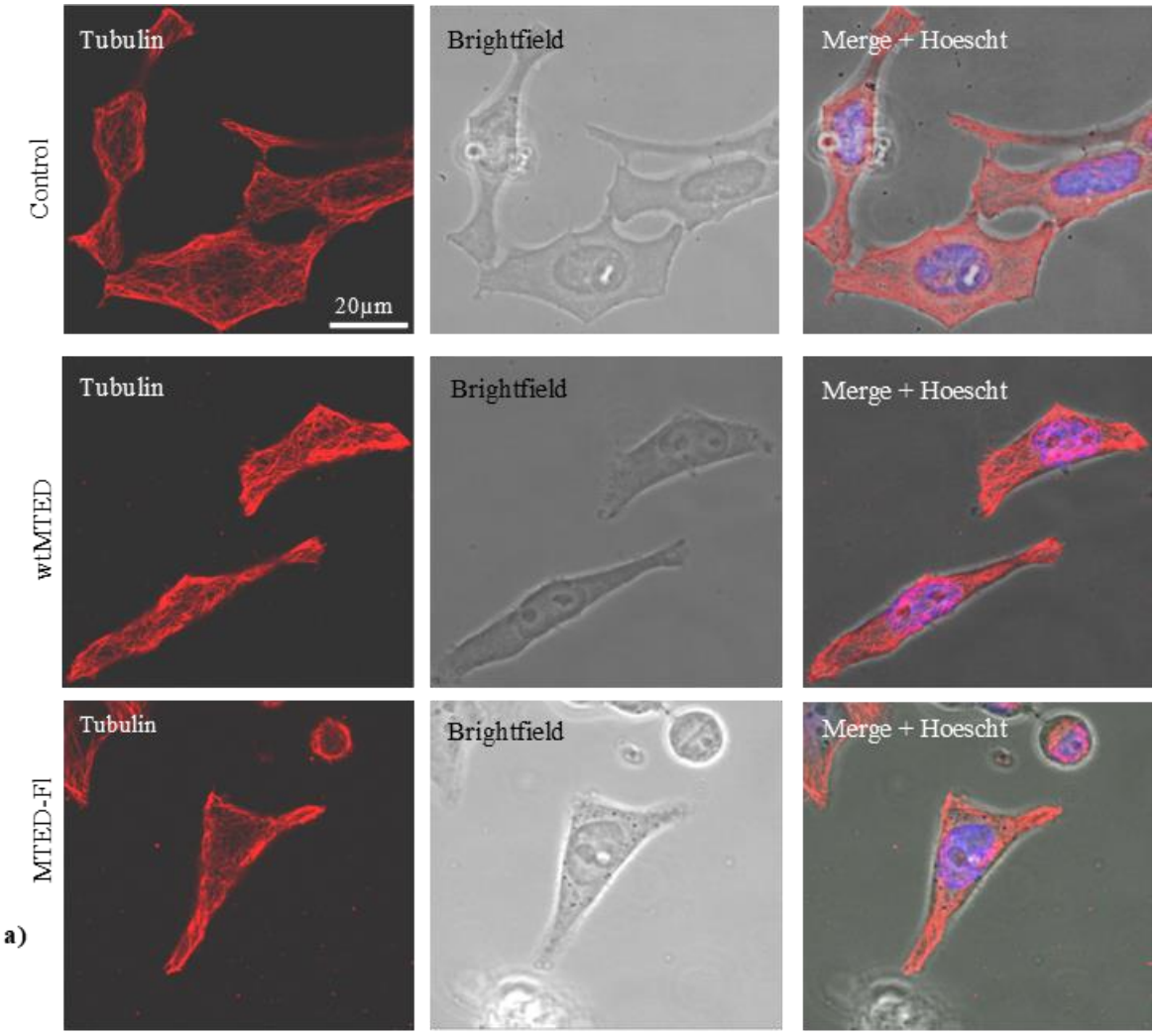

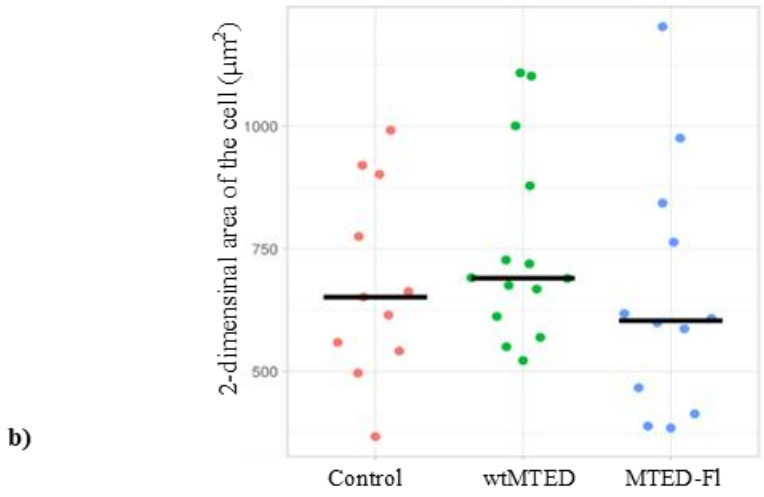

Figure 4.11) The MTED peptide cannot enter cells.

a) Confocal fluorescent and brightfield images of HeLa cells treated with wtMTED and MTED-Fl peptides and stained for α-tubulin. B) Jitter plot showing the quantified 2-dimensional area of the cell (μm^2), with each data point representing one cell. Horizontal bars denote the mean value of each dataset.

4.8. Protein transduction domains added to wtMTED allow for peptide entry into cells

Having confirmed that wtMTED does not directly enter cells, I trialled adding protein transduction domains (PTDs) to the peptide as a non-transgenetic tool to allow direct delivery of the peptide to cells.

Dixon et al. (2016) described a series of residues that were added to the amino (KRKKKGKGLGKKRKPCLRKYK; referred to as "K" onwards) and carboxyl (RRRRRQRRR; referred to as "R" onwards) termini of an RFP reporter construct. These added residues allowed rapid uptake of RFP by cells (<6 hours) without affecting cellular morphology or behaviour.

To try and achieve the same results with the MTED peptide, several new peptides with these extensions were synthesised: K-MTED-R, K-Scrambled-R, and a fluorescent version of each, K-MTED-R-Fl and K-Scrambled-R-Fl. The addition of the fluorophore would allow for visual confirmation of whether the modified peptides could enter cells. To ensure these extensions did not interfere with MTED's ability to bind to tubulin and inhibit its polymerisation, microtubule growth assays were carried out with all four newly synthesized peptides (**Figure 4.12**). K-MTED-R and K-MTED-R-Fl did inhibit tubulin polymerisation. However, an unexpected impact of the addition of these N- and C-terminal extensions was that the scrambled peptide control also inhibited microtubule growth, an activity not observed for scrambled peptide alone. These data confirm that the MTED peptide with PTD extensions retain the ability to inhibit microtubule growth. Therefore, despite the unexpected impact on the scrambled controls, these peptides were tested for their ability to enter cells and impact the microtubule network.

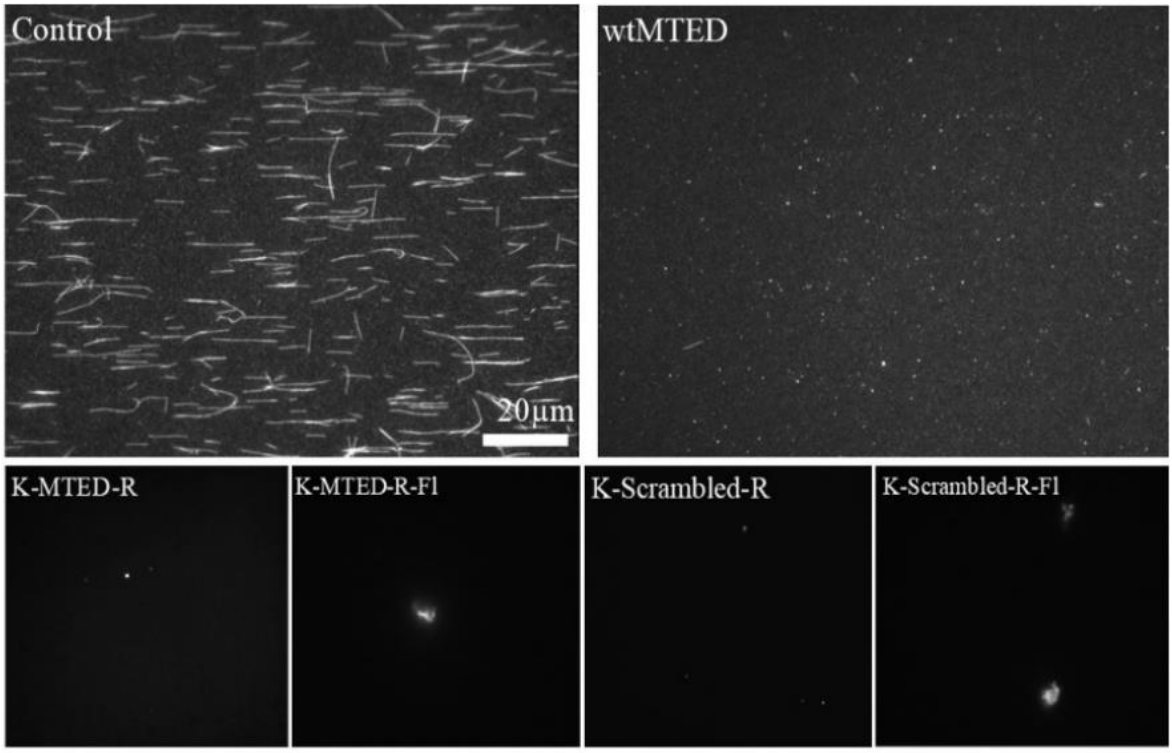

Figure 4.12) MTED and Scrambled peptides with PTDs inhibit tubulin polymerisation.

Fields of view of a microtubule growth assay carried out with wtMTED and four additional peptides with the N and C terminal PTDs. Images were not quantified as the aim of the experiment was to visualise the lack of microtubules to show that the peptides with K and R extensions bound to tubulin and inhibited microtubule growth.

Cells were incubated with 30μM peptide (K-MTED-R, K-Scrambled-R and their fluorescent counterparts) at 37°C, 5% CO_2 overnight, fixed and stained for α-tubulin and imaged the day after staining. Control cells were incubated with 1% DMSO.

Cells treated with K-MTED-R and K-Scrambled-R had an average area of 242±72μm^2, n=15; and 253±55μm^2, n=15, respectively, statistically significantly smaller than cells treated with 1% DMSO (681±187μm^2, n=11) ($p<0.0001$, t-test), and looked morphologically different (**Figure 4.13**). These data suggests that the addition of N- and C-terminal PTDs allows these peptides to enter the cell and impact the microtubule network, condensing and preventing it from extending radially throughout the cell, confirmed by cells incubated with the fluorescent versions of each peptide having internal fluorescence and being morphologically different and significantly smaller than control cells ($p<0.0001$) (**Figure 4.14**).

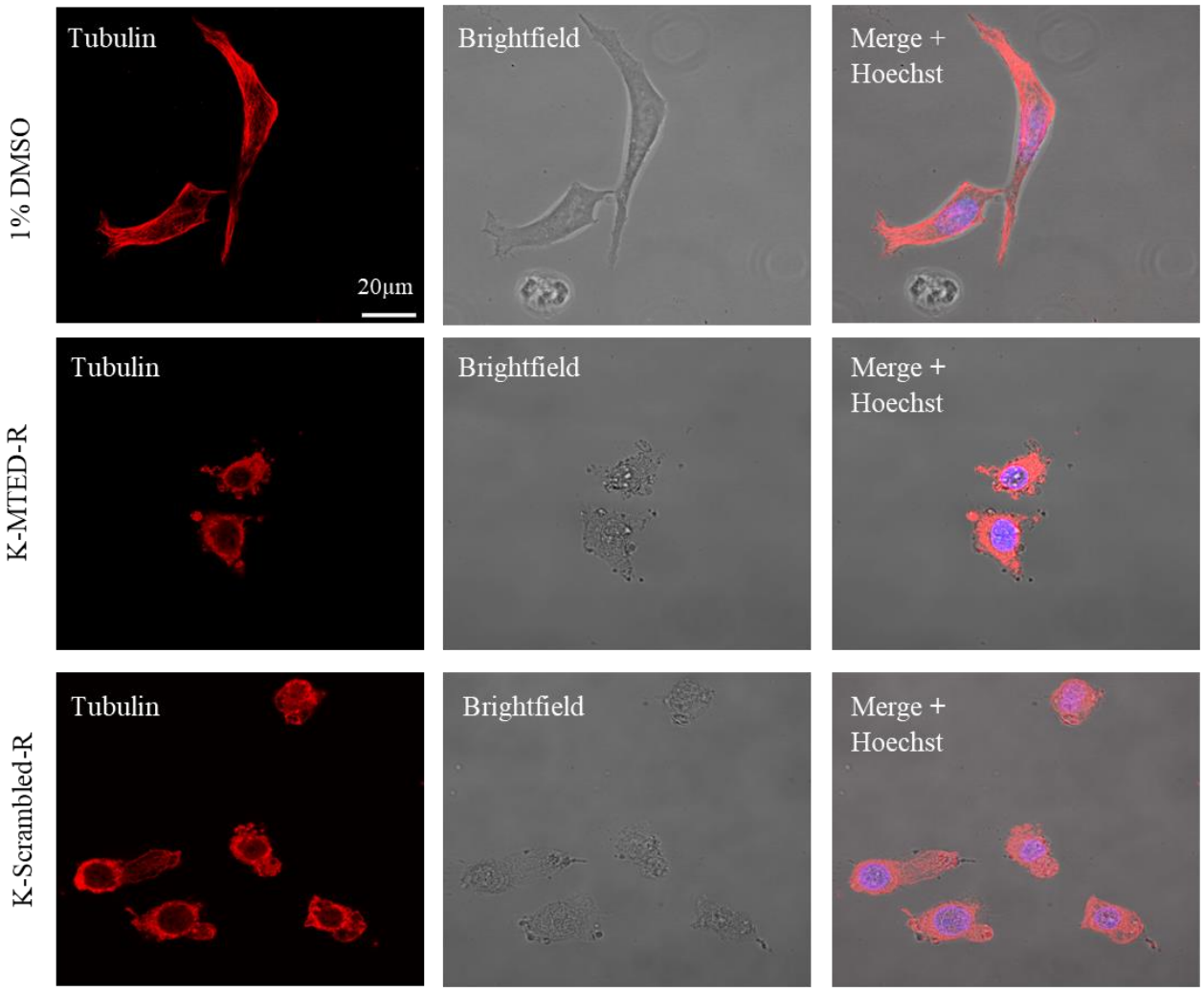

Figure 4.13) PTDs allow peptide uptake into cells.

Confocal fluorescent and brightfield images of HeLa cells treated with K-MTED-R and K-Scrambled-R. α-tubulin is stained in red, and the nucleus in blue.

a)

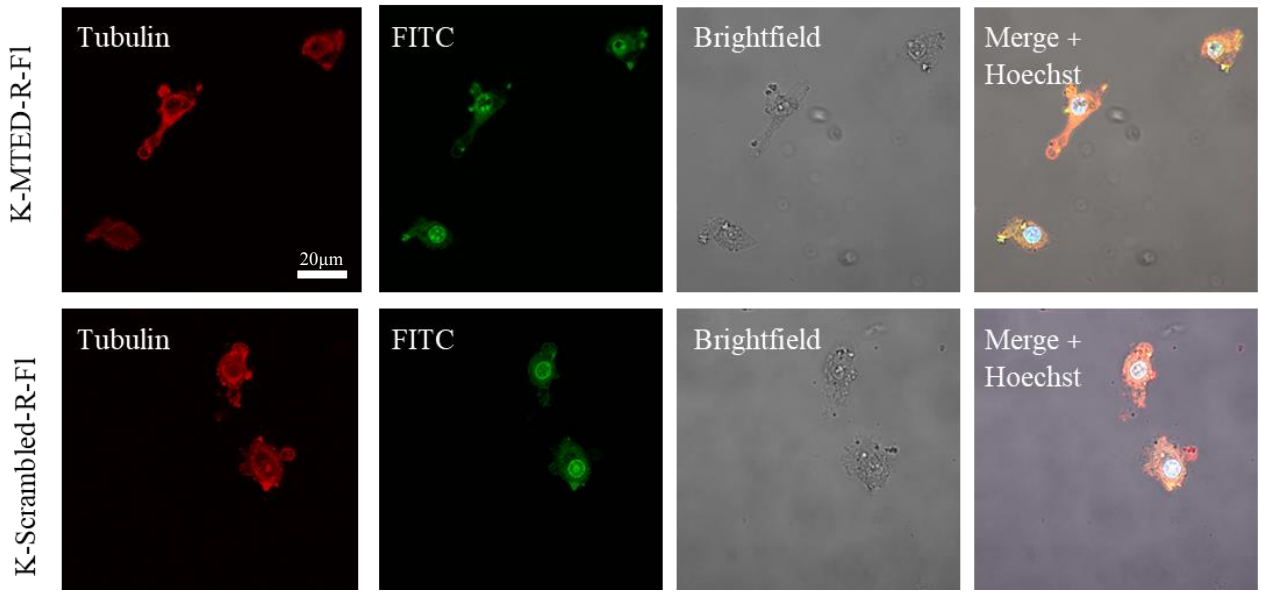

b)

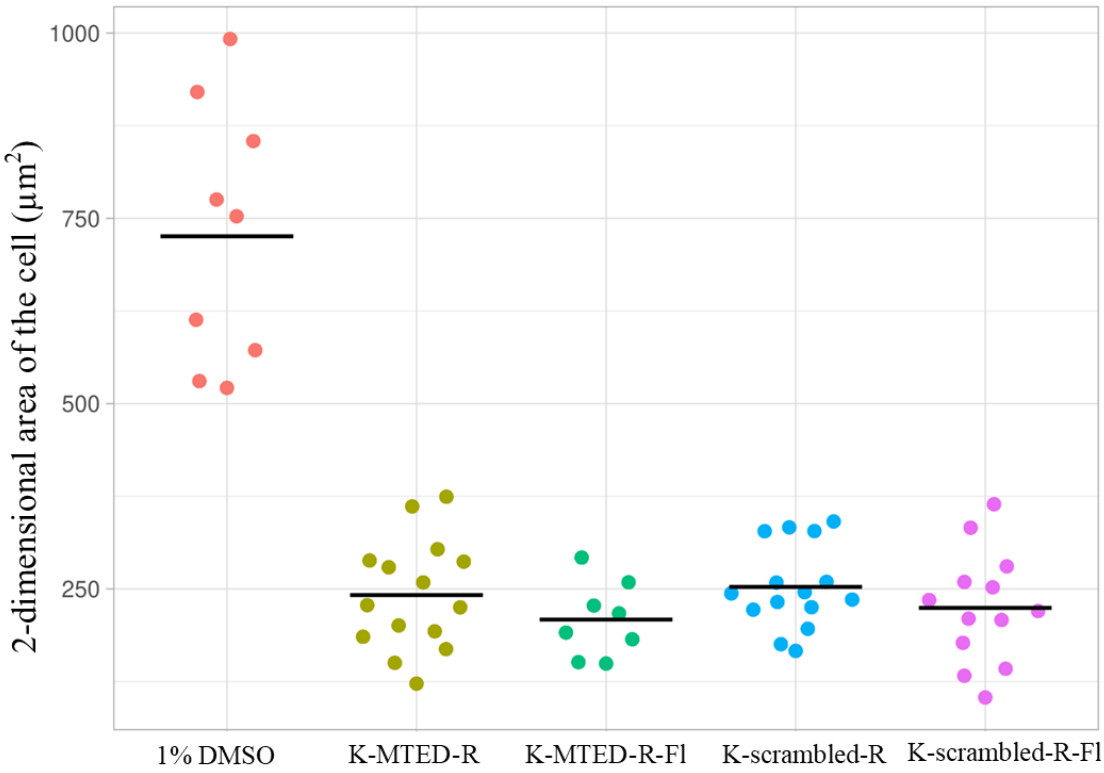

Figure 4.14) Protein transduction domains allows for peptide uptake into cells.

a) Confocal fluorescent and bright field microscopy images of HeLa cells incubated with K-MTED-R-Fl and K-Scrambled-R-Fl. α-tubulin is in red, and DNA is shown in blue. b) Jitter plot showing the quantified 2-dimensional area of the cell (µm^2) for all conditions. Each data point represents one cell. N=3, where n=the number of biological repeats.

4.9. K-MTED-R and K-Scrambled-R inhibit cell proliferation

To determine what effect the K-MTED-R and K-Scrambled-R peptides had on cell division, a proliferation assay was carried out as described in method section 2.3.7. Cells were incubated with 30µM peptide in the medium overnight at 37°C and 5% CO_2. Cells were counted every 24 hours over a 3-day period. 1% DMSO was used as a control.

48 hours after incubation, the control population was significantly larger in number than both peptide-treated populations ($p<0.05$, one way ANOVA), and this difference becomes more pronounced over the course of the assay. The K-MTED-R and K-Scrambled-R populations decreased almost to zero, while control cells continued to divide and increase in number ($p<0.001$ and $p<0.0001$ at the 48- and 72-hour time points, respectively, one way ANOVA) (**Figure 4.15**).

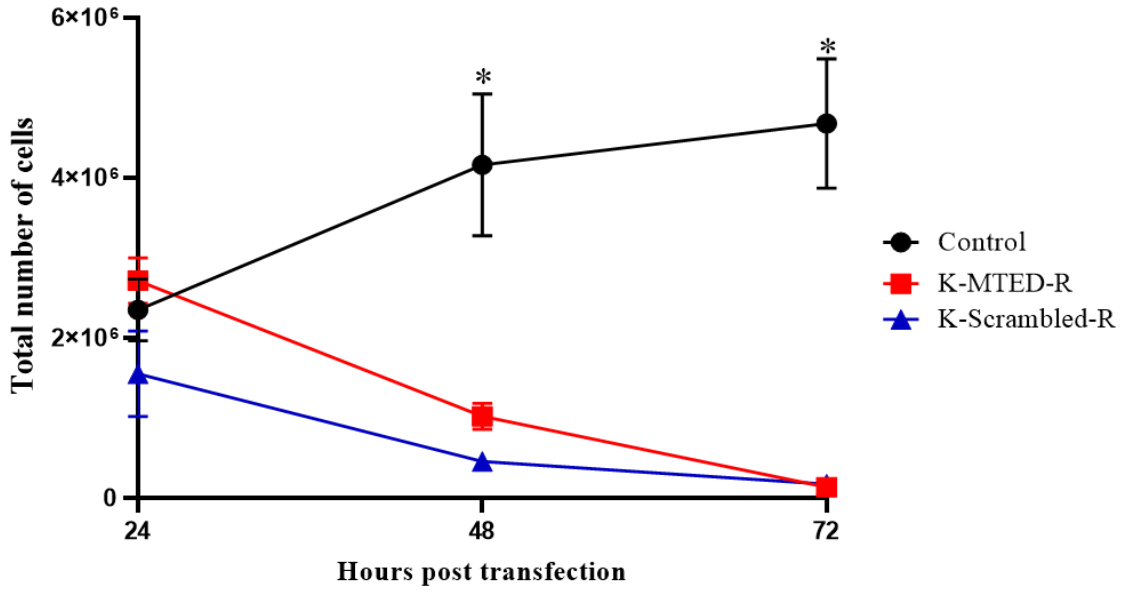

Figure 4.15) K-MTED-R and K-Scrambled-R inhibit proliferation.

Graph showing the total number of cells in each population at each time point. Astrisks represent a significant difference between the datasets. Error bars represent one standard deviation, n=3 for each sample.

4.10. K-MTED-R and K-Scrambled-R negatively impact cell viability

Brightfield images of cells treated with K-MTED-R and K-Scrambled-R show cells that have almost disintegrated, with no well-defined membrane (**Figure 4.13**). This observation, together with the data that shows K-MTED-R and K-Scrambled-R inhibit cell proliferation (**Figure 4.15**), led me to carry out a viability assay to determine whether these peptides were toxic to the cell and killing them, thereby preventing their proliferation.

A viability assay was carried out as described in section 2.3.8. Prior to counting, all cell samples were incubated with a 1:1 ratio of Trypan blue for ~3 minutes to allow for the dye to enter cells with a compromised membrane, a sign of cell death.

At the 24- and 48-hour time points, the peptide-treated samples are significantly less viable than the 1% DMSO population ($p<0.05$ at both time points, one way ANOVA). At the 72-hour mark, however, there is no significant difference in viability between the three populations ($p=0.168$, one way ANOVA). However, at this point the K-MTED-R and K-Scrambled-R populations have decreased to close to zero (**Figure 4.16**), so it is likely that the surviving population is made up of those cells that did not take up the peptide.

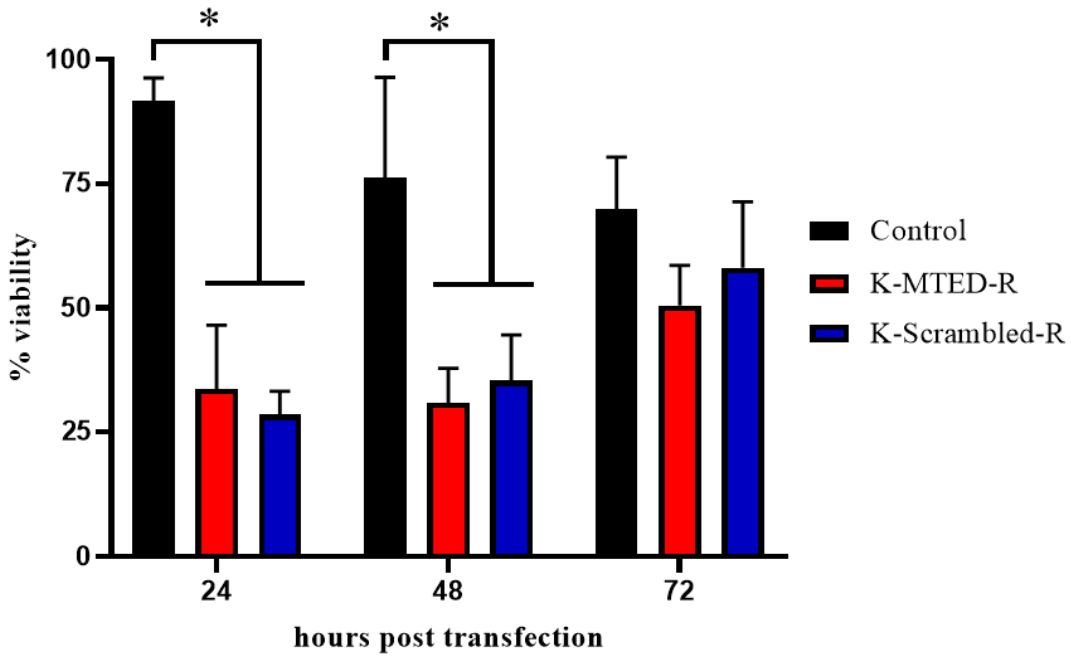

Figure 4.16) K-MTED-R and K-Scrambled-R significantly reduce cell viability.

Graph shows the mean proportion of viable cells in each population at each time point. Asterisks represent a statistically significant difference between the datasets. Error bars represent one standard deviation, n=3 for each sample, where n is the number of biological repeats.

4.11. Discussion

4.11.1. Summary

The impact of the MTED peptide on the microtubule network and cell proliferation was first studied by transfecting cells with an MTED-GFP expression plasmid. When transfected into cells, MTED-GFP almost eliminates the microtubule network, likely because it is binding to unpolymerized, heterodimeric tubulin and sequestering it. Scrambled-GFP, on the other hand, has no effect on microtubules. Cells expressing MTED-GFP did not spread on the culture surface but were contracted relative to cells expressing Scrambled-GFP and untransfected cells. Quantification of the 2D area of the cells shows that this contraction is statistically significant, verified using brightfield imaging to ensure the entire cell is affected, and not just the microtubule network.

Transfecting cells with MTED-GFP negatively impacts proliferation. During the proliferation assay, the number of cells in the MTED-GFP population decreased each day, while the number of cells in the Scrambled-GFP population remained the same. While this may seem as though the Scrambled-GFP cells are not dividing, when this data is looked at in context with the % change in population size, the Scrambled-GFP population steadily increases by 50% over each 24-hour time-period, showing that these cells are indeed dividing. By contrast, during the first 24 hours of the assay, the MTED-GFP population decreased by ~45%, a significant decrease relative to the Scrambled-GFP population.

As the FACS data shows that only 24% of cells are expressing MTED-GFP by the 96-hour mark, it is likely that the remaining 75% of cells (i.e. those not expressing the construct), are dividing at a rate similar to cells in the Scrambled-GFP population, explaining why there is no significant difference between the percentage change in population size at the 48-72- and 72-96-hour time points.

Once I had established that expression of the MTED peptide inhibits cell proliferation, I attempted to recreate this effect by adding peptide externally to the cells. If peptide could successfully be introduced, this would give more control over peptide concentrations and eliminate the complexities of transfection and the waiting time for plasmid DNA expression. It was unlikely, and ultimately proven that the wtMTED peptide cannot directly enter cells,

and so synthetic peptide with N- and C-terminal PTDs was used as a potential delivery system. Interestingly, these extensions give the scrambled peptide the ability to inhibit microtubule growth. This increase in the ability to bind to tubulin when modifying a peptide with many charged residues has previously been observed (Benôit Gigant, personal communication). As these extensions do not negate MTED's microtubule-inhibiting ability, I used first the fluorescent version of each construct to visualise peptide expression within the cell, and once this was confirmed, used the untagged versions for further investigations. As the focal point of this peptide is to inhibit microtubule polymerisation and cell division, there was no downside to testing the K-scrambled-R peptide for these abilities as well. Both peptides have a dramatic effect on the microtubule cytoskeleton, and significantly reduce the 2D area of the cell compared to control cells. Additionally, introduction of these peptides into cells significantly inhibits cell proliferation and decreases viability.

4.11.2. Limitations and future work

Unlike the previous chapter, time, more than resources, was the limiting factor here, as many results seen in this chapter could warrant further investigation. MTED's impact on proliferation, for example, is an area that can be delved into much more deeply. While the FACS data does show that the proportion of cells expressing MTED-GFP decreases over the course of the proliferation assay, and are therefore not dividing, a useful way to measure the rate of proliferation would be to use 5-ethynyl-2'-deoxyuridine (EdU). EdU is an analogue of thymidine that incorporates into newly synthesized DNA. Using flow cytometry, the proportion of cells that contain this nucleoside analogue can be measured to determine the DNA synthesis and proliferative abilities of cells (Thermo Fisher, Click-iT Flow cytometry Cell proliferation assay).

Result 4.6 shows that that a greater proportion of cells are lost during washing in the population of cells transfected with MTED-GFP compared to Scrambled-GFP. While simply counting the cells is one way to measure this, the use of crystal violet would inform on the adhesion abilities of each population. Some types of breast cancer cells form microtubule-filled cell protrusions called "microtentacles" which aid their adherence to the basal membrane (Boggs, Vitolo et al. 2015). As MTED-GFP inhibits microtubule polymerisation and

radial extension throughout the cell, microtentacle formation and subsequent adherence, measured and quantified using crystal violet, may be compromised, potentially decreasing the malignancy of the tumour, and informing on MTED's therapeutic potential.

Once the experiments involving the MTED-GFP DNA construct had shown that the peptide, when expressed in cells, significantly alters cell morphology and negatively impacts cell proliferation, a synthetic peptide was used to attempt to replicate these results. Unfortunately, the wild type peptide did not enter cells when directly added to the culture medium, and so another method was attempted.

Dixon et al. (2016) had successfully used a series of charged residues on the N- and C-termini of their reporter protein, RFP, to facilitate its uptake into cells. I attempted to re-create these results by ordering synthetic MTED (K-MTED-R) and scrambled peptide (K-scrambled-R) with the N- and C-terminal PTDs, but when I tested their microtubule-inhibition abilities in a microtubule growth assay, K-scrambled-R, as well as K-MTED-R, inhibited microtubule growth. As the scrambled peptide without any modifications does not bind to tubulin, these PTDs must somehow allow the modified peptide to bind to tubulin and inhibit its proliferation. If this is the case, then it is likely that K-MTED-R is not binding to tubulin in the same location as the wtMTED peptide. One possibility is that, as the PTDs confer a positive charge of ~17, the K-MTED-R and K-Scrambled-R peptides are attracted to the negatively charged C-terminal tail of the tubulin dimer and binding there. However, this would be unusual as the C-terminal tail of tubulin is somewhat disordered. Ultimately, a crystal structure of these peptides bound to tubulin, compared to that of wtMTED bound to tubulin would answer many questions.

When staining the microtubule network 24 hours later to visualise the impact of these peptides, the network was so distorted that at no point, either during image acquisition or post-acquisition processing, was I able to resolve individual microtubules. I believed this to be a result of the PTDs, and indeed Dixon et al. pointed out that "the extensive positive charge… can be cytotoxic"(Dixon, Osman et al. 2016). However, as they were successfully able to introduce a range of cargo into the cell without any adverse cellular affects. I re-evaluated my experimental procedure and compared it to theirs. While Dixon et al. introduced their cargo at a concentration of ~645nM/ml, I was introducing peptide at a concentration of 30µM/ml, over 46x higher. It is worth noting that Dixon et al. did not examine the microtubule cytoskeleton when carrying out their study and were only looking at uptake of their cargo of

interest and cell morphology. Therefore, it is likely that the incredibly high concentration of these positively charged PTDs was having adverse effects on the cell. Using Trypan blue, I found that 24 hours after incubation with either K-MTED-R or K-scrambled-R, less than 50% of cells remained viable, while nearly the entire population exposed to 100% DMSO in the absence of peptide was viable. This added strength to my theory that the concentration of PTDs was far too high. Unfortunately, I lacked the time and resources to carry out further investigations into this peptide, and so was unable to optimise the assay any further.

Chapter 5) A synthetic ancestral kinesin-13 is the fastest microtubule depolymeriser measured to date

5.1. Introduction

While chapters three and four focussed on MTED, a peptide that binds to the tubulin subunit and inhibits polymerisation, this chapter looks at the activity of a protein that too binds to the α/β tubulin subunit, but does so in its polymerised state, and actively depolymerises microtubules.

The tubulin gene family is thought to be one of the oldest and may have been present in the LUCA (reviewed in (Pollard and Goldman 2018)). Evidence of this can be seen in the bacterial and archaeal domains of life, which diverged prior to the emergence of the Eukaryota, encoding a tubulin-like gene, *FtsZ (*RayChaudhuri and Park 1992*)*. While sharing very little sequence homology with modern day tubulin, FstZ monomers bind GTP, assemble into protofilaments and are involved in cytokinesis (Margolin 2005). All extant Eukaryota carry genes for α- and β-tubulin, which share >75% sequence similarity across the domain, indicating that there has been little evolution amongst this gene family since the last common eukaryotic ancestor (LCEA) (Pollard and Goldman 2018).

The kinesin superfamily is the only microtubule motor protein that is known to have been present in the LCEA, as there are entire eukaryotic lineages that do not possess dynein proteins (Richards and Cavalier-Smith 2005) (Wickstead and Gull 2006, Wickstead and Gull 2007). Phylogenetic analysis of the evolutionary history of the kinesins has shown that at the very least, the LCEA encoded 11 kinesin subfamilies, one of which was the kinesin-13 subfamily of microtubule depolymerases (Wickstead and Gull 2011). There are three distinct subgroups of kinesin-13: A, B and C. Group A, which includes human KIF24, is the oldest and contains the largest number of sequences and is involved in the negative regulation of ciliogenesis. However, Group B, which includes human KIF2A, KIF2B and KIF2C/MCAK, is the best characterised (Kobayashi, Tsang et al. 2011).

MCAK is the best studied member of the kinesin-13B subfamily, a group of motor proteins that do not possess translocase activity but instead use the energy produced from their distinct ATP turnover cycle to negatively regulate microtubule length (Friel and Howard 2011). During mitosis, MCAK localises to centromeres and the spindle midzone where it facilitates the accurate attachment of spindle fibres to kinetochores by depolymerising aberrantly growing microtubules and ensures faithful segregation of sister chromatids during anaphase (Maney, Hunter et al. 1998).

Depletion of centromeric MCAK in *Xenopus Laevus* egg extracts results in defective spindle/kinetochore attachments, lagging chromosomes and errors in chromosome segregation, with some cells having 12 more kinetochores at one pole than the other, post anaphase, and similar results are observed in CHO cells when MCAK is depleted (Maney, Hunter et al. 1998, Kline-Smith, Khodjakov et al. 2004). Overexpression of MCAK in CHO cells results in abnormally large, multinucleated, and multipolar cells, with an increase in microtubule detachment from centrosomes (Ganguly, Yang et al. 2011). Additionally, overexpression of MCAK has been shown to confer resistance to microtubule-stabilising drugs such as paclitaxel, while depletion increases their sensitivity (Ganguly, Yang et al. 2011).

Accurate regulation and activity of MCAK, therefore, is crucial as the consequences of both over and under expression lead to errors in chromosomal segregation, which can result in cancer. While our existing knowledge of MCAK's structure, function and regulation has allowed for extensive research into its potential as a drug target, our understanding of the motor domain, and how it came to be so distinct from the rest of the kinesin superfamily, remains a mystery. As it is this motor domain that is responsible for MCAK's distinct role in microtubule regulation, this was the focal point of my investigations.

To address the question of how primary sequence dictates function in the kinesin family, phylogenetic analysis was used to create two reference sequences for the Kinesin-13 family motor domain (Wickstead and Gull 2006, Wickstead, Gull et al. 2010, Belsham, Alghamdi et al. 2022). The "consensus" sequence (Conc13) is a sequence that exists nowhere in nature but is a hypothetical motor that contains the residues most conserved across the kinesin-13 subfamily. The "ancestral" sequence (Anc13), is the sequence predicted to exist in the last common ancestor of the kinesin-13 subfamily, inferred from phylogenetic reconstructions (Wickstead and Gull 2006, Wickstead, Gull et al. 2010) (**Figure 5.1**). Analysis of the

depolymerisation activity of these motor domains showed that Conc13 depolymerised microtubules at a rate of 0.67±0.28µm/min^{-1}, 66% slower than MCAK, while Ancestral_13 had a depolymerisation rate of 23.05±5.23µm/min^{-1}, 11-fold higher than MCAK (2.12±0.17 µm min^{-1}) (**Figure 5.2**) (Belsham, Alghamdi et al. 2022).

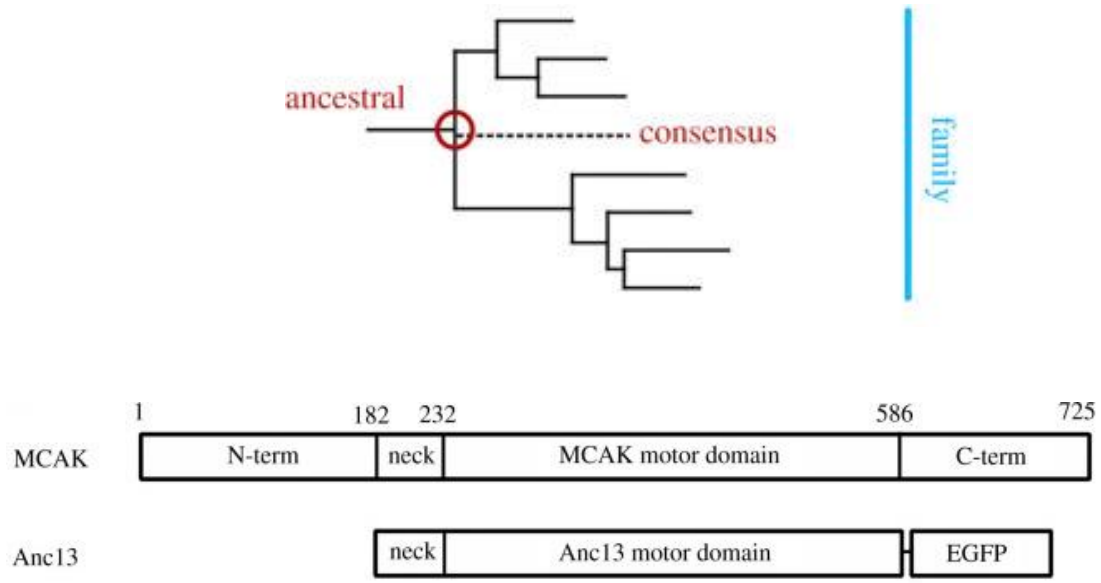

Figure 5.1) Creation of an ancestral Kinesin-13 motor domain.

A) Simplified phylogenetic tree of the Kinesin-13 family, highlighting the location of the consensus and ancestral constructs. B) Ribbon diagrams of the structure of the MCAK and Anc13 constructs. Adapted from (Belsham, Alghamdi et al. 2022).

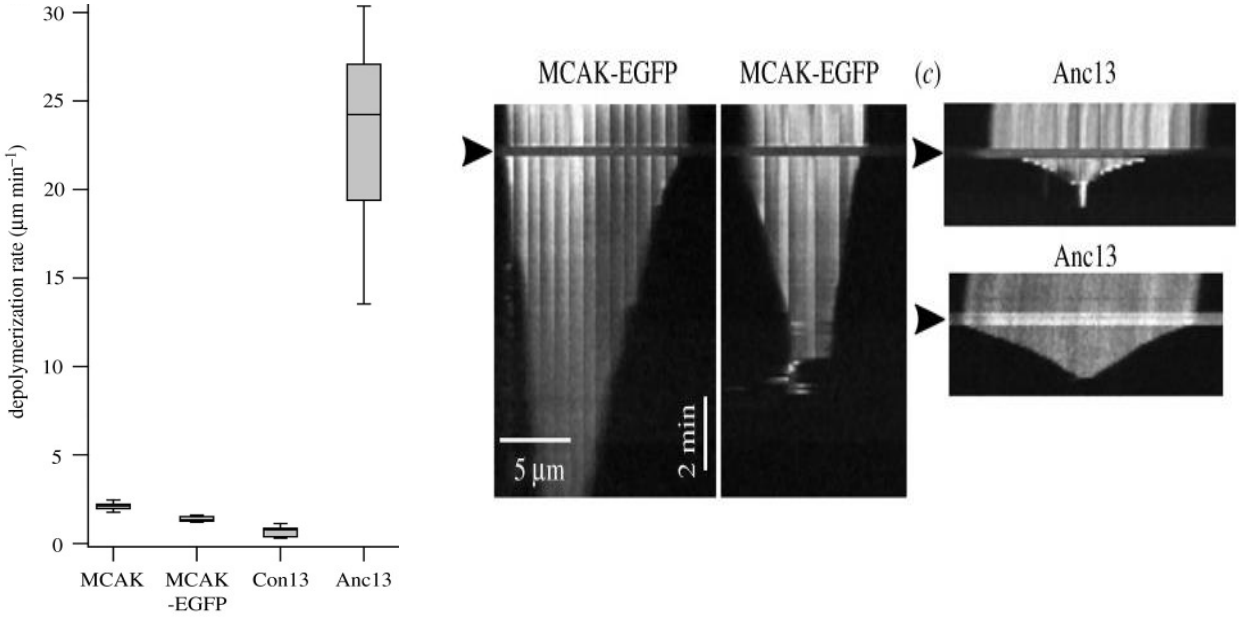

Figure 5.2) The Anc13 motor domain is an incredibly powerful microtubule depolymerase.

A) Boxplot showing the microtubule depolymerisation rates for MCAK, Conc13 and Anc13 constructs. B) Kymographs showing the changing length of the microtubule after protein addition (denoted by the black triangle). Adapted from (Belsham, Alghamdi et al. 2022).

5.2. Aims

To further understand the behaviour of the ancestral Kinesin-13, I sought to express the Ancestral13 motor domain in the context of the full length MCAK protein, known as MCAK-13, and set out the following aims for this chapter:

1. Express and purify wtMCAK and MCAK-Anc13
2. Measure the depolymerisation rate of each protein

The results of the depolymerisation assay will better inform us as to the evolutionary history of the kinesin-13 subfamily, and how they came to be so distinct from the kinesin superfamily as a whole.

5.3. Purification of wtMCAK-h6 and MCAK-Anc13-h6

pFastBac vectors containing wtMCAK and MCAK-Anc13 were already available in the Friel lab. Briefly, the pFastBac vector contains an *Autographa californica* multiple nuclear polyhedrosis virus (AcMNPV) promoter for high level recombinant protein expression in insect cells and is flanked by the left and right segments of Tn7, a bacterial transposon element (Luckow, Lee et al. 1993). I transformed these pFastBac vectors into DH10Bac cells as described in methods section 2.2.3. DH10Bac cells contain a baculovirus shuttle vector (bacmid) with an *att*Tn7 target site for the Tn7 transposon, and an additional "helper plasmid" that encodes proteins to facilitate transposition (Luckow, Lee et al. 1993). The bacmid, containing the gene of interest (wtMCAK and MCAK-Anc13, in this case), along with genes encoding baculovirus proteins, is assembled during the transformation process and subsequently purified.

Purified bacmid was then transfected into *Sf9* cells for baculovirus production. Five days after transfection, the supernatant, containing the baculovirus particles, was collected and used to infect a large culture of *Sf9* cells in suspension. After ~72 hours, infected cells were spun down, the pellet resuspended 1:2 w/v in buffer, the suspension frozen dropwise in LN_2 and stored at -80°C. To purify protein from the Sf9 cells, frozen cells were thawed in lysis buffer, the lysate centrifuged and the supernatant run through a cation-exchange followed by a nickel exchange column. Both wtMCAK and MCAK-Anc13 were purified in this way, and all samples collected during the purification process were run on an SDS-PAGE gel to determine the purity of the protein (**Figure 5.3**). wtMCAK runs to ~81kDa, while MCAK-Anc13 runs to ~83kDa.

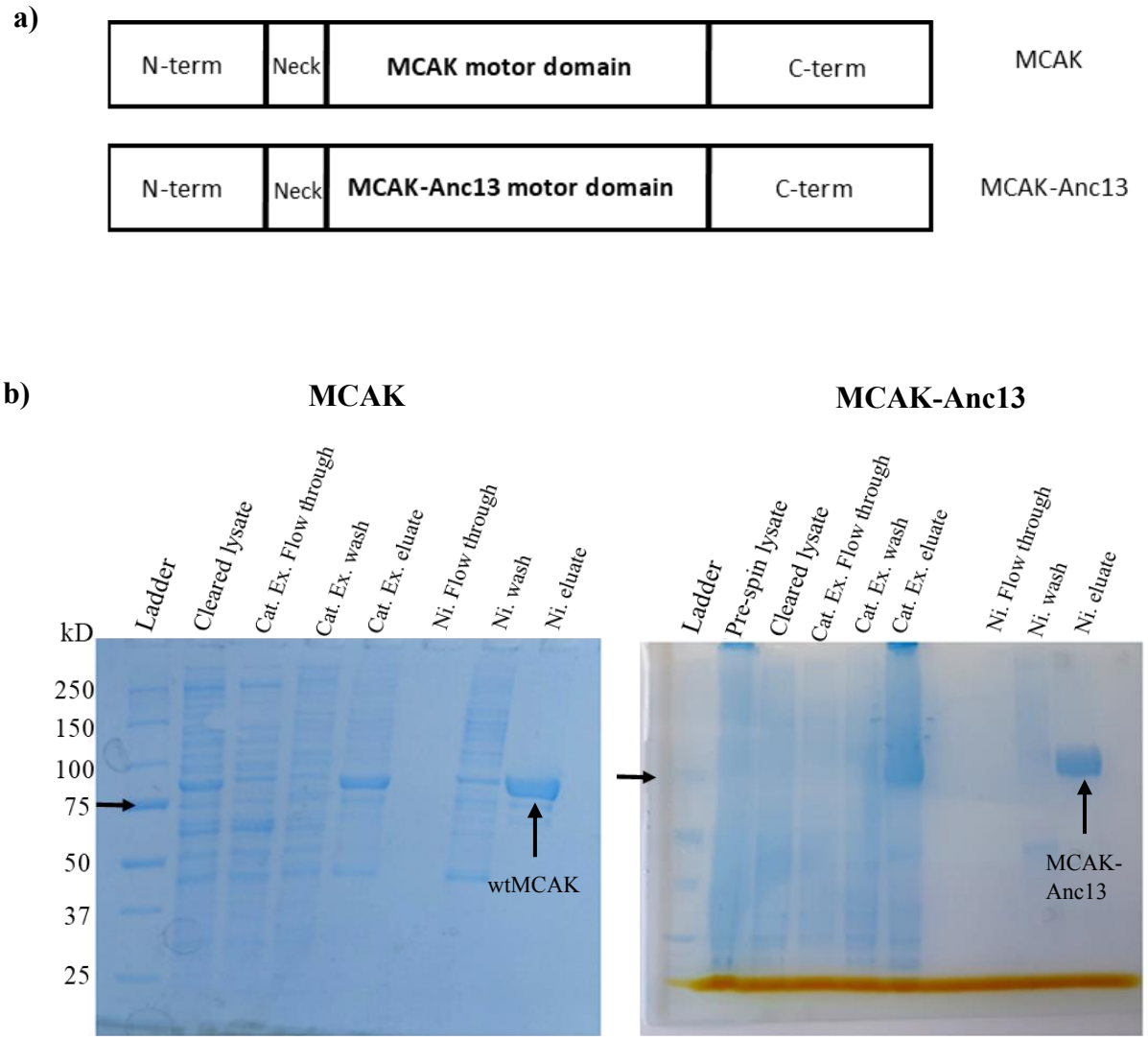

Figure 5.3) 2-step nickel affinity purification of MCAK and MCAK-Anc13

a) Ribbon diagrams showing the structure of MCAK and MCAK-Anc13, with the differing motor domains shown in bold. b) SDS-PAGE gels run with samples from MCAK-h6 purification and MCAK-Anc13-h6. The 75kDa band is highlighted on each gel, and the protein is highlighted in the final Ni. eluate.

5.4. MCAK-Anc13 depolymerises microtubules nine times faster than wtMCAK

To examine whether the Ancestral-13 motor domain retained its potent microtubule depolymerisation activity when expressed in the context of the full length MCAK protein, I carried out a microtubule depolymerisation assay with MCAK-Anc13. GMPCPP microtubules were grown and fixed onto silanised coverslips and photographed every 2 seconds for approx. 5 minutes. 40nM MCAK-Anc13 was added after one minute to visualise microtubule activity before and after protein addition. 40nM wtMCAK was used as a control and photographed every 5 seconds.

MCAK-Anc13 depolymerised microtubules at a rate of 19.50±4.87µm/min^{-1} (n=14), significantly faster than wtMCAK, with a depolymerisation rate of 2.43±0.177µm/min^{-1} (n=12) ($p<0.0001$, t-test). This shows that the ancestral motor domain retains ultra-rapid depolymerisation activity in the context of full length MCAK (Belsham, Alghamdi et al. 2022) (**Figure 5.4**).

5.5. MCAK-Anc13 promotes internal breakage of microtubules

A large number of microtubules were observed to break internally and continue to depolymerise from these newly exposed ends in the presence of MCAK-Anc13. I quantified the frequency of internal breakage for microtubules longer than 5µm in the presence of MCAK-A13 and wtMCAK. The proportion of microtubules that broke at internal sites in the presence of wtMCAK was ~5% (n=58), compared to ~70% in the presence of the MCAK-Anc13 (n=47). Microtubules that broke internally began to depolymerize from these breaks at a similar rate as from the original microtubule ends (**Figure 5.4**) (Belsham, Alghamdi et al. 2022).

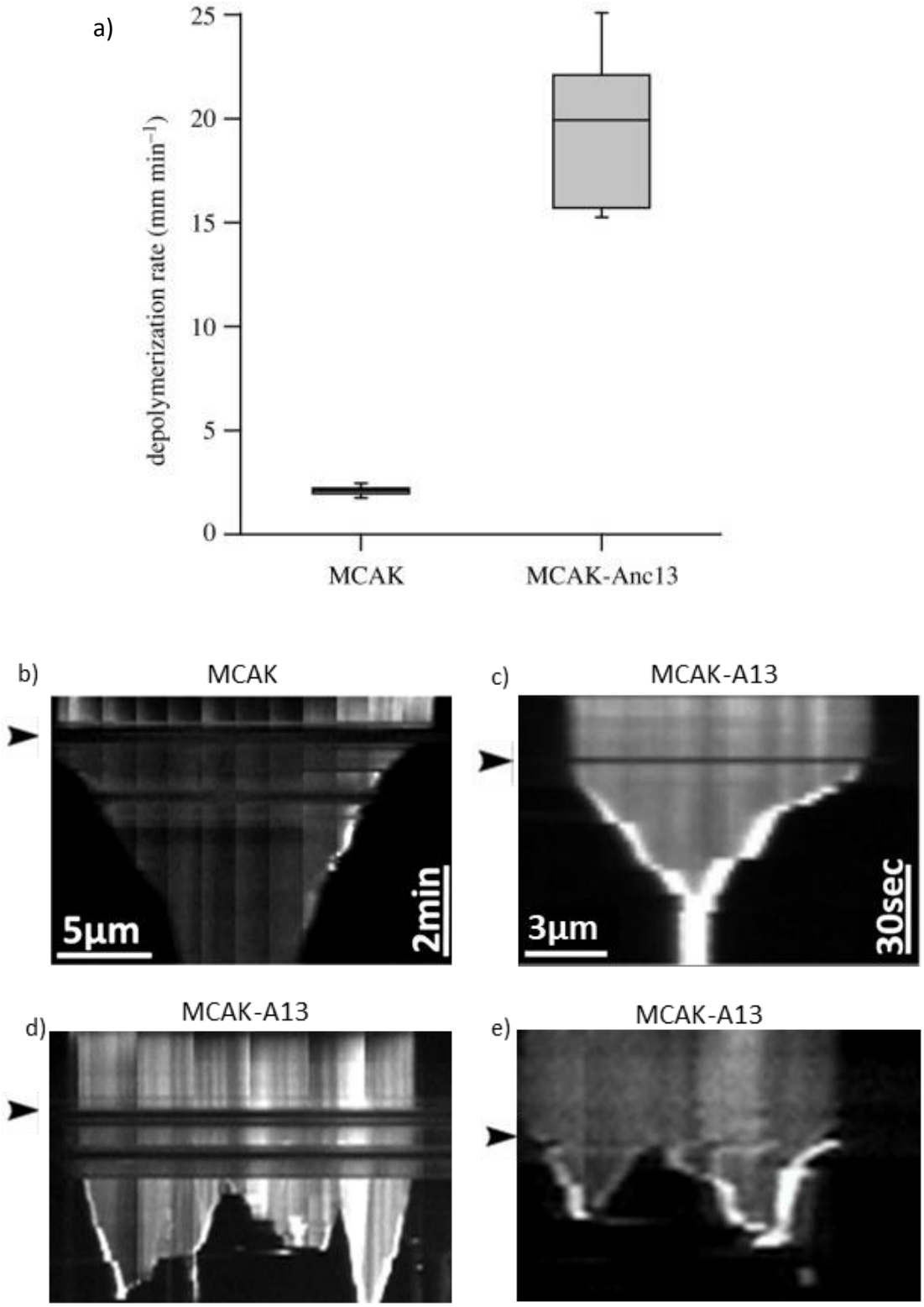

Figure 5.4) MCAK-Anc13 has extremely potent microtubule depolymerisation abilities and promotes internal breakage of microtubules.

a) Boxplot showing the depolymerisation rates of MCAK and MCAK-Anc13. b-e) kymographs showing the activity of MCAK-A13 on microtubules, depolymerising them and breaking them internally and continuing to depolymerise them from the newly exposed ends.

5.6. Discussion

The synthetic ancestral kinesin-13 motor domain has ultra-rapid depolymerisation abilities compared to the wild type MCAK protein (Belsham, Alghamdi et al. 2022). This chapter determined that, when expressed in the context of full length MCAK, this ancestral motor domain retains its potent microtubule depolymerisation abilities and causes internal breaks within the microtubule. This was a phenomenon not previously observed with MCAK and is likely to be a result of the ancestral kinesin-13's hyperactivity. The stoichiometry of ATP consumed per dimer of tubulin removed during microtubule depolymerisation by MCAK ranges from 1-20 ATPs per tubulin removed; when depolymerising GMPCPP-stabilised microtubules, MCAK removes approx. 1 tubulin dimer for every ATP consumed (Friel and Howard 2011, Belsham, Alghamdi et al. 2022). Depolymerisation of stabilised microtubules using Taxol or both GMPCPP and Taxol together, decreases MCAK's efficiency at tubulin removal to the extent that whole rounds of ATP turnover can sometimes occur without any tubulin dimers being removed (Belsham, Alghamdi et al. 2022). The ancestral kinesin-13 motor domain can depolymerise microtubules stabilised with GMPCPP, Taxol and double-stabilised microtubules, and has greater ATPase rates in solution, in the presence of unpolymerized tubulin and microtubules than MCAK, and the average number of tubulin dimers removed per ATP consumed by MCAK-Anc13 has been determined to be 5.8±1.4 (Belsham, Alghamdi et al. 2022). MCAK-Anc13 must therefore be able to bind to a tubulin dimer in microtubule lattice some distance prior to the terminal tubulin dimer and remove all those in between in one ATPase cycle (Belsham, Alghamdi et al. 2022). It is likely that, as the Kinesin-13 family evolved, such strong, uncontrolled depolymerisation was not favoured as organism complexity increased, and instead a less energetically efficient, but much more controlled motor domain evolved to allow for tight regulation of microtubule dynamics.

One further area for exploration would be the determination of the binding affinity of this MCAK-Anc13 construct for tubulin, compared to the wild type, which could further inform on the hyperactivity of this proposed Kinesin-13 ancestor and its evolution to a much more controlled depolymerase (Belsham, Alghamdi et al. 2022).

Chapter 6) Discussion

6.1. Summary and future work

The aims of this study have been to gain a better understanding of two microtubule regulatory proteins: MTED, a peptide that inhibits microtubule polymerisation, and MCAK, a microtubule depolymerase. MTED is an 18-residue motif from the N-terminus of EFA6, a cortical collapse factor that negatively regulates axonal growth through the inhibition of microtubule polymerisation. Studies have uncovered the expression, localisation, and function of this protein, with the majority of studies conducted in the nematode *C. elegans* (Casanova 2007, O'Rourke, Christensen et al. 2010, Chen, Wang et al. 2011). In 2015, Chen et al. described a motif within the disordered N-terminal domain as “a region of local protein order”, and since then, studies have identified this motif as the minimal motif necessary for microtubule inhibition (Chen, Chuang et al. 2015, Qu, Hahn et al. 2019). In 2019, Qu et al. delivered possibly the most comprehensive study into *D. melanogaster* EFA6 and the MTED motif, using both a synthetic MTED peptide and MTED DNA construct to look at its inhibition abilities in vitro and in a cellular context. This study utilised both the synthetic MTED peptide and MTED-GFP DNA construct to build on these results.

Chapter 3 showed that the MTED peptide inhibits microtubule polymerisation by direct binding to tubulin and preventing its polymerisation. This was unsurprising; the small size of the peptide was already an indication that it had no motor domain. Stathmin, an example of a microtubule regulator which too binds to the tubulin subunit and inhibits its polymerisation, is 149 residues in length (17kDa). As this too is shorter in length than the MCAK motor domain, for example (354 residues), it would have been extraordinarily surprising had MTED had depolymerisation activity, and this was proven when MTED failed to depolymerise microtubules during a MT depolymerisation assay. The inability of tubulin to polymerise in the presence of the MTED peptide, but not a Scrambled peptide, shows that the inhibition abilities of this peptide are sequence specific; following on from this, the necessity of some residues in inhibition have been determined, with the C-terminal domain not as important. These results gave the idea that the C-terminal domain would be an ideal location for tagging with a fluorophore for assays requiring a fluorescent ligand, but this was not to be as direct tagging,

and tagging following a two-residue linker, prevents the peptide from inhibiting microtubule polymerisation. Although disappointing at first, this was an interesting result. Fluorescein has a molecular weight of 332Da, making it 6x smaller than the MTED peptide, however, it is possible that the proximity of this fluorophore interferes with the peptide's inhibition abilities. Ultimately, the determination of the crystal structure of the peptide would perhaps inform on a more suitable location for fluorescent tagging. Recent personal communication from Beniôt Gigant (Institute for Integrative Biology of the Cell [I2BC] Paris-Saclay) has suggested, using X-ray crystallography, the peptide may form a β-hairpin, although this needs much more analysis before they are confident of this result. Because of the limitations posed by fluorescent tagging, fluorescence polarisation could not be used to determine the affinity of the peptide for tubulin. ITC was then attempted, but again was not successful due to the complications with peptide solubility, and so an experimental plan for Microscale Thermophoresis was eventually designed, optimised, and successfully executed to determine a K_d of 6.4 ±5.1nM. While the labelling of MTED would have been more desirable to exploit the size difference between it and the tubulin heterodimer, the fact that the scrambled peptide shows no binding further validates this figure. Additionally, the labelling of tubulin over the peptide does have its advantages now that the assay has been optimised; as there are several variants of the peptide and only one tubulin, all peptides can remain in their untagged state and used in this assay to determine their affinities for the tubulin subunit, saving a lot of time and resources. Of course, another solution exists whereby the K-MTED-R peptide can be labelled, and competition assays can be done. The Nanotemper™ molecular weight cut off for their protein labelling kits is 5kDa, and K-MTED-R is 6.2kDa. So, this peptide could successfully be labelled with Alexa 647 dye, and once the affinity of this peptide for tubulin is determined, the affinity of all the others can be determined in a competition assay. Ultimately, I believe the final decision would come down to time. As the MST has already been optimised for the current conditions, I believe it would be better to continue as is and use the labelled tubulin for future assays.

Chapter 4 looked at the impact of the peptide in cells when expressed from a DNA construct. This is an efficient way of studying the impact of this peptide in cells without having to spend time and resources trying to get the peptide into cells in the first place, without knowing what affect it would have, if any. 24 hours after transfection, the microtubule network was stained

for visualisation of the effects of the peptide, and it was shown that the 2D area of cells expressing MTED-GFP is significantly reduced compared to cells transfected with Scrambled-GFP and untransfected cells. While this was informative, the use of Z stacks might provide more information into the 3D size of the cell – as it is unlikely the contents and volume of the cell had changed, it is possible that the Z axis might be larger than conventional HeLa cells, which are notoriously flat (Dr Alan Huett, personal communication), to accommodate this. The significant reduction in the 2D size of the cell led me to the idea that these cells may be less adherent to the culture vessel, as they likely had a smaller surface area to bind with. I accounted for this by keeping the cells in the wash as well as trypsin to ensure every cell was accounted for, but there are better ways of studying this. For example, I would like to measure the force deformability of cells transfected MTED-GFP and Scrambled-GFP and compare the results of the two populations. If the microtubule network is much less structured in MTED-GFP cells, perhaps it is not able to offer the same level of structure and support to the cell, increasing its deformability. While an increase in deformability may aid in intravasation / extravasation of cancer cells, the lack of a functioning microtubule network would make it unlikely that these cells would survive the harrowing journey through the vasculature and adhere to distal tissue.

The use of the peptide in cells was a logical, but complex next step. It is unable to enter cells, as expected, and the use of the PTDs, while allowing for uptake, give the scrambled peptide microtubule inhibition abilities, and significantly decrease the viability of the cell. However, is this such a bad thing? The overall aim of developing MTED as a therapeutic is to inhibit microtubule dynamics in cancer cells, inhibiting their proliferation and inducing cell death. Of course, ensuring selectivity for cancer cells is a challenge, but could be achieved with multi-drug combinations. For example, Trilaciclib, a CDK4/6 inhibitor, is often administered to patients prior to chemotherapy to protect bone marrow, temporarily pausing proliferation in this tissue to prevent it being targeted by anti-proliferative chemotherapeutic agents (Powell & Prasad, 2021). While I am no longer able to say these effects are a direct result of peptide activity, it's not necessarily a bad thing. However, further investigations are required into the behaviour of the MTED peptide in cells to truly validate its therapeutic potential. These investigations do not necessarily need to use the extension peptides; though a logical first step would be to determine their affinity for tubulin and use this information to re-design the

experiment and introduce the peptide at a lower concentration, hopefully closer to the 645nM/ml concentration used by Dixon et al. (2016) as we know at this concentration, these PTDs do not interfere with cell morphology or function. Before this, though, microinjection, for example, would be a good way to study the peptide in cells in its wild type form, and although the sample size of microinjected cells would be quite small, we would be able to say with certainty that the peptide is within the cell. However, regardless of the data generated by the peptide, there is enough evidence to warrant further investigations into it.

Chapter 5 looked at the activity of a synthetic, ancestral kinesin-13 motor domain in the context of the full length MCAK protein. The aims of this chapter were to gain a better understanding of the evolutionary history of the kinesin-13 subfamily, and how the motor domain evolved to its current form. It was shown that MCAK-Anc13 is ~10fold faster at depolymerising microtubules than wtMCAK, and its potent activity leads to internal breakage of microtubules, which are then depolymerised from these newly exposed ends. This may indicate a different binding location to wtMCAK; the ability to severe microtubules internally means the MCAK-Anc13 construct may bind to tubulin dimers within the microtubule lattice, as opposed to the terminal dimer, and remove several dimers at once. This hyperactive motor domain was perhaps too unstable, and over time, a less potent, but much more regulated motor domain evolved.

6.2. Drug resistance to microtubule targeting agents (MTAs) and the need for more

The emphasis of this study is to learn more about this novel MTED peptide and determine whether it has the potential to be developed as a therapeutic. While there is a long way to go before arriving at a definitive answer, the initial results showing that the peptide inhibits cell proliferation as a direct result of its microtubule inhibition abilities justifies further investigation. But as there is already a host of MTAs being successfully used in chemotherapy, and in the treatment of some parasitic infections, why is there a need to develop more? It is not enough to be satisfied with the repertoire of drugs we currently have; bacteria, viruses and cancer cells continuously evolve ever more sophisticated mechanisms to avoid, survive and thrive in response to our therapeutics, and we must do the same if we don't want to lose this evolutionary arms race.

6.2.1. Post-translational modification

Resistance to MTAs can occur in many ways; tubulin, like all proteins, is regularly post-translationally modified to allow it to achieve its functional diversity. Acetylation of lysine 40 in α-tubulin subunit (αK40) is one such post-translational modification (LeDizet and Piperno 1987). αK40 resides in a loop between residues P37 and D47 of α-tubulin, and the significance of K40 in particular has led to its dubbing as the αK40 loop (Eshun-Wilson, Zhang et al. 2019). Acetylation of this residue decreases the rigidity of the microtubule, allowing for greater flexibility of the microtubule in response to mechanical stress (Nekooki-Machida and Hagiwara 2020). While this increased resistance to stress can be beneficial, acetylated microtubules are found to be more abundant in metastatic breast cancer cells, among other tumour types, where they have been associated with an increase in cancer cells' adhesion abilities to the basal membrane, facilitating invasion and metastasis (Boggs, Vitolo et al. 2015).

Increases in microtubule acetylation are associated with increased resistance to paclitaxel (Wattanathamsan, Tharattanobon et al. 2021). Treatment of non-small-cell lung cancer in mouse models using paclitaxel results in an increase in microtubule acetylation within the tumour, conferring resistance to paclitaxel's cell proliferation-inhibition abilities, and results in

no significant difference between the size of the treated and control tumours (Wattanathamsan, Tharattanobon et al. 2021).

Microtubules are acetylated by the tubulin acetyltransferase αTAT1, which is upregulated in colon cancer (Oh, You et al. 2017). Disruption of this enzyme results in a decrease in the proliferative and invasive abilities of colon cancer cells (Oh, You et al. 2017). If genetic screening of tumours can highlight upregulated genes such as αTAT1, microtubule inhibitors such as MTED could be used to inhibit microtubule proliferation in these cells, thereby preventing any acetylation from taking place and decreasing the invasiveness of these cancers.

6.2.2. Mutation and isoforms

Different tubulin isoforms and mutations within the tubulin genes are also known to offer differential resistance to MTAs (reviewed in (Roll-MEcak 2020)). All isoforms share very high sequence and structure similarity, with the main differences being found in their carboxy-terminal tails (reviewed in (Kavallaris 2010)). βI-tubulin, the most common isoform, is ubiquitously expressed in most cell types. Point mutations in this isoform, F167Y and F200Y, are thought to individually confer resistance to benzimidazole, a Tubulin Binding Agent (TBA) used in the treatment of the parasitic nematode infection cyathostomin in horses; F167Y is associated with increased resistance to benzimidazole in budding yeast and trichostrongylid nematodes, while F200Y increases benzimidazole resistance in *C. elegans* (Li, Katiyar et al. 1996, Silvestre and Cabaret 2002);(Hodgkinson, Clark et al. 2008).

The βIII-tubulin isoform, too, is associated with increased drug resistance. While mainly expressed in neuronal tissue, several studies have shown that this isoform is expressed and associated with increased aggressiveness and poor prognosis in many cancers (Kamath, Wilson et al. 2005, Lee, Cao et al. 2007, Lebok, Ozturk et al. 2016). In non-small-cell lung cancer, high βIII-tubulin mRNA expression correlates with a decrease in sensitivity to paclitaxel and decreases overall survival rate of patients post-surgery (Jiang, Yu et al. 2013). NFL-TBS.40-63 is a peptide derived from the light chain of a neurofilament containing tubulin binding sites that specifically enters glioblastoma cells, binds to the C-terminal domain of this isotype (βIII-tubulin is upregulated in glioblastoma cancers) and reduces tumour size by disrupting microtubule dynamics, all without affecting healthy cells (Berges, Balzeau et al. 2012, Balzeau,

Pinier et al. 2013, Barreau, Montero-Menei et al. 2018). It is possible that MTED, too, may have an inhibitory effect on cell proliferation within tumours. At present, it is unknown how and where MTED binds to the tubulin heterodimer; determination of the crystal structure of this peptide both in isolation and when bound to tubulin will hopefully answer these questions. If, for example, MTED binds to tubulin in a location that does not differ amongst the isoforms, it could be used as a broad-spectrum microtubule inhibitor, overcoming resistance conferred by different isoforms.

Currently, many MTAs used in chemotherapy, such as Viblastine, Colchine and Paclitaxel are small molecules, organic compounds with low molecular weight that can pass through cell membranes (reviewed in (Southey and Brunavs 2023). While these are effective chemotherapeutics, they lack specificity and can target the microtubule cytoskeleton of rapidly dividing healthy and cancerous cells alike, leading to a host of unpleasant side effects (Calinescu and Castro 2016, Wang, Gigant et al. 2023). The advantage the MTED peptide has over small molecules is that the modification of peptides is easier than that of small molecules. Peptide modification, as seen in chapter 4, can be as simple as adding a series of residues to the N- and C-termini to facilitate peptide uptake, and localisation sequences can be added to this peptide as well to allow for targeting to specific cell types. This may increase the specificity of this peptide and may allow it to function as an effective microtubule inhibitor that inhibits proliferation specifically of cancer cells, while healthy tissue remain unaffected and decreasing unpleasant side effects for patients.

Appendix I: Publications associated with this thesis

Belsham, H. R., H. M. Alghamdi, N. Dave, A. J. Rathbone, B. Wickstead and C. T. Friel (2022). "A synthetic ancestral kinesin-13 depolymerizes microtubules faster than any natural depolymerizing kinesin." Open Biol **12**(8): 220133.

Appendix II: COVID-19 impact statement

The COVID-19 pandemic resulted in a national lockdown beginning circa 10th March 2020. Many laboratories in the University of Nottingham were shut down with immediate effect, including D119 in the Medical School building, where I was based at the time and as a result, I was only able to complete two weeks of my rotation in this lab. At this time, I had not decided on a project or laboratory to join, and my cohort, consisting of students who had joined the DTP programme in September 2019, was asked to make this decision about 6 weeks earlier than in previous years. I ultimately joined the Friel lab, but due to lockdown, my first 6 months as a part of this lab were spent exclusively online, attending virtual lab meetings. During this time, my cohort were asked to write a literature review around the topic we would be researching. While this was a useful way to gain an understanding of the field, it was no substitute for practical training. The University of Nottingham Medical School reopened laboratories around the end of July. However, only senior researchers and 3rd and 4th year PhD students were allowed to return to the lab, while I was not able to return until mid. September 2020. This resulted in a full 6 months of lost laboratory time. Upon my return, the lab was divided into shifts to allow for social distancing. I was assigned the morning shift, 07:00 – 13:00 hrs, which usually required travelling to work before sunrise in winter and allowed for no extra time to re-attempt an experiment in the afternoon, for example, as the 13:00hrs was a hard deadline. As well as this, every other Friday, dubbed “Full day Friday” was the only opportunity to have a full day of work. This only happened every other week to allow both groups to get a full day, meaning that every other week was a 4-day working week on half day shifts, reducing productivity even more, to an extent where, while full days were useful, they were not enough. There were several challenges during the time the shift pattern was in place.

Firstly, I missed out on the training that comes from shadowing senior lab members during the start of my PhD. As they were severely restricted in their time as well, they were often unable to spend extra time with me and show me what to do. Many smaller laboratory rooms had a maximum occupancy of 1 person, so I was unable to watch what was being done, missing out on more training.

Secondly, training on lab equipment outside of my home lab was almost non-existent. I could not be trained on the use of ultracentrifuges, liquid nitrogen handling or microscopy for the first three months. Eventually, training slowly resumed; liquid nitrogen training could occur in person as this took place outside, but microscopy training took place over Microsoft Teams, and as such, I do not believe I received the same quality of training as I would have had it taken place in person. Ultracentrifuge training did not take place until over a year after my return to the lab.

Thirdly, much of my PhD involved mammalian cell culture in a category II laboratory. From Sept. 2020 – mid. 2021, the required equipment was again in a laboratory outside of my home lab, and so I had to coordinate with the users of the category II laboratory and work around their schedule. As they were not on a shift pattern and could work all day, they requested that I only work outside of their own working hours, which meant I often had to work from 06:00 – 09:30am. Outside of these times, I had no access to that laboratory, which severely limited the cell culture work I could do, and ultimately I was unable to generate any results during this time.

This shift pattern was in place for a full year, lifting in September 2021. Despite now returning to full time work, I was severely undertrained and still learning many techniques I believe I should have been experienced in by now. However, lab work did ultimately start progressing. Another issue arose with regards to my university issued laptop. I received a laptop upon re-joining Friel lab in September 2022, however as many of the university facilities had been closed, the PC I was given had not been wiped and re-set and as such, was still set to the previous user's settings. I could not download any applications or add my own user account for several months, and I did not know who to contact until I ultimately stumbled upon the university IT department's help pages over a year later.

Despite all the challenges posed by the COVID-19 pandemic and lockdowns, I am very proud of what I have accomplished during my PhD.

Bibliography

(2023) "WHO Model List of Essential Medicines." Web Annex A. World Health Organization Model List of Essential Medicines – 23rd List, 2023. In: The selection and use of essential medicines 2023: Executive summary of the report of the 24th WHO Expert Committee on the Selection and Use of Essential Medicines, 24 – 28 April 2023. Geneva: World Health Organization; 2023
(WHO/MHP/HPS/EML/2023.02). Licence: CC BYNC-SA 3.0 IGO.

Aguezzoul, M., A. Andrieux and E. Denarier (2003). "Overlap of promoter and coding sequences in the mouse STOP gene (Mtap6)." Genomics **81**(6): 623-627.

Andrews, P. D., Y. Ovechkina, N. Morrice, M. WAgenbach, K. Duncan, L. Wordeman and J. R. Swedlow (2004). "Aurora B regulates MCAK at the mitotic centromere." Developmental cell. **6**(2): 253-268.

Balzeau, J., M. Pinier, R. Berges, P. Saulnier, J.-P. Benoit and J. Eyer (2013). "The effect of functionalizing lipid nanocapsules with NFL-TBS.40-63 peptide on their uptake by glioblastoma cells." Biomaterials **34**(13): 3381-3389.

Barreau, K., C. Montero-Menei and J. Eyer (2018). "The neurofilament derived-peptide NFL-TBS.40-63 enters in-vitro in human neural stem cells and increases their differentiation." PLOS ONE **13**(8).

Belsham, H. R., H. M. Alghamdi, N. Dave, A. J. Rathbone, B. Wickstead and C. T. Friel (2022). "A synthetic ancestral kinesin-13 depolymerizes microtubules faster than any natural depolymerizing kinesin." Open Biol **12**(8): 220133.

Berges, R., J. Balzeau, A. C. Peterson and J. Eyer (2012). "A Tubulin Binding Peptide Targets Glioma Cells Disrupting Their Microtubules, Blocking Migration, and Inducing Apoptosis." Molecular Therapy **20**(7): 1367-1377.

Bie, L., G. Zhao, Y. P. Wang and B. Zhang (2012). "Kinesin family member 2C (KIF2C/MCAK) is a novel marker for prognosis in human gliomas." Clinical neurology and neurosurgery **114**(4): 356-360.

Boggs, A. E., M. I. Vitolo, R. A. Whipple, M. S. Charpentier, O. G. Goloubeva, O. B. Ioffe, K. C. Tuttle, J. Slovic, Y. Lu, G. B. Mills and S. S. Martin (2015). "α-tubulin acetylation elevated in metastatic and basal-like breast cancer cells promotes microtentacle formation, adhesion and invasive migration." Cancer Research **75**(1): 203-215.

Bollinger, J. A., Z. I. Imam, M. J. Stevens and G. D. Bachand (2020). "Tubulin islands containing slowly hydrolyzable GTP analogs regulate the mechanism and kinetics of microtubule depolymerization." Nature **10**(13661).

Booth, D. G., F. E. Hood, I. A. Prior and S. J. Royle (2011). "a TACC3/ch-TOG/clathrin complex stabilises kinetochore fibres by inter-microtubule bridging " The EMBO journal **30**(5): 906-919.

Bosc, C., R. Frank, E. Denarier, M. Ronjat, A. Schweitzer, J. Wehland and D. Job (2001). "Identification of novel bifunctional calmodulin-binding and microtubule-stabilizing motifs in STOP proteins." Journal of Biological Chemistry **276**(33): 30904-30913.

Boudker, O. and O. SeCheol (2015). "Isothermal titration calorimetry of ioc-coupled membrane transporters." Methods. **76**: 171-182.

Brecht, M., A. C. M. Steenvoorden, J. G. Collard, S. Luf, D. Erz, C. R. Bartram and J. W. G. Janssen (2005). "Activation ofgef-h1, a guanine nucleotide exchange factor for RhoA, byDNA transfection." International Journal of Cancer **113**(4): 533-540.

Breuss, M., J. I.-T. Heng, K. Poirier, G. Tian, X. H. Jaglin, Z. Qu, A. Braun, T. Gstrein, L. Ngo, M. Haas, N. Bahi-Buisson, M.-L. Moutard, S. Passemard, A. Verloes, P. Gressens, U. Xie, Robson, K.J.H., D. S. Rani, K. Thangaraj, T. Clausen, J. Chelly, N. J. Cowan and D. A. Keays (2012). "Mutations in the β-tubulin gene TUBB5 cause microcephaly with structural brain abnormalities." Cell Reports **2**(6): 1554-1562.

Burakov, A., E. Nadezhdina, B. Slepchenko and V. Rodionov (2003). "Centrosome positioning in interphase cells." Journal of Cell Biology **162**(6): 963-969.

Cai, S., L. N. Weaver, S. C. Ems-McClung and C. E. Walczak (2009). "Kinesin-14 family proteins HSET/XCTK2 control spindle length by cross-lnking and sliding microtubules." Molecular Biology of the Cell **20**(5): 1348-1359.

Calinescu, A.-A. and M. G. Castro (2016). "Microtubule targeting agents in glioma." Translational Cancer Research **5**(1): 54-60.

Campello, S., R. A. Lacalle, M. Bettella, S. Manes, L. Scorrano and A. Viola (2006). "Orchestration of lymphocyte chemotaxis by mitochondrial dynamics." Journal of Experimental Medicine **203**(13): 2879-2886.

Caplow, M. (1992). "Microtubule dynamics." Current Opinion in Cell Biology **4**(1): 58-65.

Casanova, J. E. (2007). "Regulation of Arf activation: the Sec7 family of guanine nucleotide exchange factors." Traffic **8**(11): 1476-1485.

Cassimeris, L. (1999). "Accessory protein regulation of microtubule dynamics throughout the cell cycle." current Opinion in Cell Biology **11**(1): 134-141.

Chang, Y.-C., P. Nalbant, J. Birkenfeld, Z.-F. Chang and G. M. Bokoch (2008). "GEF-H1 Couples Nocodazole-induced Microtubule Disassembly to Cell Contractility via RhoA." Molecular Biology of the Cell **19**: 2147-2153.

Chen, G., J. M. Cleary, A. B. Asenjo, Y. Chen, J. A. Mascaro, D. F. J. Arginteanu, J. Sosa and W. O. Hancock (2019). "Kinesin-5 Promotes Microtubule Nucleation and Assembly by Stabilizing a Lattice-Competent Conformation of Tubulin." Current Biology **29**: 2259-2269.

Chen, L., M. Chuang, T. Koorman, M. Boxem, Y. Jin and A. D. Chisholm (2015). "Axon injury triggers EFA-6 mediated destabilization of axonal microtubules via TACC and doublecortin like kinase." eLife **4**.

Chen, L., Z. Wang, A. Ghosh-Roy, T. Hubert, D. Yan, S. O'Rourke, B. Bowerman, Z. Wu, Y. Jin and A. D. Chishom (2011). "Axon regeneration pathways identified by systematic genetic screening in C. elegans." Neuron **71**(6): 1043-1057.

Cimini, D., B. Moree, J. C. Canman and E. D. Salmon (2003). "Merotelic kinetochore orientation occurs frequently during early mitosis in mammalian tissueu cells and error correction is achieved by two different mechanisms. ." Journal of cell science **116**(20): 4213-4225.

Conduit, P. T., A. Wainman and J. W. Raff (2015). "Centrosome function and assembly in animal cells." Nature reviews Molecular Biology **16**(10): 611-624.

Cooper, G. M. (2000). Structure and Organisation of Actin Filaments. The Cell: A Molecular Approach. Sunderland, MA, Sinauer Associates.

Cote, R. H. and G. G. Borisy (1981). "Head-to-tail polymerisation of microtubules in vitro." Journal of Molecular Biology **150**(4): 577-599.

Cunniff, B., A. J. McKenzie, N. H. Heintz and A. K. Howe (2016). "AMPK activity regulates trafficking of mitochondria to the leading edge during cell migration and matrix invasion." Molecular Biology of the Cell **27**(17): 2662-2674.

Cuveillier, C., J. Delaroche, M. Seggio, S. Gory-Faure, C. Bosc, E. Denarier, M. Bacia, G. Schoehn, H. Mohrbach, I. Kulic, A. Andrieux, I. Arnal and C. Delphin (2020). "MAP6 is an intraluminal protein that induces neuronal microtubules to coil." Science Advances **6**(14).

Delphin, C., D. Bouvier, M. Seggio, E. Couriol, Y. Saoudi, E. Denarier, C. Bosc, O. Valiron, M. Bisbal, I. Arnal and A. Andrieux (2012). "MAP6-F Is a Temperature Sensor That Directly Binds to and Protects Microtubules from Cold-induced Depolymerization." Journal of Biological Chemistry **287**(42): 35127-35138.

Devred, F., P. Barbier, S. Douillard, O. Monasterio, J. M. Andreu and V. Peyrot (2004). "Tau Induces Ring and Microtubule Formation from αβ-Tubulin Dimers under Nonassembly Conditions." Biocemistry **43**(32): 10520-10531.

Dhyani, P., C. Quispe, E. Sharma, A. Bahukhandi, P. Sati, D. C. Attri, A. Szopa, J. Sharifi-Rad, A. O. Docea, I. Mardare, D. Calina and W. C. Cho (2022). "Anticancer potential of alkaloids: a key emphasis to colchicine, vinblastine, vincristine, vindesine, vinorelbine and vincamine." Cancer Cell International **22**(206).

Dixon, J. E., G. Osman, G. E. Morris, H. Markides, M. Rotherham, Z. Bayoussef, A. J. El Haj, C. Denning and K. M. Shakesheff (2016). "Highly efficient delivery of functional cargoes by the synergistic effect of GAG binding motifs and cell-penetrating peptides." PNAS **113**(3): 291-299.

Do Youn Jun, J. Y. L., H. S. Park, Y. H. Lee and Y. H. Kim (2017). "Tumor suppressor protein p53-mediated repression of human mitotic centromere-associated kinesin gene expression is exerted via down-regulation of Sp1 level." PloS one **12**(12).

Domintz, S. B., M. Wagenbach, J. Decarreau and L. Wordeman (2012). "MCAK activity at microtubule tips regulates spindle microtubule length to promote robust kinetochore attachment." Journal of Cell Biology **197**(2): 231-237.

Eddy, R. J., L. M. Pierini and F. R. Maxfield (2002). "Microtubule Asymmetry during Neutrophil Polarization and Migration." Molecular Biology of the Cell **13**(12): 4470-4483.

Ems-McClung, S. C., K. M. Hertzer, X. Zhang, M. W. Miller and C. E. Walczak (2007). "The interplay of the N- and C-terminal domains of MCAK control microtubule depolymerization activity and spindle assembly." Molecular Biology of the cell. **18**(1): 282-294.

Eshun-Wilson, L., R. Zhang, D. Portran, M. V. Nachury, D. B. Toso, T. Lohr, M. Vendruscolo, M. Bonomi, J. S. Fraser and E. Nogales (2019). "Effects of α-tubulin acetylation on microtubule structure and stability." PNAS **116**(21): 10366-10371.

Fauquant, C., V. Redeker, I. Landrieu, J.-M. Wieruszeski, D. Verdegem, O. Laprevote, G. Lippens, B. Gigant and M. Knossow (2011). "Systematic Identification of Tubulin-interacting Fragments of the Microtubule-associated Protein Tau Leads to a Highly Efficient Promoter of Microtubule Assembly." Journal of Biological Chemistry **286**(38): 33358-33368.

Fife, C. M., J. A. McCarroll and M. Kavallaris (2014). "Movers and shakers: cell cytoskeleton in cancer metastasis." British Journal of Pharmacology **171**(24): 5507-5523.

Fraser, R. D. B., T. P. MacRae and A. Miller (1964). "The coiled-coil model of α-keratin structure147-156." Journal of Molecular Biology **10**(1): 147-156.

Friel, C. T. and J. Howard (2011). "The kinesin-13 MCAK has an unconventional ATPase cycle adapted for microtubule depolymerization." EMBO J **30**(19): 3928-3939.
Friel, C. T. and J. Howard (2011). "The kinesin-13 MCAK has an unconventional ATPase cycle adapted for microtubule depolymerization." EMBO **30**(19): 3928-3939.

Fudge, D. S. and J. M. Gosline (2004). "Molecular design of the α–keratin composite: insights from a matrix–free model, hagfish slime threads." Biological Sciences **271**(1536).

Ganguly, A., H. Yang and F. Cabral (2011). "Overexpression of mitotic centromere associated kinesin stimulates microtubule detachment and confers resistance to paclitaxel." Molecular Cancer Therapeutics **10**(6): 929-937.

Garcin, C. and A. Straube (2019). "Microtubules in cell migration." Essays in Biochemistry **63**(5): 509-520.

Gard, D. L. and M. W. Kirschner (1987). "Microtubule assembly in cytoplasmic extracts of Xenopus oocytes and eggs." Journal of Cell Biology **105**(5): 2191-2201.

Gardner, M. K., M. Zanic, C. Gell, V. Bormuth and J. Howard (2011). "Depolymerizing kinesins Kip3 and MCAK shape cellular microtubule architecture by differential control of catastrophe." Cell **147**(5): 1092-1103.

Gell, C., V. Bormuth, G. J. Brouhard, D. N. Cohen, S. Diez, C. T. Friel, J. H. Helenius, B. Nitzsche, H. Petzold, J. Ribbe, E. Schaffer, J. H. Stear, A. Trushko, V. Varga, P. O. Widlund, M. Zanic and J. Howard (2010). "Chapter 13 - Microtubule Dynamics Reconstituted In Vitro and Imaged by Single-Molecule Fluorescence Microscopy." Methods in Cell Biology **95**: 221-245.

Haga, R. B. and A. J. Ridley (2016). "Rho GTPases: Regulation and roles in cancer cell biology." Small GTPases **7**(4): 207-221.

Hagan, I. and M. Yanigida (1990). "Novel potential mitotic motor protein encoded by the fission yeast cut7+ gene." Nature **374**(6293): 563-566.

Helenius, J., G. Brouhard, Y. Kalaidzidis, S. Diez and J. Howard (2006). "The depolymerizing kinesin MCAK uses lattice diffusion to rapidly target microtubule ends." Nature **441**: 115-119.

Hertzer, K. M., S. C. Ems-McClung, S. L. Kline-Smith, T. G. Lipkin, S. P. Gilbert and C. E. Walczak (2006). "Full-length dimeric MCAK is a more efficient microtubule depolymerase than minimal domain monomeric MCAK." Molecular biology of the cell. **17**(2): 700-710.

Hind, L. E., W. J. B. Vincent and A. Huttenlocher (2017). "Leading from the back: the role of the uropod in neutrophil polarization and migration." Developmental Cell **38**(2): 161-169.
Hirokawa, N., Y. Noda, Y. Tanaka and S. Niwa (2009). "Kinesin superfamily motor proteins and intracellular transport." Nature Reviews Molecular Cell Biology **10**: 682-696.

Hodgkinson, J. E., H. J. Clark, R. M. Kaplan, S. L. Lake and J. B. Matthews (2008). "The role of polymorphisms at β tubulin isotype 1 codons 167 and 200 in benzimidazole resistance in cyathostomins." International Journal for Parasitology **38**(10): 1149-1160.
Horio, T. and T. Murata (2014). "The role of dynamic instability in microtubule organization." Frontiers in Plant Science **5**(511).

Howell, B., N. Larsson, M. Gullberg and L. Cassimeris (1999). "Dissociation of the Tubulin-sequestering and Microtubule Catastrophe-promoting Activities of Oncoprotein 18/Stathmin." Molecular Biology of the Cell **10**(1): 105-118.

Huang, H., J. Feng, J. Famulski, J. B. L. Rattner, G. D. Kao, R. Muschel, G. K. Chan and T. J. Yen (2007). "Tripin/hSgo2 recruits MCAK to the inner centromere to correct defective kinetochore attachments." The Journal of cell biology **177**(3): 413-424.

Hunter, A. W., M. Caplow, Coy, David L., W. O. Hancock, S. Diez, L. Wordeman and J. Howard (2003). "The Kinesin-Related Protein MCAK Is a Microtubule Depolymerase that Forms an ATP-Hydrolyzing Complex at Microtubule Ends." Molecular Cell **11**(2): 445-457.

Hyman, A. A., S. Salser, D. N. Drechsel, N. Unwin and T. J. Mitchison (1992). "Role of GTP Hydrolysis in Microtubule Dynamics:." Molecular Biology of the Cell **3**: 1155-1167.

Illingworth, C., N. Pirmadjid, P. Serhal, K. Howe and G. FitzHarris (2010). "MCAK regulates chromosome alignment but is not necessary for preventing aneuploidy in mouse oocyte meiosis I." Development **137**(13): 2133-2138.

Jiang, H., X.-M. Yu, X.-M. Zhou, WangqXiao-Hong and D. Su (2013). "Correlation between microtubule-associated gene expression and chemosensitivity of patients with stage II non-small cell lung cancer." Experimental and Therapeutic Medicine **5**(5): 1506-1510.

Johnsson, A.-K. and R. Karlsson (2010). "Microtubule-dependent localization of profilin I mRNA to actin polymerization sites in serum-stimulated cells." European Journal of Cell Biology **89**(5): 394-401.

Kadavath, H., R. V. Hofele, J. Biernat, S. Kumar, K. Tepper, H. Urlaub, E. Mandelkow and M. Zweckstetter (2015). "Tau stabilizes microtubules by binding at the interface between tubulin heterodimers." PNAS **112**(24): 7501-7506.

Kamath, K., L. Wilson, F. Cabral and M. A. Jordan (2005). "βIII-Tubulin Induces Paclitaxel Resistance in Association with Reduced Effects on Microtubule Dynamic Instability." Journal of Biological Chemistry **280**(13): 12902-12907.

Kavallaris, M. (2010). "Microtubules and resistance to tubulin-binding agents." Therapeutic Resistance **10**.

Keller, H. U., A. Naef and A. Zimmermann (1984). "Effects of colchicine, vinblastine and nocodazole on polarity, motility, chemotaxis and cAMP levels of human polymorphonuclear leukocytes." Experimental Cell Research **153**(1): 173-185.

Khodjakov, A. and C. L. Rieder (1999). "The Sudden Recruitment of γ-Tubulin to the Centrosome at the Onset of Mitosis and Its Dynamic Exchange Throughout the Cell Cycle, Do Not Require Microtubules." Journal of Cell Biology **146**(3): 585-596.

Kikuchi, K. and K. Takahashi (2008). "WAVE2- and microtubule-dependent formation of long protrusions and invasion of cancer cells cultured on three-dimensional extracellular matrices." Cancer Science **99**(11): 2252-2259.

Kirschner, M. and T. Mitchison (1986). "Beyond sself-assembly: from microtubules to morphogenesis." Cell **9**(45): 329-342.

Kline-Smith, S. L., A. Khodjakov, P. Hergert and C. E. Walczak (2004). "Depletion of centromeric MCAK leads to chromosome congression and segregation defects due to improper kinetochore attachments." Molecular biology of the cell **15**(3): 1146-1159.

Kobayashi, T., W. Y. Tsang, J. Li, W. Lane and B. D. Dynlacht (2011). "Centriolar KinesinKif24 Interacts with CP110 to Remodel Microtubules and Regulate Ciliogenesis." Cell **145**(6): 914-925.

Kochanski, R. S. and G. G. Borisy (1990). "Mode of centriole duplication and distribution." The Journal of Cell Biology **110**(5): 1599-1605.

Kollman, J. M., J. K. Polka, A. Zelter, T. N. Davis and D. A. Agard (2010). "Microtubule nucleating γ-TuSC assembles structures with 13-fold microtubule-like symmetry." Nature **466**: 879-882.

Krendel, M., F. T. Zenke and G. M. Bokoch (2002). "Nucleotide exchange factor GEF-H1 mediates cross-talk between microtubules and the actin cytoskeleton." Nature Cell Biology **4**: 294-301.

Lan, W., X. Zhang, S. L. Kline-Smith, S. E. Rosasco, G. A. Battett-Wilt, J. Shabanowitz, D. F. Hunt, C. E. Walczak and P. T. Stukenberg (2004). "Aurora B phoshorylates centromeric MCAK and regulates its localization and microtubule depolymerisation activity." Current Biology **14**(4): 273-286.

Lea, W. A. and A. Simeonov (2011). "Fluorescence Polarization Assays in Small Molecule Screening." Expert Opinion on Drug Discovery **6**(1): 17-32.

Lebok, P., M. Ozturk, U. Heilenkotter, F. Jaenicke, V. Muller, P. Paluchowski, S. Geist, C. Wilke, E. Burandt, A. Lebeau, W. Wilczak, T. Krech, R. Simon, G. Sauter and A. Quaas (2016). "High levels of class III β-tubulin expression are associated with aggressive tumor features in breast cancer." Oncology Letters **11**(3): 1987-1994.

LeDizet, M. and G. Piperno (1987). "Identification of an acetylation site of Chlamydomonas alpha-tubulin." PNAS **84**(16): 5720-5724.

Lee, K. M., D. Cao, A. Itami, P. M. Pour, R. H. Hruban, A. Maitra and M. M. Ouellette (2007). "Class III beta-tubulin, a marker of resistance to paclitaxel, is overexpressed in pancreatic ductal adenocarcinoma and intraepithelial neoplasia." Histopathology **51**(4): 539-546.

Lee, M.-H., P.-H. Wu, D. Gilkes, I. Aifuwa and D. Wirtz (2015). "Normal mammary epithelial cells promote carcinoma basement membrane invasion by inducing microtubule-rich protrusions." Oncotarget **6**(32): 32634-32645.

Lepinoux-Chambaud, C. and J. Eyer (2019). "The NFL-TBS.40-63 peptide targets and kills glioblastoma stem cells derived from human patients and also targets nanocapsules into these cells." International Journal of Pharmaceutics **566**: 218-228.

Li, J., S. K. Katiyar and T. D. Edlind (1996). "Site-directed mutagenesis of Saccharomyces cerevisiae b-tubulin : interaction between residue 167 and benzimidazole compounds." FEBS Letters **385**(2): 7-10.

Liao, G., L. Mingle, L. Van De Water and G. Liu (2014). "Control of cell migration through mRNA localization and local translation." WIREs RNA **6**(1): 1-15.

Lieuvin, A., J. C. Labbe, M. Doree and D. Job (1994). "Intrinsic microtubule stability in interphase cells." Journal of Cell Biology **124**(6): 985-996.

Liu, B. P., M. Chrzanowska-Wodnicka and K. Burridge (1998). "Microtubule Depolymerization Induces Stress Fibers, Focal Adhesions, and DNA Synthesis via the GTP-Binding Protein Rho." Cell Adhesion and Communication **5**: 249-255.

Logan, C. M. and A. S. Menko (2019). "Microtubules: Evolving roles and critical cellular interactions." Experimental Biology and Medicine **244**(15): 1240-1254.

Lolly, A. L., H. Kim, D. Srinivasan, M. Lakonishok, A. G. Larson and V. I. Gelfand (2010). "Kinesin-1 heavy chain mediates microtubule sliding to drive changes in cell shape." PNAS **107**(27): 12151-12156.

Lowe, J., H. Li, K. Downing, H and E. Nogales (2001). "Refined structure of αβ-tubulin at 3.5 Å resolution." Journal of Molecular Biology **313**(5): 1045-1057.
Lu, W., P. Fox, M. Lakonishok, M. W. Davidson and V. I. Gelfand (2013). "Initial Neurite Outgrowth in Drosophila Neurons is Driven by Kinesin-powered Microtubule Sliding." Current Biology **23**(11): 1018-1023.

Luckow, V. A., S. C. Lee, G. F. Barry and P. O. Olnis (1993). "Efficient Generation of Infectious Recombinant Baculoviruses by Site-specific Transposon-mediated Insertion of Foreign Genes into a Baculovirus Genome Propagated in Escherichia coli." American Society for Microbiology **67**(8): 4566-4579.

Macia, E., M. Partisani, C. Favard, E. Mortier, P. Zimmermann, M.-F. Carlier, P. Gounon, F. Luton and M. Franco (2008). "The Pleckstrin Homology Domain of the Arf6-specific Exchange Factor EFA6 Localizes to the Plasma Membrane by Interacting with Phosphatidylinositol 4,5-Bisphosphate and F-actin." Journal of Biological Chemistry **283**(28): 19836-19844.

Magidson, V., R. Paul, N. Yang, J. G. Ault, C. B. O'Connell, I. Tikhonenko, B. F. McEwen, A. Mogilner and A. Khodjakov (2015). "Adaptive changes in the kinetochore architectrue facilitate proper spindle assembly." Nature Cell Biology **17**(9): 1134-1144.

Maney, T., A. W. Hunter, M. Wagenbach and L. Wordeman (1998). "Mitotic centromere-associated kinesin is important for anaphase chromosome separation." The Journal of Cell Biology **142**(3): 787-801.

Maney, T., M. Wagenbach and L. Wordeman (2001). "Molecular dissection of the microtubule depolymerizing activity of mitotic centromere-associated kinesin." Journal of Biological Chemistry **276**(37): 34753-34758.

Margolin, W. (2005). "FTSZ and teh division of Prokaryotic cells and organelles." Nature Reviews Molecular Biology of the Cell **6**(11): 862-871.

Martins, G. G. and J. Kolega (2012). "A role for microtubules in endothelial cell protrusion in three-dimensional matrices." Biology of the Cell **104**(5): 271-286.

Mastronarde, D. N., K. L. McDonald, R. Ding and J. R. McIntosh (1993). "Interpolar spindle microtubules in PTK cells." The Journal of Cell Biology **123**(6): 1475-1489.

McDonald, H. B., R. J. Stewart and L. S. Goldstein (1990). "The kinesin-like ncd protein of Drosophila is a minus end-directed microtubule motor." Journal of Cell Science **63**(6): 1159-1165.

McHugh, T., J. Zou, V. A. Volkov, A. Bertin, S. K. Talapatra, J. Rappsilber, M. Dogterom and J. P. Welburn (2019). "The depolymerase activity of MCAK shows a graded response to Aurora B kinase phosphorylation through allosteric regulation." Journal of cell science **132**(4).

Meunier, S. and I. Vernos (2012). "Microtubule assembly during mitosis - from distinct origins to distinct functions?" Journal of Cell Science **125**(12): 2805-2814
.
Mingle, L. A., N. N. Okuhama, J. Shi, R. H. Singer, J. Condeelis and G. Liu (2005). "Localization of all seven messenger RNAs for the actin-polymerization nucleator Arp2/3 complex in the protrusions of fibroblasts." The Journal of Cell Science **118**(11): 2425-2433.

Montieiro, P., B. Yeon, S. S. Wallis and S. A. Godhino (2023). "Centrosome amplification fine tunes tubulin acetylation to differentially control intracellular organization." EMBO **42**(16).

Moore, A. T., K. E. Rankin, G. Von Dassow, L. Peris, M. Wagenbach, Y. Ovechkina, A. Andrieux, D. Job and L. Wordeman (2005). "MCAK associates with the tips of polymerising microtubules." The Journal of Cell Biology **169**(3): 391-397.

Moores, C. A., M. Yu, J. Guo, C. Beraud, R. Sakowicz and R. A. Milligan (2002). "A mechanism for microtubule depolymerisation by KinI kinesins." Molecular cell **9**(4): 903-909.

Nakamura, Y., F. Tanaka, N. Haraguchi, K. Mimori, T. Matsumoto, H. Inoue, K. Yanaga and M. Mori (2007). "Clinicopathological and biological significance of mitotic centreomere-associated kinesin overexpressoin in human gastric cancer." British journal of cancer **97**(4): 543-549.

Nekooki-Machida, Y. and H. Hagiwara (2020). "Role of tubulin acetylation in cellular functions and diseases." Medical Molecular Morphology **53**: 191-197.

Nguyen, H., S. Chari, D. Gruber, C. Lue, S. J. Chapin and J. C. Bulinski (1997). "Overexpression of full- or partial-length MAP4 stabilizes microtubules and alters cell growth." Journal of Cell Science **110**(2): 281-294.

Niggli, V. (2003). "Microtubule-disruption-induced and chemotactic-peptide-induced migration of human neutrophils: implications for differential sets of signalling pathways." Journal of Cell Science **116**(5): 813-822.

Nixon, F. M., Gutierrez-Caballero, C., F. E. Hood, D. G. Booth, I. A. Prior and S. J. Royle (2015). "The mesh is a network of microtubule connectors that stabilizes individual kinetochore fibres of the mitotic spindle." Elife **4**.

Nogales, E., S. G. Wolf and K. H. Downing (1998). "Structure of the alpha beta tubulin dimer by electron crystallography." Nature **391**: 199-203.

O'Rourke, S. M., S. N. Christensen and B. Bowerman (2010). "Caenorhabditis elegans EFA-6 limits microtubule growth at the cell cortex." Nature Cell Biology **12**(12): 1235-1243.

Oh, S., E. You, P. Ko, J. Jeong, S. Keum and S. Rhee (2017). "Genetic disruption of tubulin acetyltransferase, αTAT1, inhibits proliferation and invasion of colon cancer cells through decreases in Wnt1/β-catenin signaling." Biochemical and Biophysical Research Communications **482**(1): 8-14.

Ohi, R., K. Burbank, Q. Liu and T. J. Mitchison (2007). "Nonredundant functions of Kinesin-13s during meiotic spindle assembly." Current biology **17**(11): 953-959.

Ookata, K., S. Hisanaga, J. C. Bulinski, H. Murofushi, H. Aizawa, T. J. Itoh, H. Hotani, E. Okumura, K. Tachibana and T. Kishimoto (1995). "Cyclin B interaction with microtubule-associated protein 4 (MAP4) targets p34cdc2 kinase to microtubules and is a potential regulator of M-phase microtubule dynamics." The Journal of Cell Biology **128**(5): 849-862.

Palmer, R. E., D. S. Sullivan, T. Huffaker and D. Koshland (1992). "Role of Astral Microtubules and Actin in Spindle Orientation and Migration in the Budding Yeast Saccharomyces cerevisiae." The Journal of Cell Biology **119**(3): 583-593.

Parry, D. A. D., S. V. Strelkov, P. Burkhard, U. Aebi and H. Herrmann (2007). "Towards a molecular description of intermediate filament structure and assembly." Experimental Cell Research **313**(10): 2204-2216.

Patel, J. T., H. R. Belsham, A. J. Rathbone, B. Wickstead, C. Gell and C. T. Friel (2016). "The family-specific a4-helix of the kinesin-13, MCAK, is critical to microtubule end recognition. ." Open biology **6**(10).

Paul, R., R. Wollman, W. T. Silkworth, I. K. Nardi, D. Cimini and A. Mogilner (2009). "Computer simulations predict that chromosome movements and rotations accelerate mitotic spindle assembly without compromising accuracy." PNAS **106**(37): 15708-15713.

Perour, C. M., S. S. Jeffrey, M. Van De Rijn, C. A. Rees, M. B. Eisen, D. T. Ross, A. Pergamenschikov, C. F. Williams, S. X. Zhu, J. C. Lee and D. Lashkari (1999).

"Distinctive gene expression patterns in human mammary epithelial cells and breast cancers." Proceedings of the National Academy of Sciences **96**(16): 9212-9217.

Piehl, M., U. S. Tuli, P. Wadsworth and L. Cassimeris (2004). "Centrosome maturation: measurement of microtubule nucleation throughout the cell cycle by using GFP-tagged EB1." Proceedings of the National Academy of Sciences **101**(6): 1584-1588.

Pollard, T. D. and R. D. Goldman (2018). "Overview of the Cytoskeleton from an Evolutionary Perspective." Cold Spring Harbor Laboratory Press **10**.

Prosser, S. L. and L. Pelletier (2017). "Mitotic spindle assembly in animal cells: a fine balancing act." Nature reviews Molecular Cell Biology **18**(3).

Qu, Y., I. Hahn, M. Lees, J. Parkin, A. Voelzmann, K. Dorey, A. Rathbone, C. T. Friel, V. J. Allan, P. Okenve-Ramos, N. Sanchez-Soriano and A. Prokop (2019). "Efa6 protects axons and regulates their growth and branching by inhibiting microtubule polymerisation at the cortex." eLife **8**.

RayChaudhuri, D. and J. T. Park (1992). "Escherichia coli cell-division gene ftsZ encodes a novel GTP-binding protein." Nature **17**(359): 251-254.

Ren, Y., R. Li, Y. Zheng and H. Busch (1998). "Cloning and Characterization of GEF-H1, a Microtubule-associated Guanine Nucleotide Exchange Factor for Rac and Rho GTPases*." Journal of Biological Chemistry **273**(52): 34954-34960.

Richards, T. A. and T. Cavalier-Smith (2005). "Myosin domain evolution and the primary divergence of the eukaryotes." Nature **436**(7054): 1113-1118.

Rieder, C. L. (1981). "The structure of the cold-stable kinetochore fiber in metaphase PtK1 cells." Chromosoma **84**(1): 145-158.

Robbins, E., G. Jentzsch and A. Micali (1968). "The centriole cycle in synchronised HeLa cells." The Journal of Cell Biology **36**(2): 329-339.

Roll-MEcak, A. (2020). "The Tubulin Code in Microtubule Dynamics and Information Encoding." Developmental Cell **54**(1): 7-20.

Royle, S. J., N. A. Bright and L. Lagnado (2005). "Clathrin is required for the function of the mitotic spindle." Nature **434**(7037): 1152-1157.

Rubin, C. I. and G. F. Atweh (2004). "The role of stathmin in the regulation of the cell cycle." Journal of Cellular Biochemsitry **93**(2): 242-250.

Sakagami, H., s. Matsuya, H. Nishimura, R. Suzuki and H. Kondo (2004). "Somatodendritic localization of the mRNA for EFA6A, a guanine nucleotide exchange protein for ARF6, in rat hippocampus and its involvement in dendritic formation." European Journal of Neuroscience **19**(4): 863-870.

Samora, C. P., B. Mogessie, L. Conway, J. L. Ross, A. Straube and A. D. McAinsh (2011). "MAP4 and CLASP1 operate as a safety mechanism to maintain a stable spindle position in mitosis." Nature Cell Biology **13**(9): 1040-1050.

Sawin, K. E., K. LeGuellec, M. Philippe and T. J. Mitchison (1992). "Mitotic spindle organization by a plus-end-directed microtubule motor." Nature **359**(6395): 540-543.

Schaks, M., G. Giannone and K. Rottner (2019). "Actin dynamics in cell migration." Essays in Biochemistry **63**: 483-495.

Schofield, A. and O. Bernard (2013). "Tubulin polymerization promoting protein 1 (TPPP1)." Communicative & Integrative Biology **6**(6).

She, Z.-Y., N. Zhong and Y.-L. Wei (2022). "Kinesin-5 Eg5 mediates centrosome separation to control spindle assembly in spermatocytes." Chromosoma **131**: 87-105.

She, Z., N. Zhong, K. Yu, Y. Xiao, Y. Wei, Y. Lin, Y. Li and M. Lu (2020). "Kinesin-5 Eg5 is essential for spindle assembly and chromosome alignment of mouse spermatocytes." Cell Division **15**(6).

Shimo, A., C. Tanikawa, T. Nishidate, M. L. Lin, K. Matsuda, J. Park, H, T. Ueki, T. Ohta, K. Hirata, M. Fukida and Y. Nakamura (2008). "Involvement of kinesin family member 2C/mitotic centromere-associated kinesin overexpression in mammary carcinogenesis." Cancer science **99**(1): 62-70.

Shipley, K., M. Hekmat-Nejad, J. Turner, C. Moores, R. Anderson, R. Milligan, R. Sakowicz and R. Fletterick (2004). "Structure of a kinesin microtubule depolymerization machine." The EMBO Journal **23**(7): 1422-1432.

Silvestre, A. and J. Cabaret (2002). "Mutation in position 167 of isotype 1 β-tubulin gene of Trichostrongylid nematodes: role in benzimidazole resistance?" Molecular and Biochemical Parasitology **120**(2): 297-300.

Southey, M. W. Y. and M. Brunavs (2023). "Introduction to small molecule drug discovery and preclinical development." Frontiers in Drug Discovery **3**.

Strahl, H., F. Burmann and L. W. Hamoen (2014). "The actin homologue MreB organizes the bacterial cell membrane." Nature communications **5**(3442).

Su, X., W. Qiu, M. L. Gupta Jr, J. B. Pereira-Leal, S. L. Reck-Peterson and D. Pellman (2011). "Mechanisms Underlying the Dual-mode Regulation of Microtubule Dynamics by Kip3/Kinesin-8." Molecular Cell **43**(5): 751-763.

Sulimenko, V., Z. Hajkova, A. Klebanovych and P. Draber (2017). "Regulation of microtubule nucleation mediated by γ-tubulin complexes." Protoplasma **254**: 1187-1199.

Talapatra, S. K., B. Harker and J. P. Welburn (2015). "The C-terminal regionof the motor protein MCAK controls its structure and activity through a conformational switch." Elife **4**.

Tanenbaum, M. E. and R. H. Medema (2010). "Mechanisms of Centrosome Separation and Bipolar Spindle Assembly." Developmental Cell **19**: 797-806.
Tang, N. and W. F. Marshall (2012). "Centrosome positioning in vertebrate development." Journal of Cell Science **125**(21): 4951-4961.

Tanno, Y., T. S. Kitajima, T. Honda, Y. Ando, K. I. Ishiguro and Y. Watanabe (2010). "Phosphorylation of mammalian Sgo2 by Aurora B recruits PP2A and MCAK to centromeres." Genes & development **24**(19): 2167-2179.

Tolic, I. M. (2018). "Mitotic spindle: kinetochore fibers hold on tight to interpolar bundles." European Biophysics Journal **47**(3): 191-203.

Trinczek, B., J. Biernat, K. Baumann, E. Mandelkow and E. Mandelkow (1995). "Domains of Tau Protein, Differential Phosphorylation, and Dynamic Instability of Microtubules." Molecular Biology of the Cell **6**(12): 1619-1902.

Uhlen, M. O., P; Fagerberg, L; Lundberg, E; Jonasson, K; Forsberg, M; Zwahlen, M; Kampf, C; Wester, K; Hober, S; Wernerus, H; Bjorling, L; Ponten, F. (2012). Homo sapiens, epidermoid carcinoma. Cell Image Library.

Vale, R. D., T. S. Reese and M. P. Sheetz (1985). "Identification of a novel force-generating protein, kinesin, involved in microtubule-based motility." Cell **42**(1): 39-50.

Wang, D., N. Ryo, M. Morikawa, H. Yajima, S. Inoue, H. Shigematsu, M. Kikkawa and N. Hirokawa (2016). "Motility and microtubule depolymerization mechanisms of the Kinesin-8 motor, KIF19A." eLife **5**(18101).

Wang, H. W. and E. Nogales (2005). "Nucleotide-dependent bending flexibility of tubulin regulates microtubule assembly." Nature **435**: 911-915.

Wang, W., S. Cantos-Fernandes, Y. Ly, H. Kuerban, S. Ahmad, C. Wang and B. Gigant (2017). "Insight into microtubule disassembly by kinesin-13s from the structure of Kif2C bound to tubulin." Nature communications **8**(1): 1-11.

Wang, X., B. Gigant, X. Zheng and Q. Chen (2023). "Microtubule-targeting agents for cancer treatment: Seven binding sites and three strategies." MedComm-Oncology **2**(3).

Wattanathamsan, O., R. Tharattanobon, R. Rodsiri, P. Chanvorachote, C. Vinayanuwattikun and V. Pongrakhanon (2021). "Tubulin acetylation enhances lung cancer resistance to paclitaxel-induced cell death through Mcl-1 stabilization." Cell Death Discovery **7**(67).

Weaver, B. A. (2014). "How Taxon/paclitaxel kills cancer cells." Molecular Biology of the Cell **25**(18): 2677-2681.

Weaver, L. N., S. C. Ems-McClung, J. R. Stout, C. LeBlanc, S. L. Shaw, M. K. Gardner and C. E. Walczak (2011). "Kif18A Uses a Microtubule Binding Site in the Tail for Plus-end Localisation and Spindle Length Regulation." Current Biology **21**(17): 1500-1506.

Wickstead, B. and K. Gull (2006). "A "Holistic" Kinesin Phylogeny Reveals New Kinesin Families and Predicts Protein Function." Molecular Biology of the Cell **17**(4): 1734-1743.

Wickstead, B. and K. Gull (2007). "Dyneins Across Eukaryotes: A Comparative Genomic Analysis." Traffic **8**(12): 1708-1721.

Wickstead, B. and K. Gull (2011). "The evolution of the cytoskeleton." Journal of Cell Biology **194**(4): 513-525.

Wickstead, B., K. Gull and T. A. Richards (2010). "Patterns of kinesin evolution reveal a complex ancestral eukaryote with a multifunctional cytoskeleton." Evolutionary Biology **10**(110): 1471-2148.

Wieczorek, M., L. Urnavicius, S.-C. Ti, K. R. Molloy, B. T. Chait and T. M. Kapoor (2020). "Asymmetric Molecular Architecture of the Human gTubulin Ring Complex." Cell **180**: 165-175.

Wollman, R., E. N. Cytrynbaum, J. T. Jones, J. M. Scholey and A. Mogilner (2005). "Efficient chromosome capture requires a bias in the 'search-and-capture' process during mitotic-spindle assembly." Current Biology **15**(9): 828-832.

Wordeman, L. (2005). "Microtubule-depolymerizing kinesins." Current opinion in cell biology **17**(1): 82-88.

Wordeman, L. and T. J. Mitchison (1995). "Identification and partial characterization of mitotic centromere-associated kinesin, a kinesin-related protein that associates with centromeres during mitosis." Journal of Cell Biology **128**(1): 95-104.

Wordeman, L., M. Wagenbach and G. von Dassow (2007). "MCAK facilitates chromosome movement by promoting kinetochore microtubule turnover." The Journal of cell biology **179**(5): 869-879.

Wu, Z., A. Ghosh-Roy, M. F. Yanik, J. Z. Zhang, Y. Jin and A. D. Chisholm (2007). "Caenorhabditis elegans neuronal regeneration is influenced by life stage, ephrin signaling, and synaptic branching." PNAS **104**(38): 15132-15137.

Xie, J., Y. Bi, H. Zhang, S. Dong, L. Teng, R. J. Lee and Z. Yang (2020). "Cell-Penetrating Peptides in Diagnosis and Treatment of Human Diseases: From Preclinical Research to Clinical Application." frontiers in Pharmacology **11**.

Yadav, S. K., D. Stojkov, S. W. Feigelson, F. Roncato, H.-U. Simon, S. Yousefi and R. Alon (2019). "Chemokine-triggered microtubule polymerization promotes neutrophil chemotaxis and invasion but not transendothelial migration." Journal of Leukocyte Biology **105**(4): 755-766.

Yang, P., C. Yin, S. Ma, Y. Cao, C. Zhang, T. Chen and H. Zhao (2020). "Mutation analysis of tubulin beta 8 class VIII in infertile females with oocyte or embryonic defects." Clinical Genetics **99**(1): 208-214.

Yu, D., V. Pessino, S. Kuei and M. T. Valentine (2012). "Mechanical and functional properties of epothilone-stabilized microtubules†." Cytoskeleton **70**(2): 74-84.

Zonderland, J., P. Wieringa and L. Moroni (2019). "A quantitative method to analyse F-actin distribution in cells." MethodsX **6**: 2562-2569.